Superconductivity With Strongly Correlated Electrons and an Electron Phonon Interaction

by

Thomas M Hardy

A Doctoral Thesis
submitted in partial fulfilment of the requirements
for the award of
Doctor of Philosophy
of
Loughborough University

March 2009

Abstract

The effect on the stability of the superconducting phase due the addition of an electron-phonon interaction to a repulsive Hubbard model is studied. Our Hubbard-Fröhlich Hamiltonian includes electron hoping, the on-site Coulomb repulsion, vibrating ions (phonons) and the electron-phonon interaction. A Lang-Firsov transformation is used to integrate out the phonon degrees of freedom; The transformation reduces the model to simple a Hubbard Hamiltonian with an additional long range electron-electron attraction. A variational Monte Carlo technique, with a projected BCS trial function, is used to investigate the ground state energies of our transformed Hubbard-Fröhlich Hamiltonian.

For various electron densities, with a d-wave superconducting order parameter, it is found that the inclusion of the electron-phonon interaction significantly enhances the condensation energy (the energy required to break paired electrons). We show that increasing the strength of the electron-phonon interaction increases the condensation energy. It is also found that even with an infinite on-site repulsion, where the resonating valence bond state cannot exist, the EPI does still lead to a d-wave superconducting state.

In addition we examine, analytically, the coexistence of ferromagnetism and superconductivity. Allowing different masses for spin-up and spin-down electrons in a BCS type Hamiltonian two new branches in the energy spectrum are found. Including a spatially varying order parameter a new expression for the pairing amplitude of finite momentum pairs is derived.

Contents

List of Figures

List of Tables

Acknowledgements

I would like to thank my supervisors, Prof. Sasha Alexandrov, Dr Jim Hague and Dr John Samson for their support and guidance throughout my PhD.

In addition I am grateful to EPSRC for funding various conferences and schools. I would also like to thank Loughborough University for my scholarship.

Chapter 1

Introduction

In 1911 Heike Kamerlingh Onnes made the remarkable discovery, using liquid helium to cool the sample, that below 4.15K mercury has no electrical resistance. The first superconductor had been found. What follows is a brief historical overview mapping the development of electrical conduction theories with the ultimate aim of explaining superconductivity.

1.1 History of solid state physics

One of the most fundamental developments in physics was the discovery of the electron by J. J. Thomson in 1897. Since then there have been many theories to explain electronic conduction, however there are still many unsolved problems.

1.1.1 Free electrons

The first of the theories, by Drude, used kinetic theory and assumed the electrons to be a non-interacting gas colliding with stationary ions. He made the following

assumptions: (a) that there was no electron-electron interaction (known as the independent electron approximation), (b) that the collisions were only between the ions and electrons, abruptly altering the electron velocity and (c) that collisions occur with an average probability per unit time $1 / \tau$, where τ is the relaxation time. The electron gas attains thermal equilibrium through collisions with the ions. However, since the Pauli principle had been ignored, this model did not predict many measurable quantities, such as the specific heat, of metallic conductors accurately.

The next step towards a robust theory of electrical conduction came with the advent of quantum mechanics. Sommerfeld devised a model in which the electrons are confined to a cube as an approximation to the bulk limit. Applying the Schrödinger equation to this system the free electron energy spectrum and wave functions are obtained. The ground state is then created by filling the lowest energy single electron states, in a manner that obeys the Pauli exclusion principle. By using the Fermi-Dirac distribution, instead of the Maxwell-Boltzmann distribution, Sommerfeld was able to more accurately predict the specific heat [3].

However, the free electron model has a number of failures. The most striking of these is its inability to distinguish between metals and insulators. It also does not, in most cases, produce a correct value for the Hall coefficient and, for certain metals, even predicts the wrong sign. Furthermore there is no explanation for magneto-resistance. Resistivity is temperature dependent but this is only achieved within the free electron model by making the relaxation time a function of temperature with no physical foundation. Importantly within the free electron model there is no explanation for superconductivity.

1.1.2 Bloch's theorem

To progress further and make more accurate predictions, the assumption that the electrons are moving in a vacuum needs to be abandoned. Therefore the periodic potential

created by the crystalline ions needs to be included in the Schrödinger equation. To cater for the periodic potential Bloch's theorem, which states that the solutions can be written in the form of plane waves multiplied by a function that has the same periodicity as the ion lattice, must be applied. Doing so leads to the formation of energy bands of allowed energies and corresponding wave vectors in the first Brillouin zone. Depending on the filling of these bands a distinction between metals, band insulators and intrinsic semiconductors can be made.

1.1.3 Correlated Electrons

While Bloch's theorem solved a lot of the shortcomings of the free electron approximation there are still some phenomena, such as superconductivity and Mott insulators, that are left unexplained. To go beyond the Bloch theorem the independent electron approximation needs to be rejected. When the inter-electron interactions are included in the model it is considered a correlated electron system. Here the Coulomb repulsion is so strong that the motion of one electron depends on the position of all the other electrons [4]. Studying correlated electrons is a problem of huge complexity and to find any solutions again some simplifications must be made. For example, the calculation of the complete wave function, from the full Schrödinger equation, of a single iron atom with 26 electrons would require the storage of at least 10^{78} numbers [4].

The Hubbard model

One of the most basic models able to tackle electron interactions and the one studied predominantly in this thesis is the Hubbard Hamiltonian. This was first introduced by M. Gutzwiller [5], J. Hubbard [6] and J. Kanamori [7] in three separate papers while trying to explain the correlated d-electrons in the transition metals. The Hamiltonian is made up of two competing terms, the hopping term, t, which describes the move-

ment of the electron between neighbouring ions and an on-site term, U, to approximate the electronic interaction. The idea behind the Hubbard model is that the Coulomb interaction between two electrons a distance r apart is inversely proportional to r, so the largest term is when the two electrons are both on the same site and negligible otherwise. When U is positive the electron interaction is repulsive due to the Coulomb force. A negative U represents an attractive interaction due to some other overriding force. With the on-site term set to zero the electron correlation disappears and the independent electron picture is recovered. If the hopping term is set to zero the electrons become localised to each site.

One example where the effect of electronic correlation can be observed is the Mott insulator. For some materials, such as nickel oxide, conventional band theory predicts metallic behaviour: however these solids are in fact insulators, known as Mott insulators. To describe this phenomenon Mott used a thought experiment with a lattice of hydrogen like atoms and a variable lattice constant a [8]. As the lattice constant is increased the overlap between the atomic wave functions decreases, thereby reducing the likelihood of an electron hopping to another site and a metal-insulator transition occurs. This phenomenon can be described with the Hubbard model, by increasing the electron hopping integral, t, to decrease the lattice spacing. When there is exactly one electron per site, which is known as half filling, such a transition can be found when the on-site term in the Hubbard Hamiltonian is large enough relative to the hopping term.

In some cases long range ordering of the correlated electrons can lead to a lower energy, as is the case in the anti-ferromagnetic state. This occurs again at half filling for intermediate and large values of U. The Pauli exclusion prohibits hopping when an electron is surrounded by electrons of the same spin. If, however, an electron is surrounded by electrons of opposite spin then hopping is permitted. This gives a staggered configuration of up and down electrons, as shown in Fig(1.1), that increases the magnitude of the kinetic energy, though, obviously, there is still the cost of the onsite

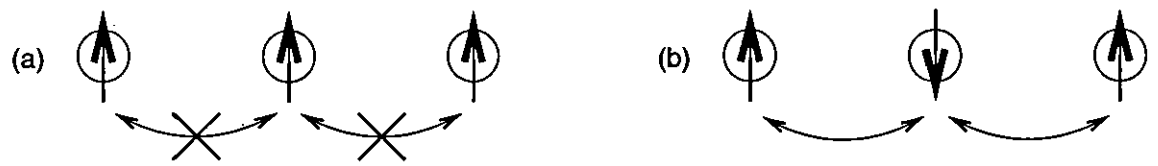

Figure 1.1: The ferromagnetic arrangement in (a) prevents hopping while the antiferromagnetic arrangement in (b) allows hopping

Hubbard U to be considered.

BCS Superconductivity

Another area in which electron correlations need to be considered is superconductivity. While attempting to understand the superconducting state it is important to realise that it is not simply a perfect conductor. One such feature that distinguishes the superconducting state from a zero resistance state is the Meissner effect, where perfect diamagnetism is displayed. Another defining feature is the isotope effect where the transition temperature depends on the isotopes of the elements in the compound. Any theory of superconductivity must explain these phenomena.

Various attempts were made at producing a theory of superconductivity, notably by London, Ginzburg and Landau; however, these were only phenomenological theories. A microscopic theory was not found until 1957, nearly half a century after the original discovery of the effect, by Bardeen, Cooper and Schrieffer [9].

A clue to the origins of the superconducting state comes from the superfluid state in ^{4}He, which displays similar properties. However electrons are fermions, obeying the Pauli exclusion principle, unlike the bosons in ^{4}He which can all be in the same state. Pairs of electrons on the other hand have spin zero or spin one and are therefore have similar properties to bosons able to form a condensate. Electrons are negatively charged particles and therefore repel each other so that a paired state does not seem

immediately achievable.

Further indication to the cause of the pairing mechanism lies with the fact that none of the good conductors are superconductors, hinting that the source of resistance, at low enough temperatures, also causes superconductivity. One of the mechanisms for resistivity comes from the reduction in the electron mean free path by scattering from vibrating lattice ions (phonons). Another clue that phonons cause conventional superconductivity is in the isotope effect; the transition temperature is (approximately) inversely proportional to the square root of the ion mass. It was also known that the presence of an electron in an ionic lattice can cause a distortion where the ions are pulled towards the electron. Due to the large mass of the ions, making the nuclei slow to return to their original positions, the distortion can persist after the electron has been removed. The persisting distortion leaves a favourable position for another electron and can lead to a retarded attraction between electrons. This led Cooper to conclude the attractive force pairing electrons is driven by a weak electron-phonon interaction. Paired electrons, known as Cooper pairs, are formed in momentum space via their weak interaction with the phonons. In real space the pairs are formed over large distances so that the intermediate electrons screen the Coulomb repulsion of the paired electrons.

Using Coopers' result, Bardeen, Cooper and Schrieffer formed a full theory of superconductivity now known as the BCS theory of superconductivity. Unfortunately it was generally perceived, based on work by P. W. Anderson and M. Cohen [10], that using BCS theory there was a maximum superconducting transition temperature of about 30K and therefore hope of finding a superconductor with a practical transition temperature was dwindling. Such low temperatures require liquid Helium and are therefore costly to achieve making conventional superconductivity impractical for many applications.

1.2 High temperature Superconductivity

In 1986 Bednorz and Müller exceeded all the predictions of the time finding a superconducting transition temperature of 35K [11] in the doped Ba-La-Cu-O compounds. Since then there have been many more high temperature superconductors with the current record, at ambient pressure, 138K with a Hg-Tl-Ba-Ca-Cu-O compound [12]. This means that it is now possible to produce a superconducting state with liquid nitrogen, a much more cost effective and commercially viable method. However despite intensive effort there is still no widely accepted theory for the high temperature superconductors.

1.2.1 General Properties of the high temperature superconductors

While trying to determine the mechanism driving the superconductivity in the cuprates it is an advantage to understand as many of their other properties as possible. Since the discovery of the cuprate superconductors a large amount of experimental data has been produced, here we give a brief overview of the experimental facts and the conclusions drawn.

In general the high T_c superconductors are not isotropic systems; the superconductivity occurs mainly in planes and the resistivity across the planes is high. They all consist of copper-oxygen planes inter spaced with charge donor planes see Fig(1.2). It is widely accepted that it is the copper-oxygen planes which are responsible for the superconductivity and a 2D model will be sufficient to describe the state. With the copper ions in a d^9 configuration there is one hole in the d shell per unit cell so a half filled effective single-band model [13], such as the Hubbard model, describes the situation of the parent compounds.

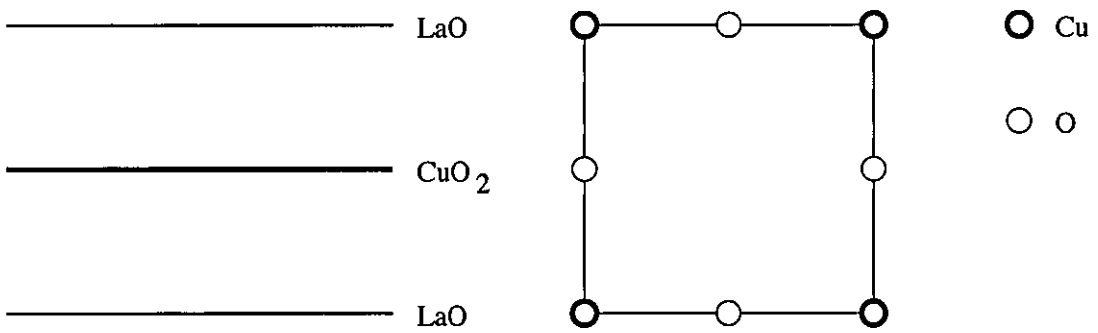

Figure 1.2: Schematic structure of LaCuO [1], layers on the left and cuprate plane on the right.

Another feature is the antiferromagnetic order, with a Néel temperature of about $T_N \approx 300K$, present when the materials are undoped, see Fig(1.3). Such a state is adequately modelled by the Hubbard Hamiltonian so the presence of anti-ferromagnetism in the parent compounds is one of the justifications for using the Hubbard model to explain superconductivity. The anti-ferromagnetism disappears when doped with either holes or electrons, allowing the formation of the superconducting state [14]. In this thesis we focus on the hole doped case, the right hand side of the phase diagram Fig(1.3), where the superconductivity persists over a large range of doping, from around 5% to 25% with the maximum transition temperature found at about 16% [1] forming the famous superconducting dome. The maximum transition temperature occurs at optimal-doping, doping levels below this are referred to as under-doped and concentrations over this as over-doped.

Like the BCS superconductors the high temperature superconductors have charge 2e carriers and exhibit the Meissner effect. The coherence length of the pairs, however, differs substantially: BCS superconductors have a coherence length of the order of 10^3Å, where as the cuprates have a coherence length of the order of 10Å [15]. Both types of superconductor exhibit an energy gap at the Fermi surface: though unlike the BCS superconductors that have an order parameter with s-wave symmetry the high-temperature superconductors have an order parameter that exhibits d-wave symmetry

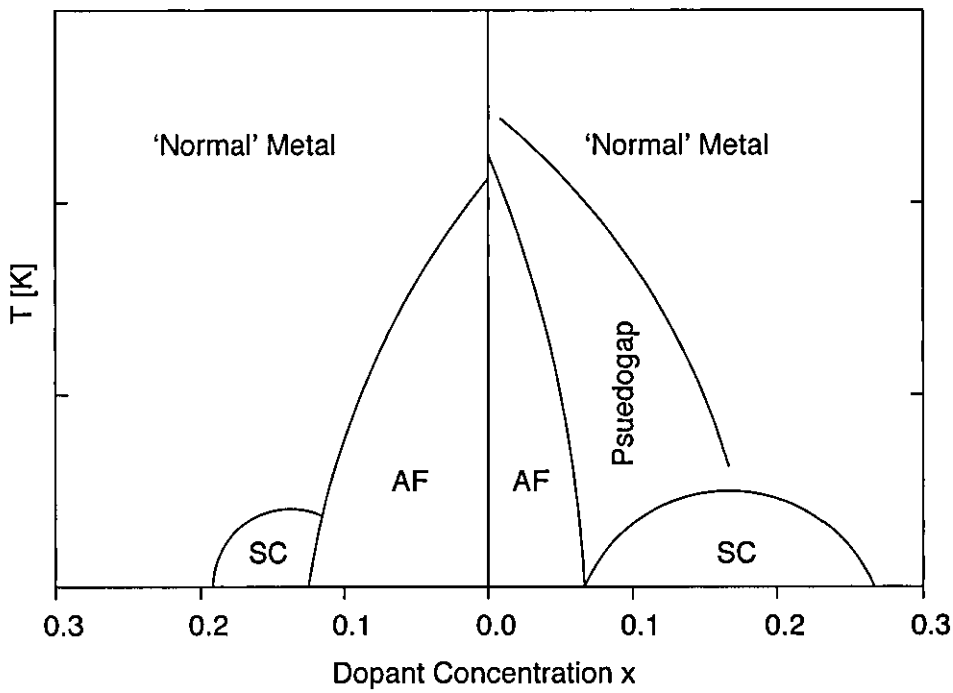

Figure 1.3: Schematic phase diagram of the high temperature superconductors, the right side shows hole doping with electron doping on the left [2]

with a sign change present in the gap function [16]. The cuprates also differ from the BCS superconductors with the presence of the pseudogap region on the phase diagram, Fig(1.3). In this region there is evidence for the existence of pairs at temperatures greater than the transition temperature [17] with a gap in the excitation spectrum. The absence of phase coherence between these pairs means that they do not result in a superconducting state. Another difference is that cuprates do not exhibit a significant conventional isotope effect on the transition temperature at optimum doping, which has led many to believe that phonons are not relevant [18].

1.2.2 Theories for the high temperature superconductors

While there is no accepted theory to explain the high T_c there are many that attempt to explain the phenomenon. One theory is based on polarons (an electron dressed by a phonon) and bipolarons as an extension of the BCS theory. The precise nature of the attractive force in BCS theory is not critical and need not be an electron phonon interaction. Various theories to explain the high Tc superconductors with a modification to the pairing mechanism of the BCS model have been proposed. Other theories ignore the electron-phonon interaction and the BCS theory completely relying on other mechanisms for pairing the electrons. One such theory is the Resonating Valence Bond (RVB) proposed by P. W. Anderson [19] in which the electrons are anti-ferromagnetically paired within the Hubbard model. In this thesis only the RVB state and electron phonon interactions are discussed.

Resonating Valence Bond theory of superconductivity

There is an ongoing debate over whether or not the Hubbard model has the essential physics required for a mechanism to provide high T_c superconductivity. The resonating valence bond theory is derived from an antiferromagnetic pairing mechanism within the strongly correlated electron regime so that the Hubbard model is an adequate base for investigating this state.

In the Hubbard model at half filling with $U \gg t$ the Mott insulating state, described earlier, exists because the onsite repulsion prevents the electrons hopping. These are virtual hopping processes, in which an electron hops to a neighbouring site, occupied by an electron of opposite spin, creating a virtual doubly occupied site. One of the two electrons on the doubly occupied site then hops back to the empty site. This virtual hopping lowers the energy by an amount $J = 4t^2/U$ called the antiferromagnetic exchange energy. This exchange energy can lead to singlet pairs: The RVB state is a

sum of all the possible singlet pairs. If holes are injected into this state then the pairs become mobile and could lead to superconductivity [19].

Results by Paramekanti *et al* [20] and Yamaji et al [21] using a variational Monte Carlo (VMC) method found a RVB d-wave superconducting state in the Hubbard model. These results are not unique and other work has led to the same conclusion. A d-wave superconducting state was also found in the $t - t'J$ model, a derivative of the Hubbard model, by Sorella et al [22] using the Green function MC method. The Dynamical Cluster approximation combined with a quantum MC technique employed by T. Maier *et al* has been used to show that the 2D Hubbard model displays a 'finite temperature instability to d-wave superconductivity' [23]. Later we repeat some of these VMC results as a validation of our own code.

Polaron and bipolaron theory of superconductivity

Contrary to the previously mentioned references, recent results, employing a Gaussian Basis MC algorithm, by Imada et al [24] indicate that the Hubbard model along with the RVB state do not contain the essential physics required for high temperature superconductivity. Earlier studies using the auxiliary field quantum MC method, by Furukawa [25] and Imada [26], find similar results. Further work using the constrained path MC technique by Zhang *et al* [27] and Guerrero *et al* [28] again find no evidence for high temperature superconductivity in the 2D Hubbard model. These results indicate that the Hubbard model may not be a likely candidate for high temperature superconductivity and we conclude that other factors may be important and should be considered.

There a number of experiments, that are often overlooked, which show the cuprates do exhibit an isotope effect, indicating phonons do contribute to the unconventional superconducting state. An oxygen isotope effect (OIE) on the effective carrier mass and a small transition temperature OIE were found in a $YBa_2Cu_30_{6.94}$ sample by Zhao

and Morris [29]. Zhao *et al* [30] found an OIE on the penetration depth in LaSrCuO compounds. Again an OIE on the effective carrier mass was found by Khasanov *et al* [31] in the YBaCuO superconductors.

Further evidence for the electron-phonon interaction in the unconventional superconductors has also been found with photoemission experiments. Angle resolved photoemission spectroscopies (ARPES) by Lanzara *et al* [32] show that the electron dynamics are strongly influenced by the presence of phonons. Another ARPES study by Gweon et al [33] find further evidence of the OIE. Other studies by Zhou et al [34] and Meevasana *et al* [35] provide additional ARPES results backing this up.

Further support for the EPI is provided by Mihailović *et al* [36] who find that the charge carriers in the high temperature superconducting state of Tl-Ba-Ca-Cu-O, Y-Ba-Cu-O, and La-Sr-Cu-O parent compounds are polarons, electrons dressed with a phonon cloud. Direct evidence for the existence of polarons in the NdCuO material was found by Calvani *et al* [37]. Using Raman scattering evidence for a strong electron phonon coupling was found by Zamboni *et al* [38] in the YBaCuO superconductor. Results by Reznik *et al* [39] suggest that the EPI plays an important role in the high-temperature superconductors.

The theory for high-temperature superconductivity driven by an EPI was originally proposed by Alexandrov and Mott [40] as an extension of the BCS model to the strong coupling limit. In this theory bound pairs of polarons, known as bipolarons, are created. Bose-Einstein condensation of the bipolarons allows the formation of a superconducting state.

Based on the above arguments, we conclude that the electron phonon interaction as well as the usual electron hopping and on-site Hubbard repulsion should be considered for a theory of unconventional superconductivity. Therefore in this thesis, we examine the Hubbard-Fröhlich model that includes in addition to the normal terms a phonon mediated effective electron-electron attraction.

1.2.3 Ferromagnetism and Superconductivity

Previously we have discussed superconductivity in an anti-ferromagnetic parent compound but it is also possible to obtain a superconducting state in a ferromagnetic system. There have been some recent results where this phenomenon has been observed in the ferromagnetic compounds UGe_2 [41], $ZrZn_2$ [42], URhGe [43] and $RuSr_2RECu_2O_8$ [44]. The theory for this state was first proposed by Fulde and Ferrell [45] and Larkin and Ovchinnikov [46] in separate papers and leads to the formation of electron pairs with a non-zero total momentum.

1.3 Outline of Thesis

The rest of this thesis is set out as follows:

In chapter 2 we describe and derive the various physical models, mathematics and approximations used in our results. We start off with a description of correlated electrons within the Hubbard model. Then we introduce lattice vibrations (phonons) and their interaction with electrons which leads into the BCS theory. Finally we introduce the Hubbard-Fröhlich model taking into account both the correlated electrons and electron phonon interaction (EPI).

Chapter 3 introduces the Monte Carlo (MC) method and its application to fermionic systems which has been used in the calculation of our numerical results. We start from statistical physics discussing the probabilities of transitions from one state to another. The MC technique and the method for calculating the relative probabilities of two states are then introduced. We then describe the application of the MC algorithm to the quantum variational principle and fermions. Various results for the Hubbard model are then examined to validate our own Variational MC method (VMC).

Novel results for the Hubbard-Fröhlich model are presented in chapter 4. A discussion

of the transformation used to average out the phononic degrees of freedom from the Hubbard-Fröhlich model is given. We then use the VMC method and the Hubbard-Fröhlich model to investigate the effects of combining strongly correlated electrons with an electron-phonon interaction. Our results, which focus on the optimally doped case, are presented. In addition some other doping levels are considered and the results are also included.

Finally in chapter 5 we diverge slightly and study analytically the coexistence of ferromagnetism and superconductivity. Here Green Functions are used to examine both zero and finite momentum paired electrons within a ferromagnetic BCS type Hamiltonian.

Chapter 2

Models

The strongly correlated electron many-body problem is one of huge complexity and very difficult to solve; even a relatively simple iron atom already has too many interactions to find the full wave functions and energies without some simplification. This chapter introduces the models and approximations upon which our results are based. The chapter concludes with a derivation of an extended Hubbard model from the Hubbard-Fröhlich model.

2.1 Electron Correlations

While the Bloch band theory produces some very useful results it fails to explain the exciting aspects caused by the electron correlations. Ignoring electron correlations, the many body Hamiltonian is a summation of the individual single particle Hamiltonians containing the kinetic and single particle potential energy, and is easily solved. Including the electron-electron interaction introduces a third term to the Hamiltonian:

$$\hat{H}_{e-e} = -\sum_i \left[\frac{\hat{p}_i^2}{2} + U(\boldsymbol{r}_i)\right] + \frac{1}{2}\sum_{ij} V(\boldsymbol{r}_i - \boldsymbol{r}_j) \tag{2.1}$$

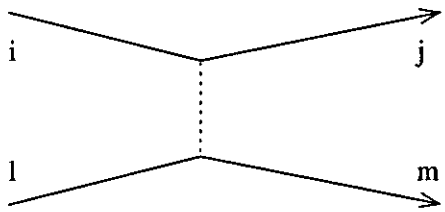

Figure 2.1: Scattering of particle from states i and l to j and m respectively.

where $\hat{p}$ is the momentum operator, $U(\boldsymbol{r}_i)$ is the periodic potential due to the lattice and $V(\boldsymbol{r}_i - \boldsymbol{r}_j)$ is the Coulomb potential between two electrons. Here we use atomic units so the electronic charge, e, the electron mass, m, Planck's constant, $\hbar$, and the term $4\pi\epsilon_0$ are all one. For the purpose of this thesis second quantisation is preferred so the interacting Hamiltonian is:

$$\hat{H}_{e-e} = \sum_{ij} t_{ij} c_i^\dagger c_j + \frac{1}{2} \sum_{ijlm} c_j^\dagger c_m^\dagger c_l c_i V_{ijlm} \tag{2.2}$$

where $c^\dagger$ and c are the usual electron creation and annihilation operators, t_{ij} and V_{ijlm} are the overlap integrals defined by:

$$t_{ij} = \int d^3\boldsymbol{r} \phi_i(\boldsymbol{r})^* \Big[-\frac{\nabla^2}{2} + U(\boldsymbol{r}) \Big] \phi_j(\boldsymbol{r}) \tag{2.3}$$

$$V_{ijlm} = \int d^3\boldsymbol{r}_1 \int d^3\boldsymbol{r}_2 \phi_j^*(\boldsymbol{r}_1) \phi_i(\boldsymbol{r}_1) V(\boldsymbol{r}_1 - \boldsymbol{r}_2) \phi_m^*(\boldsymbol{r}_2) \phi_l(\boldsymbol{r}_2).$$

The last term in the Hamiltonian describes a two electron scattering process. An electron is destroyed from state i and another created in state j representing an electron being scattered from state i to j. A similar process causes a scattering event from state l to m, as shown in Fig(2.1).

2.2 Hartree-Fock Theory

In the development of models to explain correlated electrons, the Hartree-Fock (HF) approximation is frequently used. This is built on the presumption that the single

particle problem can be used to represent the interacting problem. Each single particle is considered to be moving in the mean-field potential approximating the combined effect of the other particles and any external field present [47].

A starting point for the HF approximation is the Hartree theory which replaces the full electron-electron interaction with an interaction of a single electron with the mean electric field generated by the electron charge density:

$$\frac{1}{2}\sum_{i\neq j}\frac{1}{|\boldsymbol{r}_i-\boldsymbol{r}_j|}\rightarrow\sum_i\int d^3\boldsymbol{r}'\frac{n(\boldsymbol{r}')}{|\boldsymbol{r}_i-\boldsymbol{r}'|} \tag{2.4}$$

where $n(\boldsymbol{r}')$ is the density of all electrons. With this mean potential the Schrödinger equation is written as:

$$\Big(-\frac{\nabla^2}{2}+v_0(\boldsymbol{r})+\int d^3\boldsymbol{r}'\frac{n(\boldsymbol{r}')}{|\boldsymbol{r}_i-\boldsymbol{r}'|}\Big)\phi_i(\boldsymbol{r})=\epsilon_i\phi_i(\boldsymbol{r}). \tag{2.5}$$

Solving the Schrödinger equation gives the single particle wave-functions. The ground state is found by filling these states, starting with the lowest energy and observing the Pauli exclusion principle. From Eq(2.5) the electron density is determined:

$$n(\boldsymbol{r})=\sum_i^N|\phi_i(\boldsymbol{r})|^2 \tag{2.6}$$

which can then be inserted back into the Schrödinger equation; this is then a self-consistent problem that needs to be solved iteratively from an initial guess at the charge density. However, the Hartree theory is a poor approximation as it includes an unphysical electron interaction with itself. To improve on this a simple many-body wave-function is used: $\Phi(\boldsymbol{r}_1,...\boldsymbol{r}_N)=\phi(\boldsymbol{r}_1)\phi(\boldsymbol{r}_2)...\phi(\boldsymbol{r}_N)$. The energy of the state is then obtained using the variational method:

$$E=\frac{\langle\Phi|\hat{H}|\Phi\rangle}{\langle\Phi|\Phi\rangle} \tag{2.7}$$

This is then minimized using the constraint that the single particle wave-functions are orthonormal resulting in the Euler Lagrange equation:

$$\frac{\partial}{\partial\phi_j^*(\boldsymbol{r})}\Big[\langle\Phi|\hat{H}|\Phi\rangle+\sum\epsilon_i\int d^3\boldsymbol{r}|\phi(\boldsymbol{r}_i)|^2\Big]=0 \tag{2.8}$$

From this the single particle Schrödinger equation, Eq(2.4), is written as:

$$\Big[-\frac{\nabla^2}{2}+v_0(\boldsymbol{r})+\sum_{j\neq i}\int d^3\boldsymbol{r}'\frac{|\phi_j(\boldsymbol{r})|^2}{|\boldsymbol{r}-\boldsymbol{r}'|}\Big]\phi_i(\boldsymbol{r})=\epsilon_i\phi_i(\boldsymbol{r}) \tag{2.9}$$

This leads to the following ground state energy:

$$E_{HF}=\sum_i^N\langle i|[\hat{T}+\hat{V}_0]|i\rangle+\frac{1}{2}\sum_{i,j}^N\langle ij|\hat{U}|ij\rangle=\sum_i^N\epsilon_i+\frac{1}{2}\sum_{i,j}^N\langle ij|\hat{U}|ij\rangle \tag{2.10}$$

where the Coulomb term is defined by:

$$\langle ij|\hat{U}|ij\rangle=\int d^3\boldsymbol{r}\int d^3\boldsymbol{r}'\frac{\phi_i^*(\boldsymbol{r})\phi_j^*(\boldsymbol{r}')\phi_j(\boldsymbol{r})\phi_i(\boldsymbol{r}')}{|\boldsymbol{r}-\boldsymbol{r}'|} \tag{2.11}$$

This approximation still ignores the Pauli exclusion principle; to ensure two fermions cannot occupy the same state the Hartree-Fock approximation is needed. The HF approximation uses an antisymmetric wave-function, which can be written as a Slater determinant, so that the Pauli principle is accounted for. With the anti-symmetrised wave function the Euler-Lagrange equation becomes:

$$\Big[-\frac{\nabla^2}{2}+v_0(\boldsymbol{r})+\int d^3\boldsymbol{r}\frac{\sum_j|\phi_j(\boldsymbol{r})|^2}{|\boldsymbol{r}-\boldsymbol{r}'|}\Big]\phi_i(\boldsymbol{r})+\int d^3\boldsymbol{r}\frac{\sum_i\phi_i^*(\boldsymbol{r})\phi_i(\boldsymbol{r}')}{|\boldsymbol{r}-\boldsymbol{r}'|}\phi_i(\boldsymbol{r}')=\epsilon_i\phi_i(\boldsymbol{r}). \tag{2.12}$$

From which the ground state energy is determined:

$$E_{HF}=\sum_i\epsilon_i+\frac{1}{2}\sum_{i,j}^N[\langle ij|\hat{U}|ij\rangle-\langle ij|\hat{U}|ji\rangle] \tag{2.13}$$

where the exchange term is given by:

$$\langle ij|\hat{U}|ji\rangle=\int d^3\boldsymbol{r}\int d^3\boldsymbol{r}'\frac{\phi_i^*(\boldsymbol{r})\phi_j^*(\boldsymbol{r}')\phi_i(\boldsymbol{r}')\phi_j(\boldsymbol{r})}{|\boldsymbol{r}-\boldsymbol{r}'|}. \tag{2.14}$$

2.3 The Hubbard Model

The simplest model available for studying electron correlations is given by the Hubbard Hamiltonian. This model was first introduced by Gutzwiller [5], Hubbard [6] and

Kanamori [7], though it is generally attributed to J. Hubbard, to provide a theory of the correlated d-electrons in the transition metals where the free electron gas model had unsurprisingly failed.

The d-electrons are tightly bound to specific ions so it is feasible to think of an electron as sitting on a site. Experimentally it is found that these electrons demonstrate both band and atomic model properties. For simplicity in deriving this model Hubbard considered s-band electrons as an appropriate approximation for narrow energy bands. It is assumed that the wave functions and energies, ϵ_k, of the s-band have been calculated using a HF potential. He then used the following Hamiltonian to describe the s-band electrons:

$$\begin{aligned}\hat{H} &= \sum_k \epsilon_k (c^\dagger_{k\uparrow} c_{k\uparrow} + c^\dagger_{k\downarrow} c_{k\downarrow}) \\ &+ \frac{1}{2} \sum_{k_1 k_2 k'_1 k'_2} \sum_{\sigma_1 \sigma_2} \langle k_1 k_2 | \frac{1}{r} | k'_1 k'_2 \rangle c^\dagger_{k_1\sigma_1} c^\dagger_{k_2\sigma_2} c_{k'_2\sigma_2} c_{k'_1\sigma_1} \\ &- \sum_{kk'} \sum_\sigma [2\langle kk' | \frac{1}{r} | kk' \rangle - \langle kk' | \frac{1}{r} | k'k \rangle] v_k c^\dagger_{k\sigma} c_{k\sigma}\end{aligned} \tag{2.15}$$

where:

$$\langle k_1 k_2 | \frac{1}{r} | k'_1 k'_2 \rangle = \int \frac{\psi^*_{k_1}(x) \psi_{k'_1}(x) \psi^*_{k_2}(x') \psi_{k'_2}(x')}{|x - x'|} dx dx' \tag{2.16}$$

is the overlap integral between Bloch states and v_k are the occupation numbers of the states in the band. The first two terms describe the electron motion in the HF mean potential and the electron-electron interaction, as per Eq(2.2). The last term of the Hamiltonian is to ensure the interactions of the band aren't counted twice. The Hamiltonian can be written using Wannier functions, which are defined as:

$$\phi(x) = \frac{1}{\sqrt{N}} \sum_k \psi_k(x) \tag{2.17}$$

So that the wave functions become:

$$\psi_k(x) = \frac{1}{\sqrt{N}} \sum_i e^{ik.R_i} \phi(x - R_i) \tag{2.18}$$

summing over all sites in the lattice. The Fourier transform of the creation and annihilation operators are:

$$c^{\dagger}_{k\sigma} = \frac{1}{\sqrt{N}} \sum_i e^{-ik.R_i} c^{\dagger}_{i\sigma} \qquad c_{k\sigma} = \frac{1}{\sqrt{N}} \sum_i e^{ik.R_i} c_{i\sigma}. \tag{2.19}$$

Substitution of these equations into the Hamiltonian yields:

$$\begin{aligned} \hat{H} &= -\sum_{ij} t_{ij}(c^{\dagger}_{i\uparrow}c_{j\uparrow} + c^{\dagger}_{i\downarrow}c_{j\downarrow}) \\ &+\frac{1}{2}\sum_{ijkl}\sum_{\sigma_1\sigma_2}\langle ij|\frac{1}{r}|kl\rangle c^{\dagger}_{i\sigma_1}c^{\dagger}_{j\sigma_2}c_{l\sigma_2}c_{k\sigma_1} \\ &-\sum_{ijkl}[2\langle ij|\frac{1}{r}|kl\rangle - \langle ij|\frac{1}{r}|kl\rangle]v_{jl}(c^{\dagger}_{i\uparrow}c_{k\uparrow} + c^{\dagger}_{i\downarrow}c_{k\downarrow}) \end{aligned} \tag{2.20}$$

where

$$t_{ij} = \frac{1}{N}\sum_k \epsilon_k e^{ik.(R_i - R_j)} \tag{2.21}$$

$$\langle ij|\frac{1}{r}|kl\rangle = \int \frac{\psi^*(\boldsymbol{x}-\boldsymbol{R}_k)\psi(\boldsymbol{x}-\boldsymbol{R}_i)\psi^*(\boldsymbol{x}'-\boldsymbol{R}_j)\psi(\boldsymbol{x}'-\boldsymbol{R}_l)}{|\boldsymbol{x}-\boldsymbol{x}'|} d\boldsymbol{x}d\boldsymbol{x}' \tag{2.22}$$

and

$$v_{jl} = \frac{1}{N}\sum_k v_k e^{ik.(R_i - R_j)} \tag{2.23}$$

For the bandwidth to be small the interatomic spacing must be large relative to the size of the atomic orbitals.. So all terms other than $\langle ii|1/r|ii\rangle$, which is defined as the on-site Hubbard repulsion U, are relatively small and the Hamiltonian can be approximated to:

$$\hat{H}_{HM} = -\sum_{ij} t_{ij}(c^{\dagger}_{i\uparrow}c_{j\uparrow} + c^{\dagger}_{i\downarrow}c_{j\downarrow}) + U\sum_i \hat{n}_{i\uparrow}\hat{n}_{i\downarrow} - \mu\sum_i(\hat{n}_{i\uparrow} + \hat{n}_{i\downarrow}) \tag{2.24}$$

This is known as the Hubbard Hamiltonian, $\hat{H}_{HM}$. The simplest solution to this is found by setting U to zero. The chemical potential term, μ, is constant when the number of particles is fixed and can be ignored. Then only the kinetic term of the Hamiltonian remains. This can be referred to as the tight binding model:

$$\hat{H}_{tb} = -\sum_{ij} t_{ij}(c^{\dagger}_{i\uparrow}c_{j\uparrow} + c^{\dagger}_{i\downarrow}c_{j\downarrow}) \tag{2.25}$$

In real space this is not diagonal. To diagonalise the Hamiltonian a transformation to momentum space needs to be performed. Writing the creation and annihilation operators in terms of momentum space operators:

$$c_{i\sigma}^{\dagger} = \frac{1}{\sqrt{N}} \sum_{\boldsymbol{k}} e^{i\boldsymbol{k}.\boldsymbol{R}_i} c_{\boldsymbol{k}\sigma}^{\dagger} \qquad c_{i\sigma} = \frac{1}{\sqrt{N}} \sum_{\boldsymbol{k}} e^{-i\boldsymbol{k}.\boldsymbol{R}_i} c_{\boldsymbol{k}\sigma} \tag{2.26}$$

Substituting these equations into the Hamiltonian:

$$\hat{H}_{tb} = -\sum_{ij\sigma} \sum_{\boldsymbol{kp}} \frac{t_{ij}}{N} e^{i(\boldsymbol{k}.\boldsymbol{R}_i - \boldsymbol{p}.\boldsymbol{R}_j)} c_{\boldsymbol{k}\sigma}^{\dagger} c_{\boldsymbol{p}\sigma} \tag{2.27}$$

If only nearest neighbour hops are allowed then $\boldsymbol{R}_j = \boldsymbol{R}_i + \boldsymbol{\tau}$ where $\boldsymbol{\tau}$ are the primitive lattice vectors

$$\begin{aligned} \hat{H}_{tb} &= -\sum_{i\tau\sigma} \sum_{\boldsymbol{kp}} \frac{t}{N} e^{i(\boldsymbol{R}_i(\boldsymbol{k}-\boldsymbol{p})-\boldsymbol{p}.\boldsymbol{\tau})} c_{\boldsymbol{k}\sigma}^{\dagger} c_{\boldsymbol{p}\sigma} = -\sum_{\tau\sigma} \sum_{\boldsymbol{kp}} t\delta_{\boldsymbol{kp}} e^{-i\boldsymbol{p}.\boldsymbol{\tau}} c_{\boldsymbol{k}\sigma}^{\dagger} c_{\boldsymbol{p}\sigma} \\ \hat{H}_{tb} &= -\sum_{\tau\sigma\boldsymbol{k}} t e^{-i\boldsymbol{k}.\boldsymbol{\tau}} c_{\boldsymbol{k}\sigma}^{\dagger} c_{\boldsymbol{k}\sigma} \end{aligned} \tag{2.28}$$

When creating a many-body wave-function the states are filled in momentum space lowest energy first. It is for this reason the energy spectrum needs to be known. For a simple cubic lattice the following energy spectrum is found, Fig(2.2):

$$\epsilon_{\boldsymbol{k}} = -2t[\cos(k_x a) + \cos(k_y a) + \cos(k_z a)]. \tag{2.29}$$

2.3.1 The Gutzwiller projection operator

Using the Hubbard Hamiltonian, Gutzwiller [5] proposed a solution that didn't ignore the potential energy term. As it is only the on-site Coulomb repulsion that contributes to the potential energy in the Hamiltonian he suggested a wave-function in which the doubly occupied sites are eliminated or suppressed. Reducing the number of doubly occupied sites reduces the energy cost associated with the on-site Coulomb repulsion

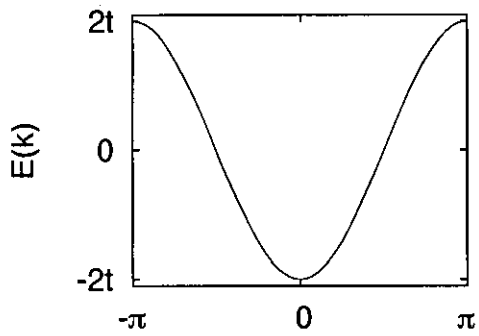

Figure 2.2: 1D tight binding energy spectrum E as a function of k.

at the expense of the hopping term. The basic wave-function is an anti-symmetrised product of Bloch functions of the occupied states written in second quantized form as:

$$|\psi\rangle = \prod_{k} c^{\dagger}_{k\uparrow} c^{\dagger}_{k\downarrow} |0\rangle \tag{2.30}$$

where the product is over the lowest momentum states in the first Brillouin zone. The optimized wave-function is then found by applying Gutzwiller's projection operator to the base wave-function:

$$|\psi_g\rangle = \prod_{i} [1 - (1-g)\hat{n}_{i\uparrow}\hat{n}_{i\downarrow}]|\psi\rangle \tag{2.31}$$

where $0 \leq g \leq 1$. This is a Jastrow type variational wave function [48] in which only the onsite correlation is considered. When $g = 1$ the original tight binding wave-function is recovered and corresponds to the $U = 0$ case. For infinite U, $g = 0$ so that there are no doubly occupied sites. For intermediate values of U/t there is a trade off between the suppression of the potential energy and reduction in kinetic energy.

2.3.2 Anti-Ferromagnetism

As stated earlier, in the case of a half filled lattice, one electron per site, the ground state, under certain circumstances, is the Néel state. Away from half filling the anti

ferromagnetism can persist in the form of a spin density wave, which destroys the spin and translational symmetry of the original lattice. A new lattice is formed with a unit cell twice the size of the previous lattice, therefore halving the Brillouin zone and forming two energy bands. A gap between the upper and lower bands allows a lowering of the energy.

To describe the SDW state the Hubbard Hamiltonian is split into two terms, the first, a self consistent field (SCF) or Hartree-Fock and the second a residual term that can be neglected, see for example P. Fulde's book [49]:

$$\hat{H} = \hat{H}_{SCF} + \hat{H}_{RES} \tag{2.32}$$

by introducing:

$$\delta n_{i\sigma} = n_{i\sigma} - \langle n_{i\sigma} \rangle. \tag{2.33}$$

The two terms of the Hamiltonian are then:

$$\hat{H}_{SCF} = -t \sum_{<ij>\sigma} (c^{\dagger}_{i\sigma} c_{j\sigma} + c^{\dagger}_{j\sigma} c_{i\sigma}) + U \sum_{i\sigma} \langle n_{i-\sigma} \rangle n_{i\sigma} + E_0 \tag{2.34}$$

and

$$\hat{H}_{RES} = U \sum_{i} \delta n_{i\uparrow} \delta n_{i\downarrow} \tag{2.35}$$

where:

$$E_0 = U \sum_{i} \langle n_{i\uparrow} \rangle \langle n_{i\downarrow} \rangle \tag{2.36}$$

The SDW state leads to the formation of a bipartite lattice built with two sub-lattices A and B each with a net magnetisation Fig(2.3).

$$\langle n_{i\sigma} \rangle = \frac{1}{2}(1 + \sigma m_0 e^{-i\boldsymbol{Q}\boldsymbol{R}_i}) \tag{2.37}$$

where $\boldsymbol{Q} = (\pi, \pi, \pi)$ in 3D, $\boldsymbol{Q} = (\pi, \pi)$ in 2D and $\boldsymbol{Q} = \pi$ in 1D is the antiferromagnetic reciprocal lattice vector and $\sigma = \pm 1$ depending on the spin. The overall magnetisation of the lattice remains zero, however the sub lattices have a magnetisation m_0 given by:

$$m_{0A} = \langle n_{iA\uparrow} - n_{iA\downarrow} \rangle \qquad m_{0B} = \langle n_{iB\downarrow} - n_{iB\uparrow} \rangle \tag{2.38}$$

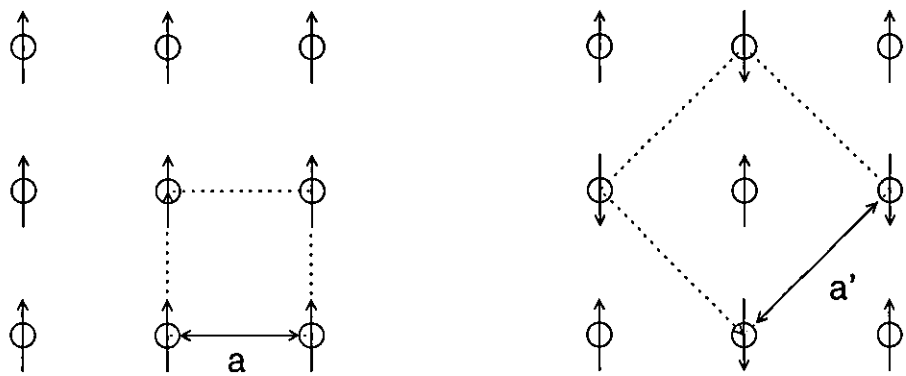

Figure 2.3: The anti-ferromagnetic lattice has a unit cell that is twice as big as the paramagnetic lattice. In the 2D example here, the new lattice constant is defined by $a' = \sqrt{2}a$.

Substitution of these equations into the SCF Hamiltonian yields:

$$\hat{H}_{SCF} = -t \sum_{<ij>\sigma} (c^{\dagger}_{i\sigma} c_{j\sigma} + c^{\dagger}_{j\sigma} c_{i\sigma}) + \frac{U}{2} \sum_{i\sigma} (1 + \sigma m_0 e^{-i\boldsymbol{Q}\boldsymbol{R}_i}) n_{i\sigma} + E_0 \tag{2.39}$$

Writing the real space creation and annihilation operators in terms of their momentum space counterparts the following form of the Hamiltonian is obtained.

$$H_{SCF} = -\sum_{\mathbf{k}\sigma} \left[(\epsilon(\boldsymbol{k}) + \frac{U}{2}) c^{\dagger}_{\boldsymbol{k},\sigma} c_{\boldsymbol{k},\sigma} + (\epsilon(\boldsymbol{k}+\boldsymbol{Q},\sigma) + \frac{U}{2}) c^{\dagger}_{\boldsymbol{k}+\boldsymbol{Q},\sigma} c_{\boldsymbol{k}+\boldsymbol{Q},\sigma} + \frac{U}{2} \sigma m_0 (c^{\dagger}_{\boldsymbol{k},\sigma} c_{\boldsymbol{k}+\boldsymbol{Q},\sigma} + c^{\dagger}_{\boldsymbol{k}+\boldsymbol{Q},\sigma} c_{\boldsymbol{k},\sigma}) \right] + E_0 \tag{2.40}$$

This Hamiltonian is diagonalised using the Bogoliubov transformation [50]. This involves writing new quasiparticle operators in terms of the electron operators, neglecting the spin subscript for convenience:

$$\begin{aligned} \alpha_{\boldsymbol{k}} &= u_{\boldsymbol{k}} c_{\boldsymbol{k}} + \sigma v_{\boldsymbol{k}} c_{\boldsymbol{k}+\boldsymbol{Q}} & \alpha^{\dagger}_{\boldsymbol{k}} &= u_{\boldsymbol{k}} c^{\dagger}_{\boldsymbol{k}} + \sigma v_{\boldsymbol{k}} c^{\dagger}_{\boldsymbol{k}+\boldsymbol{Q}} \\ \beta_{\boldsymbol{k}} &= u_{\boldsymbol{k}} c_{\boldsymbol{k}+\boldsymbol{Q}} - \sigma v_{\boldsymbol{k}} \boldsymbol{k} c_{\boldsymbol{k}} & \beta^{\dagger}_{\boldsymbol{k}} &= u_{\boldsymbol{k}} c^{\dagger}_{\boldsymbol{k}+\boldsymbol{Q}} - \sigma v_{\boldsymbol{k}} c^{\dagger}_{\boldsymbol{k}} \end{aligned} \tag{2.41}$$

Like the electrons they replace, these new quasiparticles are also fermions and therefore

must obey the anti-commutation rules:

$$\begin{aligned} 1 = \{\alpha_k^\dagger, \alpha_k\} = (u_k c_k + \sigma v_k c_{k+Q})(u_k c_k^\dagger + \sigma v_k c_{k+Q}^\dagger) + \\ (u_k c_k^\dagger + \sigma v_k c_{k+Q}^\dagger)(u_k c_k + \sigma v_k c_{k+Q}) \\ 1 = u_k^2 + v_k^2 \end{aligned} \tag{2.42}$$

giving a useful identity for determining the values of u_k and v_k that diagonalise the Hamiltonian. The other fermion anti-commutation relations follow by definition:

$$0 = \{\alpha_k^\dagger, \alpha_p\}_{k \neq p} = \{\alpha_k, \alpha_k\} = \{\alpha_k^\dagger, \alpha_k^\dagger\} = \{\alpha_k^\dagger, \beta_k\} = \{\alpha_k, \beta_k\} \tag{2.43}$$

The electron creation and annihilation operators are written in terms of the quasi-particles. Then on substitution, in terms of the new quasiparticles the Hamiltonian is:

$$\begin{aligned} \hat{H}_{SCF} = \sum_k \Big[(\epsilon(k) + \frac{U}{2})(u_k^2 \alpha_k^\dagger \alpha_k - \sigma u_k v_k \alpha_k^\dagger \beta_k + v_k^2 \beta_k^\dagger \beta_k - \sigma u_k v_k \beta_k^\dagger \alpha_k) + \\ + (\epsilon(k+Q) + \frac{U}{2})(u_k^2 \beta_k^\dagger \beta_k + \sigma u_k v_k \beta_k^\dagger \alpha_k + v_k^2 \alpha_k^\dagger \alpha + \sigma u_k v_k \alpha_k^\dagger \beta_k) + \\ \frac{U}{2} \sigma m_0 [u_k^2 \alpha_k^\dagger \beta_k + \sigma u_k v_k \alpha_k^\dagger \alpha_k - \sigma u_k v_k \beta_k^\dagger \beta_k - v_k^2 \beta_k^\dagger \alpha^\dagger]_k + \\ + u_k^2 \beta_k^\dagger \alpha_k - \sigma u_k v_k \beta_k^\dagger \beta_k + \sigma u_k v_k \alpha_k^\dagger \alpha_k - v_k^2 \alpha_k^\dagger \beta_k] \Big] + E_0 \end{aligned}$$

For a SDW state with $\epsilon(k) = -2t[\cos(k_x a) + \cos(k_y a) + \cos(k_z a)]$, $\epsilon(k+Q) = -\epsilon(k)$. Summations are now over the reduced Brillouin zone defined by the new lattice vectors. Still the Hamiltonian is not diagonal; to diagonalise it the off diagonal terms must equal zero:

$$2\epsilon(k) u_k v_k + \frac{U}{2} \sigma m_0 (u_k^2 - v_k^2) = 0 \tag{2.44}$$

Solving this equation it is found that:

$$u_k^2 = \frac{1}{2}\Big(1 + \frac{\epsilon(k)}{\sqrt{\epsilon(k)^2 + \Delta^2}}\Big) \qquad v_k^2 = \frac{1}{2}\Big(1 - \frac{\epsilon(k)}{\sqrt{\epsilon(k)^2 + \Delta^2}}\Big) \tag{2.45}$$

where $\Delta = \frac{U}{2} m_0$. Using $E_k = \sqrt{\epsilon(k)^2 + \Delta^2}$ and $u_k v_k = \Delta / 2E$ to simplify the equations. The diagonal form of the Hamiltonian is then:

$$\hat{H}_{SCF} = \sum_k \Big[\Big(\frac{U}{2} - E\Big) \alpha_k^\dagger \alpha_k + \Big(\frac{U}{2} + E\Big) \beta_k^\dagger \beta_k \Big] + E_0 \tag{2.46}$$

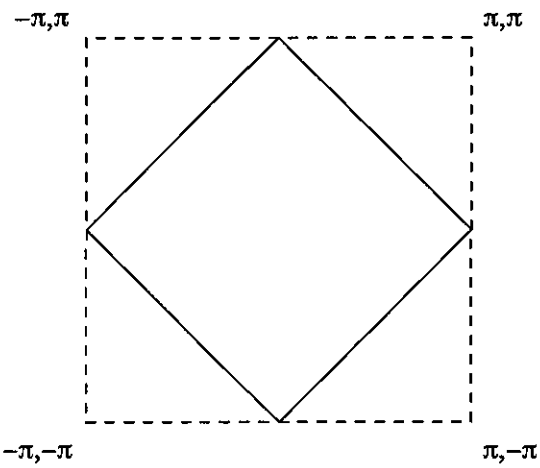

Figure 2.4: AFM Brillouin zone (Solid) and Paramagnetic Brillouin zone (Dashed)

The ground state of the SDW for the half filled band Hamiltonian is:

$$|\Phi_{AF}\rangle = \prod_{k\sigma} \alpha^{\dagger}_{k\sigma}|0\rangle \tag{2.47}$$

where the product is over all the momentum points in the reduced zone. Again to ensure the filling of the momentum states is done in the correct order the energy $E = \langle\psi|H|\psi\rangle$ (where $H = -t\sum_{\tau i} c^{\dagger}_i c_{i+\tau}$) is needed:

$$\langle\psi|H|\psi\rangle = -\frac{t}{N}\sum_{\tau r_i}[u_k e^{-ikr_i} + \sigma v_k e^{-i(k+\pi)r_i}][u_k e^{ik(r_i+\tau)} + \sigma v_k e^{i(k+\pi)(r_i+\tau)}]. \tag{2.48}$$

In 1D this leads to the following energy spectrum:

$$E_k = -\frac{t}{N}[u_k^2\cos(ka) + v_k^2\cos((k+\pi)a)]. \tag{2.49}$$

Examining these two energy bands reveals the expected gap to lower the energy Fig(2.5).

2.4 Electron Phonon Interactions

Up until this point, because the mass of the ion is much greater than that of the electrons the motion of the ions has been neglected. If this condition is relaxed and

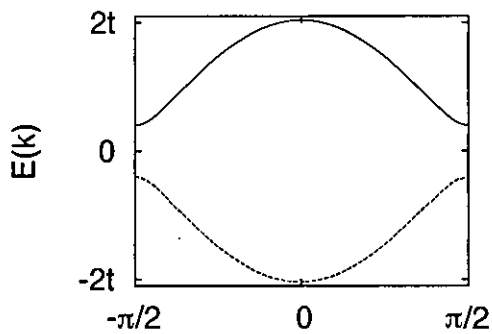

Figure 2.5: Anti-ferromagnetic energy spectrum.

the ionic motion is examined it is possible to explain the fascinating phenomenon of superconductivity.

In fact the ions in general do not deviate far from their equilibrium positions given by the Bravais lattice. The ions oscillate around their equilibrium positions in quantized units known as phonons according to the Hamiltonian for the harmonic oscillator which can be written as:

$$\hat{H}_{ph} = \frac{\hat{p}^2}{2m} + \frac{k}{2}\hat{x}^2 \tag{2.50}$$

where $\omega = \sqrt{k/m}$. Solving this gives the well known result $E = \omega(n + 1/2)$. A more elegant solution to this problem is found by introducing two new operators known as lowering and raising operators:

$$a = \sqrt{\frac{m\omega}{2}}\left(\hat{x} + \frac{i\hat{p}}{m\omega}\right) \qquad a^\dagger = \sqrt{\frac{m\omega}{2}}\left(\hat{x} - \frac{i\hat{p}}{m\omega}\right) \tag{2.51}$$

These operators are Hermitian conjugates of each other. With these operators the harmonic oscillator Hamiltonian is written in second quantisation as:

$$\hat{H}_{ph} = \omega_{\boldsymbol{k}}(a^\dagger_{\boldsymbol{k}} a_{\boldsymbol{k}} + \frac{1}{2}) \tag{2.52}$$

where $a^\dagger_{\boldsymbol{k}}$ and $a_{\boldsymbol{k}}$ are the creation and annihilation operators for phonons and obey the bosonic commutation relations. These phonons distort the lattice breaking its perfect periodicity which in turn affects the electron motion.

To describe this situation when phonons are accounted for, a new Hamiltonian that includes the electron phonon interaction is required. Such a Hamiltonian was developed by Fröhich in the 1950s, see for example [51], and consists of three terms:

$$\hat{H} = \hat{H}_{ph} + \hat{H}_{e-e} + \hat{H}_{e-ph} \tag{2.53}$$

where $\hat{H}_{ph}$ is the phonon Hamiltonian from Eq(2.52), $\hat{H}_{e-e}$ is the interacting electron Hamiltonian discussed above and $\hat{H}_{e-ph}$ is the Hamiltonian describing the electron phonon interaction. Here we describe briefly the derivation of the Hamiltonian, the details are discussed in Mahan [52] and Gross [47]. The electron-phonon potential takes the form:

$$\hat{H}_{e-ph} = \sum_i V(\boldsymbol{r}_i), \tag{2.54}$$

where the potential is the sum of the interaction from every site in the lattice:

$$V(\boldsymbol{r}_i) = \sum_j \tilde{V}_{e-ph}(\boldsymbol{r}_i - \boldsymbol{R}_j). \tag{2.55}$$

The ion position $\boldsymbol{R}_j$ can be written in terms of the lattice vectors $\boldsymbol{R}_{j0}$ and a small displacement $\boldsymbol{Q}_j$ so that $\boldsymbol{R}_j = \boldsymbol{R}_{j0} + \boldsymbol{Q}_j$. A Taylor expansion in powers of $\boldsymbol{Q}_j$ of the electron-phonon interaction gives:

$$\tilde{V}(\boldsymbol{r}_i - \boldsymbol{R}_{j0} + \boldsymbol{Q}_j)_{e-ph} = \tilde{V}_{e-ph}(\boldsymbol{r}_i - \boldsymbol{R}_{j0}) + \boldsymbol{Q}_j.\nabla\tilde{V}_{e-ph}(\boldsymbol{r}_i - \boldsymbol{R}_{j0}) + O(\boldsymbol{Q}_j^2)... \tag{2.56}$$

If the displacement is small, as it must be in solids, then terms $O(\boldsymbol{Q}_j^2)$ and higher can be neglected. The zero-order term is the periodic potential mentioned earlier that gave rise to the Bloch states and energy bands and is not considered as part of the electron phonon Hamiltonian. This means the Hamiltonian is of the form $\hat{H}_{e-ph} = \hat{H}_0 + V$ where V is a perturbation to the periodic potential. The Fourier transform of the interaction is:

$$\tilde{V}_{e-ph}(\boldsymbol{r}) = \frac{1}{N}\sum_{\boldsymbol{q}} \tilde{V}_{e-ph}(\boldsymbol{q})e^{i\boldsymbol{q}.\boldsymbol{r}} \tag{2.57}$$

and the Fourier transform of the derivative is:

$$\nabla\tilde{V}_{e-ph}(\boldsymbol{r}) = \frac{i}{N}\sum_{\boldsymbol{q}} \boldsymbol{q}\tilde{V}_{e-ph}(\boldsymbol{q})e^{i\boldsymbol{q}.\boldsymbol{r}} \tag{2.58}$$

The interaction then takes the form:

$$V(\boldsymbol{r}) = i\frac{i}{N}\sum_{\boldsymbol{q}} e^{i\boldsymbol{q}.\boldsymbol{r}}\tilde{V}_{e-ph}(\boldsymbol{q})\boldsymbol{q}.\sum_{j}\boldsymbol{Q}_j e^{-i\boldsymbol{q}.\boldsymbol{R}_{j0}} \tag{2.59}$$

Rewriting the deviation, $\mathbf{Q_j}$, using the form of the lowering and raising operators defined in Eq(2.51) ignoring constants:

$$\begin{aligned}\sum_{j}\boldsymbol{Q}_j e^{-i\boldsymbol{q}.\boldsymbol{R}_{j0}} &= -\sum_{\boldsymbol{q}'j} e^{i(-\boldsymbol{q}+\boldsymbol{q}').\mathbf{R}_{j0}}\xi_{\boldsymbol{q}}(\mathbf{a}_{\boldsymbol{q}'}+\mathbf{a}^{\dagger}_{-\boldsymbol{q}'}) \\ &= \xi_{\boldsymbol{q}}(a_{\boldsymbol{q}}+a^{\dagger}_{-\boldsymbol{q}})\end{aligned} \tag{2.60}$$

where $\xi_{\boldsymbol{q}}$ is the polarization direction of the phonon. So the interaction is written now as:

$$V(\boldsymbol{r}) = \sum_{\boldsymbol{q}} e^{i\boldsymbol{r}.\boldsymbol{q}}V(\boldsymbol{q})\mathbf{q}.\xi_{\boldsymbol{q}}(\mathbf{a}_{\boldsymbol{q}}+\mathbf{a}^{\dagger}_{-\boldsymbol{q}}) \tag{2.61}$$

The term $\mathbf{q}.\xi = \mathbf{0}$ for transverse phonons so the interaction disappears. The interaction is then written using second quantisation forms of the electron and phonon operators:

$$\hat{H}_{e-ph} = \sum_{\boldsymbol{q},\mathbf{k}} V(\boldsymbol{q})\mathbf{q}.\xi\mathbf{c}^{\dagger}_{k+q}\mathbf{c}_k(\mathbf{a}_{\boldsymbol{q}}+\mathbf{a}^{\dagger}_{-\boldsymbol{q}}). \tag{2.62}$$

This Hamiltonian describes the absorption or emission of a phonon with momentum $\mathbf{q}$ by an electron in state $\mathbf{k}$ causing it to scatter to a new state $\mathbf{k}+\mathbf{q}$.

2.4.1 Attractive Electron-Electron Interactions

Arguably the most fascinating result of the electron-phonon interaction is superconductivity. The BCS theory of Superconductivity is based on work by Fröhlich in 1950 [53] that showed that the electron-phonon interaction can lead to an attractive force between the electrons and therefore be the cause of superconductivity. Cooper [54] then demonstrated that the normal state in a metal was unstable in the presence of an attractive interaction, no matter how small.

Cooper then considered two electrons, with opposite spin and the centre of mass at rest. Here the role of the electron Fermi gas is only to prohibit further occupation of

the states inside the Fermi sphere. The orbital part of the wave-function of the pair is written as an expansion of plane waves [55]:

$$\psi(\boldsymbol{r}-\boldsymbol{r}') = \sum_{\boldsymbol{k}} g(\boldsymbol{k}) e^{i\boldsymbol{k}(\boldsymbol{r}-\boldsymbol{r}')} \tag{2.63}$$

where $g(\boldsymbol{k})$ is the probability amplitude of finding one electron in state $\boldsymbol{k}$ and the other in $-\boldsymbol{k}$. The filled Fermi sea ensures $g(\boldsymbol{k}) = 0$ for states $\boldsymbol{k} < \boldsymbol{k}_F$. For these two electrons the Schrödinger equation is written:

$$-\frac{1}{2}(\nabla_1^2 + \nabla_2^2)\psi(\boldsymbol{r}-\boldsymbol{r}') + V(\boldsymbol{r}-\boldsymbol{r}')\psi(\boldsymbol{r}-\boldsymbol{r}') = \Big[E + \boldsymbol{k}_F^2\Big]\psi(\boldsymbol{r}-\boldsymbol{r}') \tag{2.64}$$

E is the energy of the electron with respect to the Fermi energy. Substituting the plane wave form of the wave-function into the Schrödinger equation:

$$\boldsymbol{k}^2 g(\boldsymbol{k}) + \sum_{\boldsymbol{k}'} g(\boldsymbol{k}') V_{\boldsymbol{k}\boldsymbol{k}'} = (E + 2E_F) g(\boldsymbol{k}) \tag{2.65}$$

where:

$$V_{\boldsymbol{k}\boldsymbol{k}'} = \frac{1}{L^3}\int V(\boldsymbol{r}) e^{-i(\boldsymbol{k}-\boldsymbol{k}')\cdot\boldsymbol{r}} d\boldsymbol{r} \tag{2.66}$$

is the matrix element for the interaction of the electrons in states $\boldsymbol{k}$ and $\boldsymbol{k}'$. If there is an attractive interaction then the approximation:

$$V_{\boldsymbol{k}\boldsymbol{k}'} = -\frac{V}{L^3} \qquad \text{if} \qquad \frac{\boldsymbol{k}^2}{2} < E_F + \hbar\omega_D \tag{2.67}$$

and $V_{\boldsymbol{k}\boldsymbol{k}'} = 0$ otherwise is used. The attraction is assumed constant and attractive within the the Debye energy of the Fermi energy. Using this the Schrödinger equation can be simplified to

$$\Big(-\boldsymbol{k}^2 + E + 2E_F\Big) g(\boldsymbol{k}) = -\frac{V}{L^3}\sum_{\boldsymbol{k}'} g(\boldsymbol{k}') \tag{2.68}$$

which must be a constant C. From this we can define $g(\boldsymbol{k}) = C/(-\boldsymbol{k}^2 + E + 2E_F)$, which then leads to the self consistent equation:

$$1 = \frac{V}{L^3}\sum_{\boldsymbol{k}'} \frac{1}{-E + \boldsymbol{k}'^2 - 2E_F} \tag{2.69}$$

using the substitution:

$$\xi' = \boldsymbol{k}^2 - E_F \tag{2.70}$$

and the density of states

$$N(\xi') = \frac{1}{(2\pi)^3} 4\pi \boldsymbol{k}'^2 \frac{d\boldsymbol{k}'}{d\xi'} \tag{2.71}$$

the sum can can be written as an integral:

$$1 = \frac{1}{2}\int_0^{\omega_D} N(\xi')\frac{1}{2\xi' - E} d\xi' = \frac{1}{2} N(0) V \ln \frac{E - 2\omega_D}{E}. \tag{2.72}$$

From this it can be seen that there is a bound state for any attraction given by:

$$E = -2\omega_D e^{\left(-\frac{2}{N(0)V}\right)} \tag{2.73}$$

So far, in this section, the cause of the attraction has not been examined. As stated earlier the electron attraction is attributed by Fröhlich to the exchange of phonons between electrons. However there are two competing interactions, a Coulomb repulsion and a phonon induced attraction. For the net interaction to be attractive the phonon term must dominate. The matrix element of the Coulomb repulsion between the initial state a and final state b is written [55]:

$$\langle a|\hat{H}_c|b\rangle = \int d\boldsymbol{r}_1 d\boldsymbol{r}_2 e^{-i\boldsymbol{k}.(\boldsymbol{r}_1 - \boldsymbol{r}_2)} U_c(\boldsymbol{r}_1 - \boldsymbol{r}_2) e^{-i\boldsymbol{k}.(\boldsymbol{r}_1 - \boldsymbol{r}_2)} = U_{\boldsymbol{q}} \tag{2.74}$$

The phonon term is described by the process where one electron emits a phonon with momentum $-\boldsymbol{q}$ scattering to the state $\boldsymbol{k}+\boldsymbol{q}$ and the phonon is then absorbed by another electron scattering to the state $\boldsymbol{k}' - \boldsymbol{q}$. The matrix element between the initial and final states governed by the indirect phonon scattering from the intermediate states i is:

$$\langle a|\hat{H}_{ind}|b\rangle = \sum_i \langle a|\hat{H}_{e-ph}|i\rangle \frac{1}{2}\left(\frac{1}{E_b - E_i} + \frac{1}{E_a - E_i}\right)\langle i|\hat{H}_{e-ph}|b\rangle \tag{2.75}$$

$$\langle a|\hat{H}_{ind}|b\rangle = \frac{|W_{\boldsymbol{q}}|^2}{\hbar}\left(\frac{1}{\omega - \omega_{\boldsymbol{q}}} - \frac{1}{\omega + \omega_{\boldsymbol{q}}}\right) \tag{2.76}$$

From this the net matrix element between states a and b is:

$$\langle a|\hat{H}|b\rangle = U_{\boldsymbol{q}} + \frac{2|W_{\boldsymbol{q}}|^2}{\hbar}\frac{\omega_{\boldsymbol{q}}}{\omega^2 - \omega_{\boldsymbol{q}}^2} \tag{2.77}$$

This produces a negative interaction when $\omega < \omega_{\boldsymbol{q}}$ and $U_{\boldsymbol{q}}$ is small.

2.5 BCS Theory of Superconductivity

Using the Cooper pairs Bardeen, Cooper and Schreiffer constructed a Hamiltonian to describe superconductivity [9]:

$$\hat{H} = -\sum_{k} \xi_k [c^{\dagger}_{k\uparrow} c_{k\uparrow} + c^{\dagger}_{-k\downarrow} c_{-k\downarrow}] + \sum_{kk'} V_{kk'} c^{\dagger}_{k\uparrow} c^{\dagger}_{-k'\downarrow} c_{-k'\downarrow} c_{k\uparrow} \tag{2.78}$$

Here BCS used the approximation $V_{kk'} = -2E_p$, where E_p is a positive quantity depending on the strength of the electron-phonon interaction, when $|\xi_k - \xi_{k'}| < \omega_D$. It is useful to quantify the strength of the attraction by multiplying the approximate attractive potential by the density of electron states:

$$\lambda = -2E_p N(E_f) \tag{2.79}$$

BCS theory is applicable to the case when the electrons are weakly coupled to the phonons so that $\lambda \ll 1$ Following the method described by e.g. Alexandrov [15] the BCS Hamiltonian can then be written as:

$$\hat{H} = -\sum_{k} \xi_k [c^{\dagger}_{k\uparrow} c_{k\uparrow} + c^{\dagger}_{-k\downarrow} c_{-k\downarrow}] + \Delta_k c^{\dagger}_{k\uparrow} c^{\dagger}_{-k\downarrow} + \Delta^{*}_k c_{-k\downarrow} c_{k\uparrow} + \frac{|\Delta^2_k|}{2E_p} \tag{2.80}$$

where:

$$\Delta_k = -2E_p \sum_{k'} \Theta(\omega_D - |\xi_{k'}|) \langle\langle c_{-k\downarrow} c_{k\uparrow} \rangle\rangle \tag{2.81}$$

The diagonalization of this Hamiltonian uses a Bogoliubov transformation:

$$\begin{aligned} \alpha_k &= u_k c_{k\uparrow} - v_k c^{\dagger}_{-k\downarrow} \qquad & \alpha^{\dagger}_k &= u_k c^{\dagger}_{k\uparrow} - v_k c_{-k\downarrow} \\ \beta_k &= u_k c_{-k\downarrow} + v_k c^{\dagger}_{k\uparrow} \qquad & \beta^{\dagger}_k &= u_k c^{\dagger}_{-k\downarrow} + v_k c_{k\uparrow} \end{aligned} \tag{2.82}$$

The new particles, α and β, are fermions and must obey the anti-commutation rules given by Eq(2.42). This again produces the identity $1 = u^2_k + v^2_k$. In terms of the quasiparticles the electron operators are given by:

$$\begin{aligned} c_{k\uparrow} &= u_k \alpha_k + v_k \beta^{\dagger}_k \qquad & c^{\dagger}_{k\uparrow} &= u_k \alpha^{\dagger}_k + v_k \beta_k \\ c_{-k\downarrow} &= u_k \beta_k - v_k \alpha^{\dagger}_k \qquad & c^{\dagger}_{-k\downarrow} &= u_k \beta^{\dagger}_k - v_k \alpha_k \end{aligned} \tag{2.83}$$

Substitution of these operators in to the Hamiltonian leads to the following non-diagonal form:

$$\begin{aligned}\hat{H}_k = -[\xi_k(u_k^2 - v_k^2) - \Delta_k u_k v_k - \Delta_k^* u_k v_k]\alpha^\dagger\alpha + \\ [\xi_k(u_k^2 - v_k^2) - \Delta_k u_k v_k - \Delta_k^* u_k v_k]\beta^\dagger\beta + \\ +[2\xi_k u_k v_k + \Delta_k u_k^2 - \Delta_k^* v_k^2]\alpha^\dagger\beta^\dagger + [2\xi_k u_k v_k + \Delta_k u_k^2 - \Delta_k^* v_k^2]\beta\alpha + \\ \frac{|\Delta^2|}{2E_p} + 2\xi_k v_k^2 + u_k v_k \Delta_k + u_k v_k \Delta_k^*\end{aligned} \tag{2.84}$$

where the k index has been dropped and $\hat{H} = \sum_k \hat{H}_k$ has been used for simplicity. Setting off diagonal terms, $\alpha^\dagger\beta^\dagger$ and $\alpha\beta$ to zero will produce a diagonalised Hamiltonian. So solving:

$$2\xi_k u_k v_k + \Delta u_k^2 - \Delta v_k^2 = 0 \tag{2.85}$$

leads to the following solutions for u and v:

$$u_k^2 = \frac{1}{2}(1 + \frac{\xi_k}{\sqrt{\Delta_k^2 + \xi_k^2}}) \qquad v_k^2 = \frac{1}{2}(1 - \frac{\xi_k}{\sqrt{\Delta^2 + \xi_k^2}}) \tag{2.86}$$

$$u_k v_k = -\frac{\Delta}{2\sqrt{\xi_k^2 + \Delta^2}}$$

Using these results the diagonal form of the Hamiltonian in terms of the quasiparticles is:

$$\hat{H}_k = \sqrt{\Delta_k^2 + \xi_k^2}(\alpha^\dagger\alpha + \beta^\dagger\beta) + E_0 \tag{2.87}$$

where:

$$E_0 = \frac{|\Delta^2|}{2E_p} + 2[\xi_k v_k^2 + u_k v_k \Delta_k] \tag{2.88}$$

The BCS ground state contains no quasiparticles so is obtained by removing them from the vacuum state:

$$\phi_0 = A \prod_k \alpha_k \beta_k |0\rangle \tag{2.89}$$

Normalization requires that:

$$1 = A^2 \langle 0| \prod_k \beta_k^\dagger \alpha_k^\dagger \alpha_k \beta_k |0\rangle \tag{2.90}$$

writing the quasiparticles in terms of electron operators and expanding it is seen that:

$$A^2 \prod_k (u_k^2 v_k^2 + v_k^4) = 1 \qquad A = \prod_k \frac{1}{v_k} \tag{2.91}$$

so the ground state wave function is:

$$|\phi_0\rangle = A \prod_k (u_k c_{k\uparrow} - v_k c_{-k\downarrow}^\dagger)(u_k c_{-k\downarrow} + v_k c_{k\uparrow}^\dagger)|0\rangle \tag{2.92}$$

$$|\phi_0\rangle = \prod_k [u_k - v_k c_{-k\downarrow}^\dagger c_{k\uparrow}^\dagger]|0\rangle$$

Substitution of the quasiparticle operators into the order parameter Eq(2.81) and expanding gives:

$$\Delta_k = -2E_p \sum_{k'} \langle\langle u_{k'}^2 \beta_{k'} \alpha_{k'} + u_{k'} v_{k'} \beta_{k'} \beta_{k'}^\dagger - u_{k'} v_{k'} \alpha_{k'}^\dagger \alpha_{k'} - v_{k'}^2 \alpha_{k'}^\dagger \beta_{k'}^\dagger \rangle\rangle \tag{2.93}$$

The off diagonal terms are zero and $\beta_{k'}\beta_{k'}^\dagger = 1 - \beta_{k'}^\dagger \beta_{k'}$ so that:

$$\Delta_k = -2E_p \sum_{k'} u_{k'} v_{k'} (1 - \langle\langle \beta_{k'}^\dagger \beta_{k'} + \alpha_{k'}^\dagger \alpha_{k'} \rangle\rangle) \tag{2.94}$$

where $\langle\langle \alpha_k^\dagger \alpha_k \rangle\rangle$ and $\langle\langle \beta_k^\dagger \beta_k \rangle\rangle$ are the average number of α and β particles given by the Fermi-Dirac distribution f_k

$$\Delta = E_p \sum_{k'} \frac{\Delta}{\epsilon_{k'}} (1 - 2f_{k'}) \tag{2.95}$$

where $\epsilon_k = \sqrt{\xi_k + \Delta_k^2}$ and $f_k = (e^{\frac{\epsilon_k}{T}} + 1)^{-1}$ is the Fermi-Dirac distribution. Using the identity $1 - 2f_k = \tanh \frac{\epsilon_k}{2T}$ the equation for Δ can be written as:

$$\Delta = \frac{E_p V}{(2\pi)^3} \int_{k'} dk' \frac{\Delta \tanh \frac{\epsilon_{k'}}{2T}}{\epsilon_{k'}} \tag{2.96}$$

where the relation $\sum_k F((k) = V/(2\pi)^3 \int F((k) dk = 4\pi \int k^2 dk$ has been used. Using $\lambda = 2E_p N_E$ and the fact that the DOS is approximately constant around the Fermi surface gives the

$$\Delta = \lambda \Delta \int_0^{\omega_D} d\epsilon \frac{\tanh \frac{\epsilon_k}{2T}}{\epsilon_k} \tag{2.97}$$

$\Delta = 0$ is the trivial solution, representing the normal state. The non-trivial solution, $\Delta \neq 0$, at zero temperature, for the superconducting state, is found as follows. In the ground state, $T = 0K$, there are no excitations so Δ is given by:

$$\Delta = \lambda\Delta \int_0^{\omega_D} \frac{d\xi}{\sqrt{\xi^2 + \Delta^2}} \tag{2.98}$$

Integration gives, in the weak coupling limit $\Delta \ll \omega_D$:

$$\frac{1}{\lambda} = \left[\ln|\epsilon + \sqrt{\epsilon^2 + \Delta^2}| \right]_0^{\omega_D} \qquad \frac{1}{\lambda} = \ln 2\omega_D - \ln\Delta \tag{2.99}$$

$$\Delta = 2\omega_D e^{(\frac{-1}{\lambda})}$$

2.6 The Resonating Valence Bond State

While there are many competing theories trying to explain the High T_c superconductors, it is the Resonating Valence Bond (RVB) state that is to be used for the majority of this thesis. The idea of a RVB state was first proposed by Pauling [56] then by Anderson [57] as a 'A New Kind of Insulator'. After the discovery of the High T_c superconductors Anderson then proposed that RVB state was the underlying cause [19].

The RVB state is made up with pairs of mobile anti-ferromagnetically coupled electron pairs. A single electron pair, on a N site lattice, is described by the wave-function:

$$b_\tau^\dagger|0\rangle = \frac{1}{\sqrt{N}} \sum_j c_{j\uparrow}^\dagger c_{j+\tau\downarrow}^\dagger |0\rangle = \frac{1}{\sqrt{N}} \sum_{\boldsymbol{k}} e^{i\boldsymbol{k}.\boldsymbol{\tau}} c_{\boldsymbol{k}\uparrow}^\dagger c_{-\boldsymbol{k}\downarrow}^\dagger |0\rangle \tag{2.100}$$

where τ is a lattice vector. The full wave-function needs to include nearest neighbours so the pair creation operator is defined as:

$$b^\dagger = \sum_{\tau=(nn)} b_\tau^\dagger \qquad b^\dagger = \sum_{\boldsymbol{k}\boldsymbol{\tau}} e^{i\boldsymbol{k}.\boldsymbol{\tau}} c_{\boldsymbol{k}\uparrow}^\dagger c_{-\boldsymbol{k}\downarrow}^\dagger |0\rangle \tag{2.101}$$

From this an N electron wave-function from $N/2$ pairs is constructed.

$$|\Psi\rangle = (b^\dagger)^{\frac{N}{2}}|0\rangle \tag{2.102}$$

Anderson then constructed the RVB wave-function by projecting out all the doubly occupied sites using the Gutzwiller projection operator from Eq(2.31) with $g = 0$. This can be shown to be the same as a BCS wave-function when projected onto a state with a fixed number of elctrons.

2.7 The Hubbard-Fröhlich Model

Variational Monte Carlo results have demonstrated the existence of a d-wave superconducting state within the Hubbard [21] and the t-j models [20], though it may not be the ground state. However, there is evidence of an isotope effect on the charge carrier mass within the high T_c superconductors, see for example Ref [29] suggesting phonons play an important role. For this reason it was decided to include an electron-phonon interaction into the model which we refer to as the Hubbard-Fröhlich model (HFM):

$$\hat{H}_{CFM} = \sum_{ij} t_{ij}(\tilde{c}^{\dagger}_{i\uparrow}\tilde{c}_{j\uparrow}+\tilde{c}^{\dagger}_{i\downarrow}\tilde{c}_{j\downarrow})+U\sum_{i}\hat{n}_{i\uparrow}\hat{n}_{i\downarrow}+\sum_{m}\left[\frac{\hat{P}^2_m}{2M}+\frac{\xi^2_m M\omega^2}{2}\right]-\sum_{mn\sigma} f_m(n)\tilde{c}^{\dagger}_{n\sigma}\tilde{c}_{n\sigma}\xi_m \tag{2.103}$$

Here ξ_m is the ion displacement M is the ion mass $\hat{P}_m$ is the ion momentum operator and $f_m(n)$ is the screened Fröhlich force function. The force function is used to describe the interaction of an ion on site m and electron on site n and given by:

$$f_m(n) = \frac{\kappa}{[(m-n)^2+1]^{3/2}} e^{-\frac{|m-n|}{R_{sc}}} \tag{2.104}$$

A Lang-Firsov transformation is used to integrate out the phonon terms reducing the Hamiltonian the following form:

$$\tilde{H}_{HFM} = \sum_{\mathbf{n}\neq\mathbf{n}',\sigma} \tilde{t}c^{\dagger}_{\mathbf{n}'\sigma}c_{\mathbf{n}\sigma} + \tilde{U}\sum_{\mathbf{n}}\hat{n}_{\mathbf{n}\uparrow}\hat{n}_{\mathbf{n}\downarrow} - \lambda W \sum_{\mathbf{n}\neq\mathbf{n}',\sigma\sigma'} \Phi(\mathbf{n}-\mathbf{n}')\hat{n}_{\mathbf{n}'\sigma'}\hat{n}_{\mathbf{n}\sigma} \tag{2.105}$$

Details of this procedure are given in section 4.2. Our variational Monte Carlo algorithm along with the new Hamiltonian EqHFH is used to investigate the effects of varying the EPI strength at various electron densities.

Chapter 3

Introduction to Variational Monte Carlo

This chapter introduces the Variational Monte Carlo (VMC) simulation used to estimate the ground state energy of the various wave-functions and models examined in this thesis. The VMC method combines the quantum variational theory with the widely used Monte Carlo (MC) algorithm.

We then describe preliminary results collected during the development of the VMC code. To ensure the code was working properly we have checked our results against other published results and limiting cases, where the exact energies are known. We have re-examined three different phases of the Hubbard model; paramagnetic, antiferromagnetic and superconducting.

3.1 Statistical Physics

This section gives a brief overview of statistical physics upon which the MC algorithm is based. For any given physical system there is some, exact or approximate, Hamiltonian describing the states within it [58]. Each state then has an associated energy defined by the Hamiltonian.

At any time the system will be in one of these states μ. At a time dt later there is some finite probability $R(\mu \rightarrow \nu)dt$ of being in a new state ν where $R(\mu \rightarrow \nu)$ is the transition rate going from μ to ν. For convenience it is usually assumed that the transition rate is time independent. At some time, t, there is a probability or weight $w_\mu(t)$ of being in the state μ. If the transition rate is known a master equation can be written describing the time evolution of the weight:

$$\frac{dw_\mu}{dt} = \sum_\nu [w_\nu(t)R(\nu \rightarrow \mu) - w_\mu(t)R(\mu \rightarrow \nu)] \tag{3.1}$$

i.e the sum of all transitions into the state μ minus the sum of all the transitions out of μ. It is clear at time t the system will be in a state so $\sum_\mu w_\mu(t) = 1$.

With the knowledge of these weights, found by solving the master equation, the expectation value of a quantity Q at time t is calculated as:

$$\langle Q \rangle = \sum_\mu w_\mu(t)Q_\mu \tag{3.2}$$

When a configuration is reached in which the two terms, $[w_\nu(t)R(\nu \rightarrow \mu)$ and $w_\mu(t)R(\mu \rightarrow \nu)$, in the master equation cancel, the rate of change of the weight with respect to time is zero. This means that the weights are fixed and an equilibrium state has been achieved. At this point the weight gives the equilibrium probability of a certain state being occupied;

$$p_\mu = \lim_{t\rightarrow\infty} w_\mu(t) \tag{3.3}$$

In general, for an equilibrium system, these probabilities are given by the Boltzmann

distribution;

$$p_\mu = \frac{e^{-\beta E_\mu}}{\sum_\nu e^{-\beta E_\nu}} \tag{3.4}$$

where the sum in the denominator is the partition function $Z = \sum_\nu e^{-\beta E_\nu}$ and $\beta = 1/kT$. It is the main aim of a MC simulation to estimate expectation values by mimicking the 'random' behaviour of the real system.

3.2 Basic Principles of Monte Carlo Simulation

A MC simulation aims to recreate the random nature of a system, making random transitions from one state to another according to the probabilities of the two states. In doing this it is sufficient to find the relative weights of the various states and from this get an estimation of an expectation value: Using the Boltzmann distribution Eq(3.4) to define the weights it can be seen that the expectation value of Q is:

$$\langle Q \rangle = \frac{\sum_\mu Q_\mu e^{-\beta E_\mu}}{\sum_\mu e^{-\beta E_\mu}} \tag{3.5}$$

In practice this sum is only feasible for very small systems. As an illustration of the size of the problem, even for a simple Ising model on a 10x10 lattice there are 2^{100} or over 10^{30} possible states. There is very little hope of being able to sample every state in such system. With a MC simulation the idea is not to sample all the states but a representative sample of the most likely states with some probability p_μ. So the MC estimate of the expectation value $\langle Q \rangle_{MC}$ over a sub set of the possible states $\{\mu_1, \mu_2..\mu_M\}$:

$$\langle Q \rangle_{MC} = \frac{\sum_{i=1}^{M} p_{\mu_i} Q_\mu e^{-\beta E_{\mu_i}}}{\sum_{j=1}^{M} p_{\mu_j} e^{-\beta E_{\mu_j}}}. \tag{3.6}$$

As the number of samples increases so does the accuracy of the estimate.

The states need to be chosen according to their relative probabilities, a method called importance sampling. In the majority of MC algorithms the states are selected with a frequency based on their Boltzmann probabilities. Replacing the probabilities with

their Boltzmann representation Eq(3.4) the estimation simplifies to:

$$\langle Q \rangle_{MC} = \frac{1}{M} \sum_{i=1}^{M} Q_{\mu_i} \tag{3.7}$$

So that the probability disappears from the average. The probabilities of the states enter via the frequency with which they are chosen during the simulation. Over a long enough simulation the number of times a state is chosen, n_μ, divided by the total number of samples, N, approaches the equilibrium probability.

$$p_\mu = \lim_{N \to \infty} \frac{n_\mu}{N} \tag{3.8}$$

3.2.1 Markov Chains

The majority of MC simulations use a series of Markov processes to generate a chain of random states. A Markov process creates a random new state ν from the state μ with a transition probability $P(\mu \to \nu)$. These transition probabilities should be independent of time and depend only on the states μ and ν. The sum of the transition probabilities must be one, i.e it must result in a state:

$$\sum_{\nu} P(\mu \to \nu) = 1 \tag{3.9}$$

It is allowable to generate the same state, so $P(\mu \to \mu)$ is not necessarily zero. On the other hand, generation of the same state must not occur with probability $P(\mu \to \mu) = 1$, the system would be permanently stuck in the one state.

To ensure the correct probabilities are created, Markov chains are subject to two further conditions; The first is known as ergodicity. This condition states that starting from any one state it must be possible to access all other states (assuming that the chain is long enough). While it is allowed to have some transition probabilities set to zero there must be a 'random walk' through sample space from any one state to all others within the system. In relation to the Hubbard model a half filled lattice with infinite U, where

only single electron hops are allowed, breaks this condition. Once in a configuration where all double occupancy has been removed then no hopping is allowed and the system becomes frozen in this state, unable to access any other.

The other condition to be satisfied is detailed balance. This is used to guarantee that the states are weighted with the desired probabilities. Reusing the fact that at equilibrium the probability of a transition into a state equals the probability out:

$$\sum_{\nu} p_\nu P(\nu \rightarrow \mu) = \sum_{\nu} p_\mu P(\mu \rightarrow \nu) \tag{3.10}$$

This will always be satisfied if the following condition is obeyed:

$$p_\nu P(\nu \rightarrow \mu) = p_\mu P(\mu \rightarrow \nu) \tag{3.11}$$

It is this equation that the condition of detailed balance refers to. Rearranging this equation the condition of detailed balance is defined by the ratios:

$$\frac{P(\nu \rightarrow \mu)}{P(\mu \rightarrow \nu)} = \frac{p_\mu}{p_\nu} \tag{3.12}$$

When the probabilities of the two states are given by the Boltzmann probabilities the ratio is [58]:

$$\frac{p_\mu}{p_\nu} = e^{-\beta(E_\mu - E_\nu)} \tag{3.13}$$

3.2.2 Statistical Errors in MC Calculations

As with all numerical techniques the Monte Carlo method is not exact and the results have some error associated with them. In fact with the randomness inherent in the method some statistical error in the result is inevitable. It is common to refer to a MC simulation as a 'computer experiment' [58] and errors can be treated in the same manner as with an experimental data set.

For a set of independent measurements a good estimate of the error is given by the standard error [59]:

$$\sigma = \sqrt{\frac{\langle m^2 \rangle - \langle m \rangle^2}{n-1}} \tag{3.14}$$

where $\langle m^2 \rangle$ is the average of the measurement squared, $\langle m \rangle^2$ is the square of average and n is the number of samples. For this to be an accurate estimation the measurements should be independent. With a MC simulation this is often not the case with two successive measurements often being highly correlated.

To reduce the effect of the correlation between measurements there are a number of methods. The methods that we use is the blocking method. For this the n measurements are split into n_B blocks. The deviation of the average measurement over the blocks is then used to calculate the standard deviation;

$$\sigma = \sqrt{\frac{\langle m_B^2 \rangle - \langle m_B \rangle^2}{n_B - 1}} \tag{3.15}$$

This method is unfortunately sensitive to the block size n, but provided the block size is correct this produces a good error estimation. For a good error estimation the block size should be greater than the correlation time.

3.3 The Metropolis Algorithm

To generate Markov chains with the desired properties, one of the most common Monte Carlo methods is the Metropolis algorithm. This algorithm Fig(3.1) was first introduced by N. Metropolis *et al* in 1953 [60] for the calculation of macroscopic properties of substances consisting of interacting molecules.

To decrease the size of the problem the particles are placed in a random configuration within a reduced system, maintaining the same particle density; This introduces a finite size error. Randomly selecting one particle, R_n, it is then moved in a random fashion according to:

$$R_n(x, y) \rightarrow R_n(x + \alpha\xi_1, y + \alpha\xi_2) \tag{3.16}$$

where α is the maximum allowed moving distance, ξ_1 and ξ_2 are random numbers numbers in the range $-1 \leq \xi_i \leq 1$. If this move takes the system into a lower energy

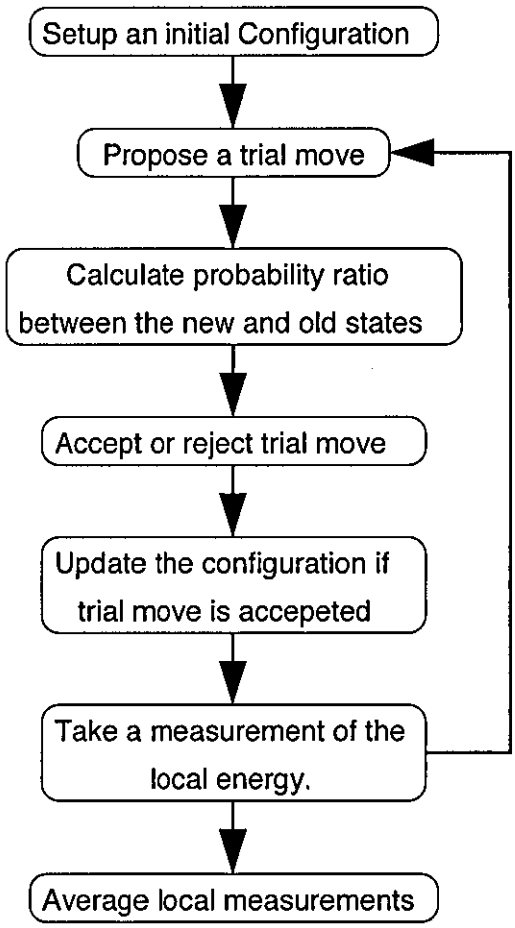

Figure 3.1: Flow chart for the Monte Carlo method.

state the move is automatically accepted. If the change in energy ΔE is negative, the move is to a configuration with a higher energy, then the move is accepted based on the probability $e^{-\Delta E\beta}$. A new random number between 0 and 1 is generated: if this is less than $e^{-\Delta E\beta}$ then the move is accepted. Then regardless of whether or not the move has been accepted a measurement of the desired quantities for the system in that state are made. The expectation value of the quantity is then given by Eq(3.6).

If for some reason the acceptance ratio is very low then the statistical correlation between successive measurements is high. In this case a measurement can be made every n^{th} step so that the statistical correlation between measurements is reduced. This

does not affect the expectation value as it reduces the weight of every state equally.

3.4 The Variational Monte Carlo Method

The application of the Monte Carlo technique to a quantum system was first introduced by Macmillan [61] in 1965. A Monte Carlo method was used to evaluate the configuration space integral of a bosonic variational wave function in the calculation of ground state properties of He^4 according to the variational principle.

3.4.1 The Variational Principle

The variational principle is used to calculate an upper bound for the ground state energy of a Hamiltonian $\hat{H}$. The energy of a trial wave function $|\Psi_T\rangle$, that need not necessarily be normalised, is then given by [62]:

$$E = \frac{\langle \Psi_T | \hat{H} | \Psi_T \rangle}{\langle \Psi_T | \Psi_T \rangle} \tag{3.17}$$

with the denominator required if the trial wave function has not been normalised. Using completeness the trial wave function can be expressed as a linear superposition of the true wave functions Ψ as $\Psi_T = \sum_n c_n \Psi_n$. Substituting into the numerator yields:

$$\langle \Psi_T | \hat{H} | \Psi_T \rangle = \sum_n |c_n|^2 E_n \tag{3.18}$$

The lowest of the energies E_n is the ground state. If the trial wave function equals the exact ground state wave function then the coefficients c_n are all zero except c_0 and $E = E_0$. If the trial wave function is different to the true wave function then $E > E_0$ so the variational energy provides an upper bound to the ground state energy.

3.4.2 Monte Carlo Integration

McMillan then applied the MC technique to determine the variational energy. As before the expectation value of the operator for the quantity Q is calculated as:

$$\langle Q \rangle = \int Q(\boldsymbol{r}_1 ... \boldsymbol{r}_N) P_N(\boldsymbol{r}_1 ... \boldsymbol{r}_N) d\tau \tag{3.19}$$

In this case, as the system is based on N Bosonic particles at positions $\boldsymbol{r}_1 ... \boldsymbol{r}_N$, the weights of the configuration$P_N(\boldsymbol{r}_1 ... \boldsymbol{r}_N)$ are given by the square of the wave function $\Psi_N(\boldsymbol{r}_1 ... \boldsymbol{r}_N)$. When the configurations are chosen according to their probability distribution $P_N(R^i) = \Psi^2(R^i)$, $R^i = \boldsymbol{r}_1 ... \boldsymbol{r}_N$ then Eq(3.6) can be used to approximate the expectation value .

The Metropolis algorithm is used to generate a sequence on configurations where each configuration is chosen with a frequency that, when run for long enough, approaches its probability. The only difference here is that rather than choosing the states based on their Boltzmann weights they are chosen according to their quantum probabilities which are given by the square of the wave function

3.4.3 VMC Applied to Fermions

For a system of fermions the VMC procedure is almost identical. The difficulty arises because of the anti-symmetric nature of the wave function. Once this has been dealt with the square of the wave function defines the probability of a certain configuration, as is the case for bosons. An effective method for the calculation of the relative probability of two fermionic configurations was first introduced by Ceperley et al [63] in 1977 while examining the ground state properties of He^3.

As before, the aim of this procedure is to minimise the energy of a trial wave function, according to the variational principle, to find an upper bound to the ground state energy. Once the values of the variational parameters that give the minimum energy

have been found then other properties can also be calculated.

As before, to start with the fermions are placed in a random configuration R_μ. A random move of any one of the fermions is proposed to take the system from the configuration R_μ to R_ν. The relative probabilities q^2 of the two states are calculated:

$$q^2 = \frac{|\Psi(R_\nu)|^2}{|\Psi(R_\mu)|^2} \tag{3.20}$$

The move is then accepted automatically if it is a more probable state $q^2 \geq 1$. If $q^2 < 1$ then the move is accepted if a random number ξ between 0 and 1 is less than q^2.

For fermions the wave function must be anti-symmetric so that on exchange of two particles a minus sign is introduced. To construct a properly anti-symmetrised wave function it is usual to use a Slater determinant.

$$\Psi(R) = \begin{pmatrix} e^{ik_1.r_1} & e^{ik_2.r_1} \\ e^{ik_1.r_2} & e^{ik_2.r_2} \end{pmatrix} \tag{3.21}$$

so that the wave function is written explicitly with the desired symmetry;

$$\Psi(R) = e^{ik_1.r_1}e^{ik_2.r_2} - e^{ik_1.r_2}e^{ik_2.r_1} \tag{3.22}$$

Unfortunately the calculation of a determinant with a computer scales with the number of particles as N^3. To get round this Ceperley [63] introduced a trick for calculating the ratio of determinants between two states that scales as N^2.

The trick uses the fact that the inverse of the transpose of a matrix $[A]$ is equal to the matrix of cofactors divided by its determinant $|A|$ (see [64] and [65]):

$$[A^T]^{-1} = \frac{[C_A]}{|A|}. \tag{3.23}$$

The definition of the cofactor element C_{ij} means that it is independent of the ith row and jth column. From this it can be seen that ratio of determinants q of two matrices that differ only on row i is given by [64];

$$\frac{\mathrm{Det(A_{new})}}{\mathrm{Det(A_{old})}} = q = \sum_{j=1}^{N} \tilde{A}_{i,j,\mathrm{old}} A_{i.j,\mathrm{new}} \tag{3.24}$$

where $\tilde{A}_{i,J}$ is the element in the ith row and jth column of the inverse of the transpose of matrix $[A]$, $[\tilde{A}] = [A^T]^{-1}$. For the case of the Slater Determinant used here, when moving particle i, the ratio of determinants, q is found using:

$$q = \sum_{j=1}^{N} \tilde{D}_{j,i,\text{old}} \Phi_j(\boldsymbol{r}_i) \tag{3.25}$$

where $\Phi_j(\boldsymbol{r}_i)$ is the wave function of an electron on site $\boldsymbol{r}_i$ in momentum state j. This allows a relatively quick way of determining the probability ratio between two configurations. While the calculation of the inverse of a matrix is computationally very expensive it is only a one-off event and insignificant when the number of samples is large. If the trial move is accepted then the inverse of the transpose of the new matrix can be calculated using;

$$\tilde{D}_{jk,\text{new}} = \begin{cases} \frac{\tilde{D}_{jk}}{q}, \text{ if } k = i \\ \tilde{D}_{jk} - \frac{\tilde{D}_{jk}}{q}\Big[\sum_{l=1}^{N} \tilde{D}_{lk}\Phi_l(\boldsymbol{r}_j)\Big] \text{if } k \neq i \end{cases} \tag{3.26}$$

3.5 VMC for the Hubbard Model

Now that the general VMC technique has been introduced, the application to the Hubbard model can be discussed. The first such application was performed by Yokoyama and Shiba [66] in 1986, with further studies in Ref [67].

3.5.1 Trial Wave Functions

The first step is the construction of a suitable trial wave function. The simplest example is the projected paramagnetic wave function, $|\Psi_{\text{Para}}\rangle$, [66]:

$$|\Psi_{\text{Para}}\rangle = \prod_j [1 - (1-g)n_{j\uparrow}n_{j\downarrow}]|\Phi_{\text{Para}}\rangle \tag{3.27}$$

with $0 \leq g \leq 1$ and $|\Phi_{\text{Para}}\rangle$ is the product of the slater determinants of the up and down electrons;

$$|\Phi_{\text{Para}}\rangle = |M_\uparrow||M_\downarrow| \tag{3.28}$$

and the elements of the matrices for the paramagnetic case are given by the free electron wave functions;

$$M_{i,j,\sigma} = e^{ik_i.r_{j\sigma}} \tag{3.29}$$

where k_i are the allowed momenta and $r_{j\sigma}$ is the position of the j^{th} electron with spin σ.

For the antiferromagnetic wave function, $|\Psi_{AFM}\rangle$, [68];

$$|\Psi_{AFM}\rangle = \prod_j [1 - (1-g)n_{j\uparrow}n_{j\downarrow}]|\Phi_{AFM}\rangle \tag{3.30}$$

where again $|\phi_{AFM}\rangle = |M_\uparrow||M_\downarrow|$. To get a real space representation of the trial wave-function $\alpha^\dagger_{k,\sigma} = u_k a^\dagger_{k,\sigma} + \sigma v_k a^\dagger_{k+Q,\sigma}$, for use in the simulation, the standard result, $\langle r|k\rangle = e^{ikr}$ is used:

$$\langle r|\alpha^\dagger_{k,\sigma}|0\rangle = u_k e^{ikr} + \sigma v_k e^{i(k+\pi)r} \tag{3.31}$$

Which can be used to define the matrix elements:

$$M_{i,j,\sigma} = u_{k_i} e^{ik_i.r_{j\sigma}} + \sigma v_{k_i} e^{i(k_i+\pi).r_{j\sigma}} \tag{3.32}$$

where the symbols are as derived in section(2.3.2):

$$u^2_{k_i} = \frac{1}{2}\Big[1 - \frac{\xi_{k_i}}{\sqrt{\xi^2_{k_i} + \Delta^2}}\Big] \qquad v^2_{k_i} = \frac{1}{2}\Big[1 + \frac{\xi_{k_i}}{\sqrt{\xi^2_{k_i} + \Delta^2}}\Big] \tag{3.33}$$

To ensure the quasiparticle number operator can be implemented into the VMC code, when acting on the vacuum state it must produce zero:

$$\langle 0|n_\alpha|0\rangle = \langle 0|(u_k a^\dagger_k + \sigma v_k a^\dagger_{k+Q})(u_k a_k + \sigma v_k a_{k+Q})|0\rangle = 0 \tag{3.34}$$

So the number operator needs no modification for the VMC. The antiferromagnetic wave function introduces a second variational parameter Δ. This increases the size of the parameter space, making the task of finding the minimum energy much more computationally intensive.

The superconducting wave function is slightly more complicated. The standard form of the BCS wave function, in which the particle number varies, is not suitable for VMC.

As before the number operator acting on the ground state must produce zero. The number operator $\alpha_k^\dagger \alpha_k$ acting on vacuum gives the following surprising result:

$$\begin{aligned} \langle 0|n_k|0\rangle &= \langle 0|u_k^2 c_{k\uparrow}^\dagger c_{k\uparrow} - u_k v_k c_{k\uparrow}^\dagger c_{-k\downarrow}^\dagger - u_k v_k c_{-k\downarrow} v_k c_{k\downarrow} + v_k^2 c_{-k\downarrow}^\dagger c_{k\downarrow}|0\rangle \quad (3.35) \\ \langle 0|n_k|0\rangle &= v_k^2 \end{aligned}$$

Demonstrating that this is not a vacuum with respect to the quasiparticles, and that this form is not suitable for our VMC simulation.

One method by Yokoyama et al [69] involves the transformation to new set of creation and annihilation operators. A new vacuum with respect to these particles is then formed. Another way to write the BCS wave function in an appropriate form is to project it onto a fixed particle number state [70]. The starting point is a projected BCS wave function [71];

$$|\Psi_{Sup}\rangle = P_N P_G \prod_k \left[u_k + v_k c_{k\uparrow}^\dagger c_{-k\downarrow}^\dagger\right]|0\rangle \quad (3.36)$$

where P_N projects onto a fixed particle number sate and P_G is the Gutzwiller projection operator. Ignoring the normalisation of the wave function it can be rewritten as:

$$|\Psi_{Sup}\rangle = P_N P_G \prod_k \left[1 + a_k c_{k\uparrow}^\dagger c_{-k\downarrow}^\dagger\right]|0\rangle \quad (3.37)$$

by defining $a_k = u_k/v_k$. Application of the particle number projection operator leads to

$$|\Psi_{Sup}\rangle = P_G\Big[\sum_k a_k c_{k\uparrow}^\dagger c_{-k\downarrow}^\dagger\Big]^{N/2}|0\rangle \quad (3.38)$$

So that the required real space representation of the trial function is:

$$|\Psi_{Sup}\rangle = P_G\Big[\sum_{j,l} a(j,l) c_{j\uparrow}^\dagger c_{l\downarrow}^\dagger\Big]^{N/2}|0\rangle \quad (3.39)$$

where we have defined:

$$a(j,l) = \frac{1}{N_s}\sum_k \frac{v_k}{u_k} e^{ik.(r_l - r_j)} \quad (3.40)$$

and N_s is the number of lattice sites. Using the results from Eq(2.86) we define $v_k/u_k = \Delta/(\xi_k + \sqrt{\xi^2 + \Delta^2})$. At $\Delta = 0$, a_k is also zero, therefore the trial function is zero and undefined so the simulation will not run.

3.5.2 Details of the VMC Simulations

Now the details of the VMC method for the Hubbard model are discussed. To start with the electrons are placed in a random configuration $\boldsymbol{R}_\mu$, with no two electrons of the same spin on the same site. A new configuration $\boldsymbol{R}_\nu$ is then generated by picking an electron at random and moving it to one of its nearest neighbours, a trial move. If the move takes the electron off the lattice then it re-enters on the site on the opposite side enforcing the periodic boundary conditions.

To determine whether or not the trial move is accepted the probability ratio between the two states is required. As before this is given by the ratio of the squared wave functions:

$$\frac{P(\boldsymbol{R}_\nu)}{P(\boldsymbol{R}_\mu)} = \frac{|\Psi(\boldsymbol{R}_\nu)|^2}{|\Psi(\boldsymbol{R}_\mu)|^2} \tag{3.41}$$

Our trial wave functions described above are written as a Gutzwiller projection of a Slater determinant;

$$|\Psi_T\rangle = \prod_j [1-(1-g)n_{j\uparrow}n_{j\downarrow}]|\Phi_T\rangle \tag{3.42}$$

For a specific configuration μ, expansion of the product, in which a factor of g is picked up for every doubly occupied site, yields

$$|\Psi_{T\mu}\rangle = g^{N_D}|\Phi_{T\mu}\rangle \tag{3.43}$$

where N_D is the number of doubly occupied sites. Thus the probability ratio is:

$$\frac{P(\boldsymbol{R}_\nu)}{P(\boldsymbol{R}_\mu)} = g^{2\delta d}\left|\frac{|M_{\uparrow\nu}|}{|M_{\uparrow\mu}|}\frac{|M_{\downarrow\nu}|}{|M_{\downarrow\mu}|}\right|^2 \tag{3.44}$$

where δd is the change in double occupancy. The ratio of determinants q between the old and new states is calculated using Ceperley's method. As only one electron is ever moved one of these determinant ratios is always one. The trial move is then accepted if a random number $0 \leq \xi \leq 1$ satisfies $\xi < P(\boldsymbol{R}_\nu)/P(\boldsymbol{R}_\mu)$. If the move is accepted then the electron position, inverse matrix, double occupancy and long range attraction are updated.

After this, assuming sufficient moves have been made to allow the system to reach equilibrium, the local energy is measured. The basic Hubbard model is written as:

$$\hat{H} = -t \sum_{<ij>} c_i^\dagger c_j + U \sum_i n_{i\uparrow} n_{i\downarrow} \tag{3.45}$$

The local energy, of the state μ is then given by;

$$E_L = \frac{\hat{H}\Psi_\mu(\boldsymbol{r})}{\Psi_\mu(\boldsymbol{r})} \tag{3.46}$$

Applying the Hamiltonian to the wave function results in two terms. The first (the kinetic energy) includes the trial move and the second is simply the number of doubly occupied sites. Unfortunately the kinetic energy of the local configuration must include all allowed hops of every electron and is not readily calculated. However the energy of one specific hop, i.e. the trial move, is known. The Monte Carlo simulation is then used to sample the possible hops within each configuration and average the local hopping energy. So the local energy is written as:

$$E_L = -t \sum_j \sum_\sigma \sum_a \frac{|M_{\uparrow\nu}|}{|M_{\uparrow\mu}|} \frac{|M_{\downarrow\nu}|}{|M_{\downarrow\mu}|} + UN_d \tag{3.47}$$

where N_d is the number of doubly occupied sites and $\Phi(\boldsymbol{i}-\boldsymbol{j})$ is the interaction between electrons on sites $\boldsymbol{i}$ and $\boldsymbol{j}$. The calculation of the determinant ratio has already been performed. To measure the double occupancy we calculate the doubly occupancy of the initial configuration and update this when necessary as the electrons move.

For the HFM we have an extra term given by:

$$\lambda W \sum_{\mathbf{n}\neq\mathbf{n}',\sigma\sigma'} \Phi(\mathbf{n}-\mathbf{n}')\hat{n}_{\mathbf{n}'\sigma'}\hat{n}_{\mathbf{n}\sigma}. \tag{3.48}$$

This means we need to make the additional measurement:

$$\lambda W \sum_{i,j} \Phi(\boldsymbol{i}-\boldsymbol{j}) \tag{3.49}$$

for the local configuration energy. Again we make an initial measurement of the long range electron interaction and update as the electrons move. A look-up table, to store

all the possible interactions, is used so that the interaction is not calculated every time an electron moves.

To ensure there are no problems with degeneracy it is important to choose the boundary conditions of the system carefully. So that trial wave function has the correct symmetries it is necessary to completely fill degenerate momentum states [63]. To lift or reduce the degeneracy it is possible to add a small momentum $\delta\mathbf{k}$ to the states. However this introduces a phase factor $exp[-i2\pi\delta k]$ to the kinetic energy when an electron crosses a boundary. This phase factor needs to be removed by multiplying the local kinetic energy by $exp[i2\pi\delta k]$ when the electron crosses the lattice boundary if there is a momentum offset in that direction.

In the case of the superconducting state a combination of periodic and anti-periodic boundary conditions are used, giving $\delta\boldsymbol{k} = 0.5\boldsymbol{k}_y$. Here the form of the wave function means that the order parameter Δ can not equal zero. With the d-wave state this means that $k_x \neq k_y$, which is avoided by choosing such boundary conditions. The phase factor $exp[-i\pi]$ is then -1 whenever an electron moves across the anti-periodic boundary.

3.6 Paramagnetic Results

Here we present results for the paramagnetic wave function Eq(3.27) and describe the evaluation of the results.

The results are calculated as follows. The raw data is created by scanning from $g = 1$ to $g = 0$ in steps of $\delta g = 0.01$ and measuring the kinetic energy, given by $-t\langle c_i^\dagger c_j\rangle$, and double occupancy, defined by $\langle n_{i\uparrow} n_{i\downarrow}\rangle$, at every point, producing data like that shown in fig(3.2). This graph clearly demonstrates the effect of the competition between the electron hopping and onsite repulsion and the role of the Gutzwiller projection operator in controlling their contributions. As $g \rightarrow 0$, minimising the on site potential energy,

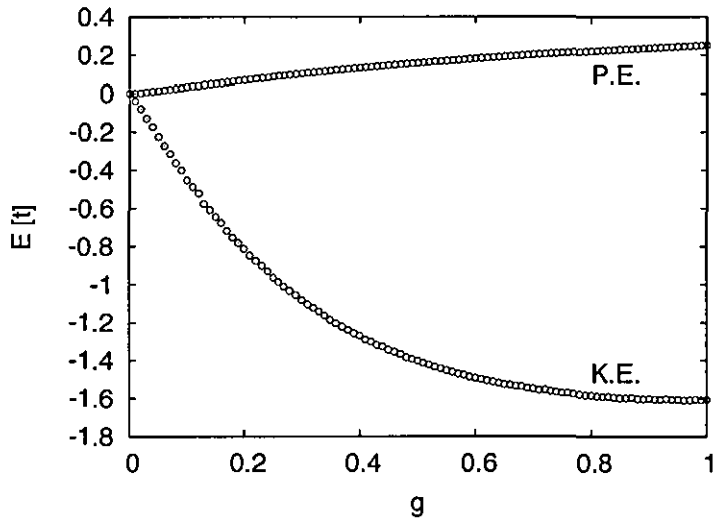

Figure 3.2: Competition between kinetic and potential energy per electron on a half-filled 14x14 2D square lattice with $U = 1$, which is equivalent to the average double occupancy, the error bars are smaller than the point size.

$U\langle n_{i\uparrow} n_{i\downarrow}\rangle$, the kinetic energy tends to zero, so that the elimination of double occupancy prevents the motion of the electrons. The on site potential energy favours localised electrons, with one electron per site, while kinetic energy favours mobile electrons.

For verification the results are examined in two limiting cases where exact results are known. For a half filled lattice with $g = 0$, which corresponds to $U = \infty$, both the kinetic energy and double occupancy should tend to zero, this is found to be the case Fig(3.2). In the other limit, $g = 1$, i.e when there is no suppression of double occupancy, the double occupancy per electron should be 0.25, which can, again, be seen in the results. In the same limit, which corresponds to $U = 0$, there is no electron correlation so the tight binding kinetic energy should be recovered. In this case the total, non-interacting, energy $E_T = \sum_{\mathbf{k}} \xi_{\mathbf{k}}$ is the sum of the energy of all occupied momentum points. The energy per electron E is calculated for an infinite lattice by integrating up to the Fermi surface:

$$E = \frac{1}{(2\pi)^3} \int \xi_{\mathbf{k}} d\mathbf{k} \tag{3.50}$$

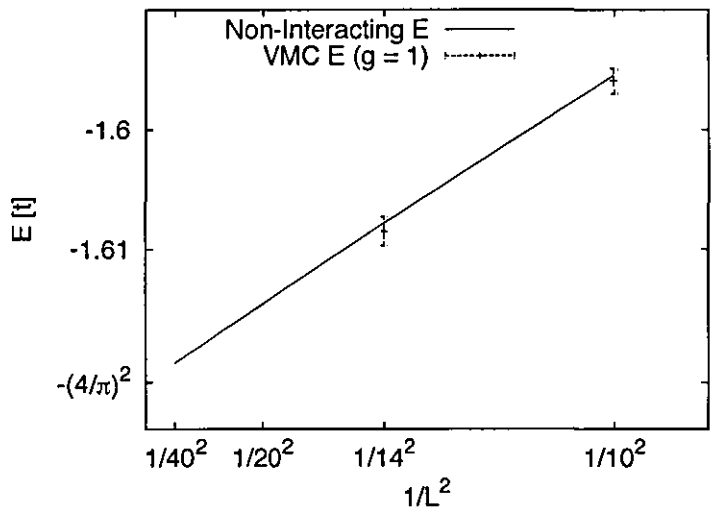

Figure 3.3: Finite size scaling effect for the kinetic energy for a 2D square lattice.

Thus for 1D, 2D and 3D respectively we get:

$$E = -\frac{4}{\pi}t \qquad E = -\left(\frac{4}{\pi}\right)^2 t \qquad E = -\left(\frac{4}{\pi}\right)^3 t \tag{3.51}$$

There is some small discrepancy between the $g = 1$ VMC results ($[-1.606 \pm 0.002]t$ for a 14x14 lattice) and the theoretical kinetic energy in the continuum limit. This is a finite size error that reduces as the lattice size is increased, see Fig(3.3). The finite lattice non-interacting energy is calculated at the start of the simulations and used to check the value of the VMC kinetic energy at $g = 1$.

As a further verification of the code, simulations were performed at low electron densities where the kinetic energy should tend to $-2dt$ when there is just one spin-up and one spin-down electron on an infinite lattice, where d is the dimensionality of the system. In this limit the potential energy will tend to 0. Our result approach these limits in both cases Fig(3.4).

From the raw data the total energy $E(g) = E_{ke}(g) + N_{do}(g)U$ as a function of g can be constructed for any value of U desired from the kinetic energy, $E_{ke}(g)$, and double occupancy, $N_{do}(g)$, data. Once the energy as a function of g, for a specific U, has been found the minimum energy is easily located. Examples of the variation of energy with

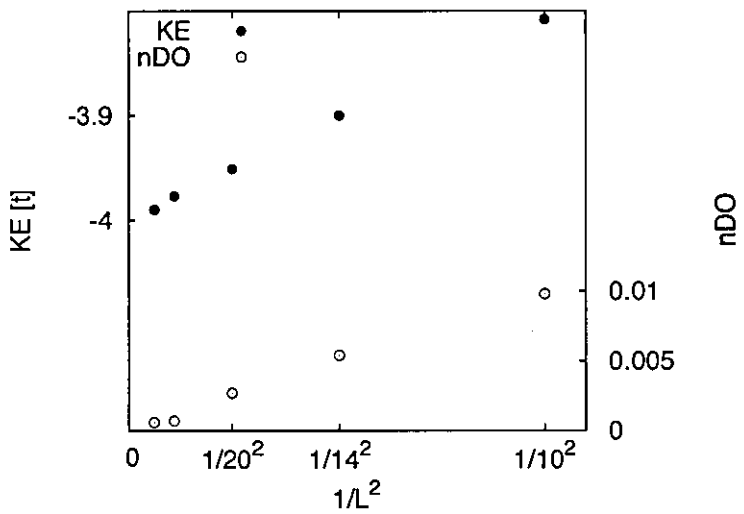

Figure 3.4: The kinetic energy (KE) and number of doubly occupied sites (nDO), per electron, in the dilute limit for 10x10, 20x20 30x30 and 40x40 2D lattices tending to -4 and 0 respectively, the error bars are smaller than the point size

g are shown in Fig(3.5). For $U = 0$ the minimum energy is found at $g = 1$, decreasing g inhibits the electron hopping increasing the energy. As U is increased the minimum shifts to smaller values of g. For values of g smaller than the minimum, the reduction in potential energy is counteracted by the rise of the kinetic energy, larger values lower the kinetic energy at the expense of the on site potential.

We then plot the minimum total energy, at values of $U = 0, 1, 2, 3, 4, 6, 8, 10, 12$, for the 30 site 1D system, Fig(3.6), 14x14 site 2D system, Fig(3.7) and the 6x6x6 site 3D system, Fig(3.8). These graphs show that the effect of increasing U is to raise the energy of the system. This is due to the competition between the two terms; the kinetic energy favours mobile electrons while the on site repulsion favours localised electrons Our results are compared with those by Yokoyama et al [66] and no disagreement is found. In these results the error bars are smaller than the point size.

In the 1D system our energies are higher than the exact solution by Lieb [72] see [66], shown in table (3.1), based on the Bethe ansatz [73]. In the weak correlation regime

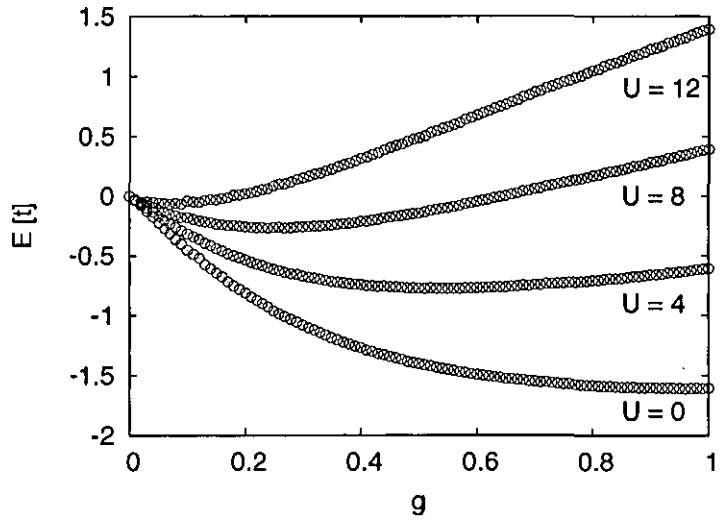

Figure 3.5: Total energy as a function of g, $E(g)$, for $U = 0, 4, 8, 12$, with the respective minima at $g = 1, 0.58, 0.24, 0.07$, on a half-filled 14x14 2D square lattice, again, the error bars are smaller than the point size

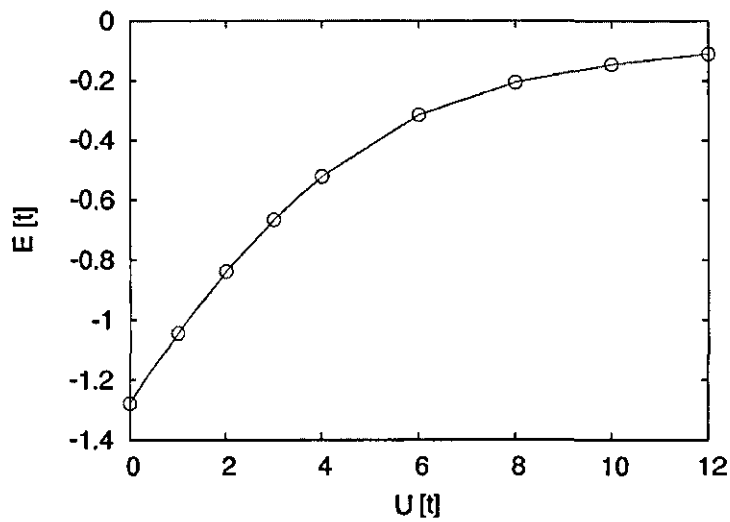

Figure 3.6: $E(U)$ for the half filled, 30 site, 1D system with a paramagnetic wavefunction, for the values of onsite repulsion $U = 0, 1, 2, 3, 4, 6, 8, 10, 12$ with minimum values at $g = 1, 0.86, 0.66, 0.56, 0.45, 0.29, 0.18, 0.14, 0.08$ respectively, note the errors are smaller than the points.

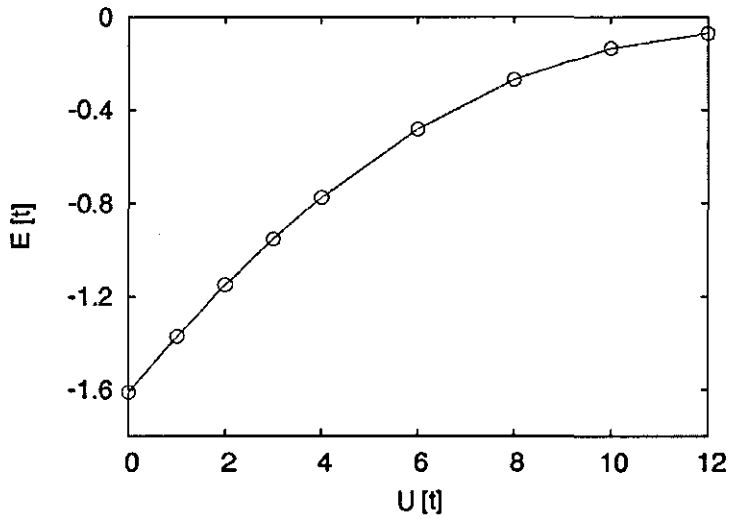

Figure 3.7: $E(U)$ for the half filled, 14x14 site. 2D system with a paramagnetic wave-function, for the values of onsite repulsion $U = 0, 1, 2, 3, 4, 6, 8, 10, 12$ with minimum values at $g = 1, 0.85, 0.71, 0.65, 0.57, 0.41, 0.27, 0.15, 0.07$ respectively, here the points are larger than the errors.

our results are close to the exact solution. However in the strong correlation regime there is a significant difference and an anti-ferromagnetic wave function [74] is likely to be closer to the exact result.

3.7 Antiferromagnetic Results

The next step in the development of the VMC code was to implement the anti-ferromagnetic trial function discussed earlier Eq(3.30). Our AFM results are detailed in this section.

The paramagnetic and anti-ferromagnetic energies $E(U)$ are compared for the 30 site 1D, Fig(3.9), 14x14 site 2D, Fig(3.10) and 6x6x6 site 3D, Fig(3.11) systems. In these graphs the data points are larger than the error bars. For all three systems an electron density $\rho = 1$ was used . In all cases for moderate and large values of U/t there is

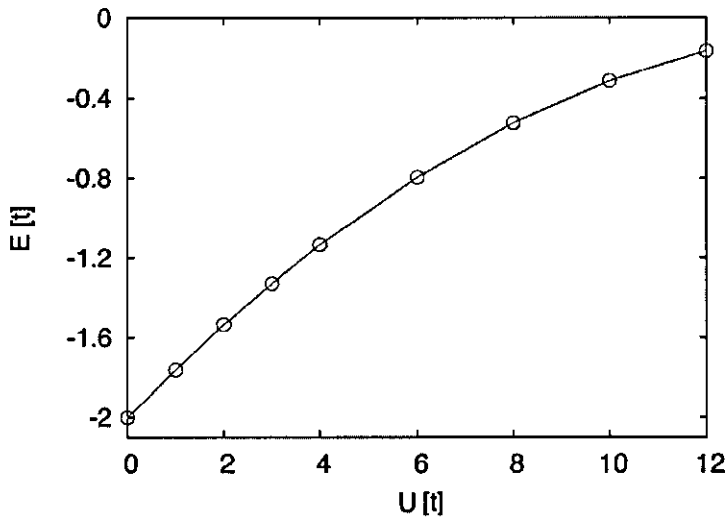

Figure 3.8: $E(U)$ for the half filled, 6x6x6, site 3D system with a paramagnetic wavefunction, for the values of onsite repulsion $U = 0, 1, 2, 3, 4, 6, 8, 10, 12$ with minimum values at $g = 1, 0.91, 0.78, 0.69, 0.58, 0.47, 0.38, 0.24, 0.15$ respectively, again error bars are within the points.

a lowering of energy due to the long range anti-ferromagnetic ordering. We present the variational parameters that minimise the energies for the various values of U/t in tables, (3.1), (3.2) and (3.3) for the 1, 2 and 3D systems respectively. Examining the variational parameters we see that as U increases so does the antiferromagnetic order Δ leading to a lowering of the kinetic and total energy.

Again our results agree with those of Yokoyama et al [68] and tend to the limiting case at $g = 1$. For the 1D state the VMC energies are higher than the exact energies by Leib [72], see Table(3.1), indicating that in the 1D system the AFM state is not the ground state.

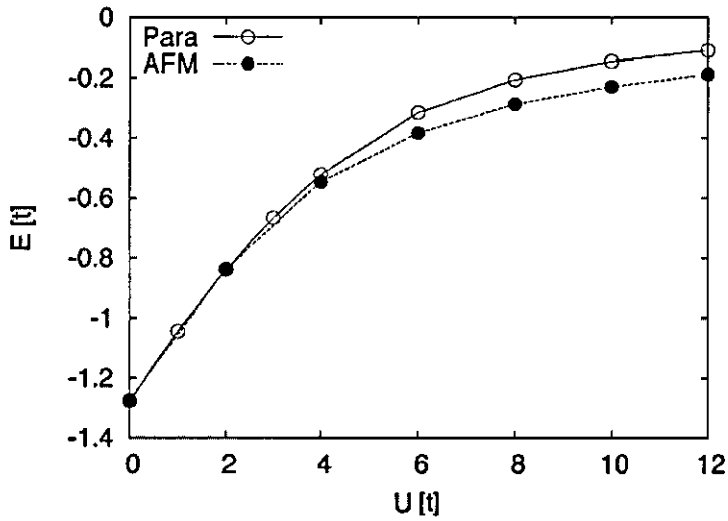

Figure 3.9: $E(U)$ for the 30 site 1D system with the paramagnetic and antiferromagnetic wave-functions.

Table 3.1: Variational and exact results for the half filled 1D 30 site antiferromagnetic system.

U/t	0	2	4	6	8	10	12
g	1.00	0.70	0.50	0.40	0.35	0.30	0.20
Δ	0	0.15	0.3	0.55	0.75	0.9	1.15
E/t (VMC)	-1.274	-0.837	-0.546	-0.383	-0.287	-0.229	-0.188
$\pm$	0.001	0.001	0.001	0.003	0.003	0.002	0.002
E/t (Exact)	-1.274	-0.847	-0.581	-0.423	-0.339	-0.266	-0.242

Table 3.2: Results for the half filled 2D 14x14 site antiferromagnetic system.

U/t	0	2	3	4	6	8	10	12
g	1.00	0.75	0.70	0.65	0.55	0.50	0.45	0.40
Δ	0	0.10	0.35	0.45	0.90	1.30	1.50	1.60
E/t (VMC)	-1.618	-1.170	-0.992	-0.842	-0.632	-0.493	-0.400	-0.335
$\pm$	0.001	0.001	0.001	0.003	0.003	0.002	0.002	0.002

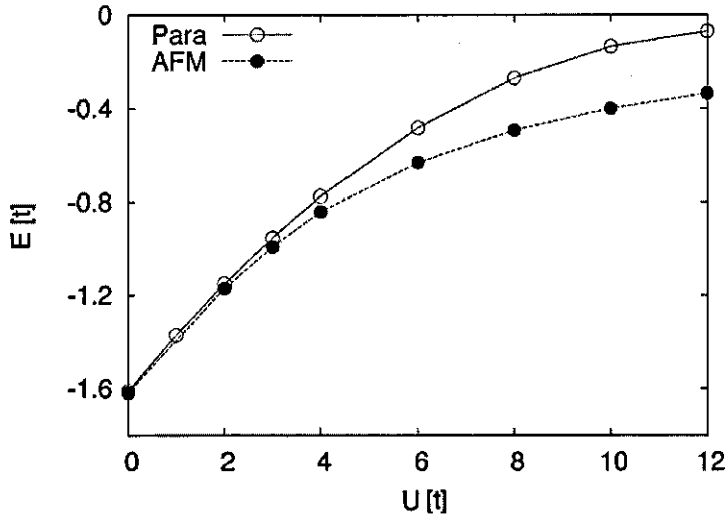

Figure 3.10: $E(U)$ for the 14x14 site 2D system with the paramagnetic and antiferromagnetic wave-functions.

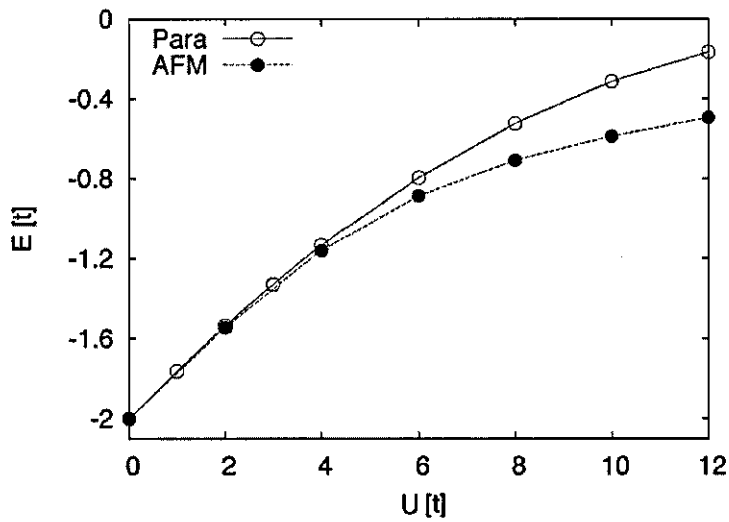

Figure 3.11: $E(U)$ for the 6x6x6 site 3D system with the paramagnetic and antiferromagnetic wave-functions.

Table 3.3: Results for the half filled 3D 6x6x6 site antiferromagnetic system.

U/t	0	2	4	6	8	10	12
g	1.00	0.80	0.65	0.60	0.60	0.535	0.525
Δ	0	0.15	0.35	0.80	1.50	1.80	2.40
E/t (VMC)	-1.998	-1.545	-1.160	-0.886	-0.708	-0.588	-0.495
$\pm$	0.002	0.002	0.005	0.005	0.003	0.004	0.005

3.8 Superconducting Results

Here we present our results using a superconducting wave function with s, $\Delta_{\mathbf{k}} = \Delta$, extended s, $\Delta_{\mathbf{k}} = \Delta(\cos \mathbf{k_x} + \cos \mathbf{k_y})$, and d, $\Delta_{\mathbf{k}} = \Delta(\cos \mathbf{k_x} - \cos \mathbf{k_y})$, wave order parameters, in an effort to determine the ground state of the Hubbard model. We use a 10x10 2D square lattice with 84 electrons, 42 spin-up and 42 spin-down and a value of $U/t = 8$. We then minimise the energy varying g and μ for a given value of Δ. Improvements to the efficiency of the code were made, the complexity of the trial wave function and corresponding increase in the parameter space, that needs to be searched to minimise the energy, means that the larger lattices used previously are no longer feasible.

Our results are presented in Fig(3.12). We repeat the findings of Yamaji *et al*: There is no superconducting state for the s and extended s wave order parameters and a minimum energy of $(-0.7375 \pm 0.0003)t$ per site at $\Delta = 0.08$ with a d-wave order-parameter. From this and the previous two paramagnetic and anti-ferromagnetic comparisons we conclude that our VMC method has been implemented correctly.

This leads to a condensation energy, $E(0) - E(\Delta)$, of $(0.0017 \pm 0.0006)t$ per electron. The wave function cannot handle $\Delta = 0$, it would always be zero, so here $E(0)$ refers to the energy at $\Delta = 0.01$. However as we know from Imada et al's results [24] because of finite size errors this condensation energy is overestimated. In fact the actual condensation energy may be much smaller and insufficient to explain the superconducting

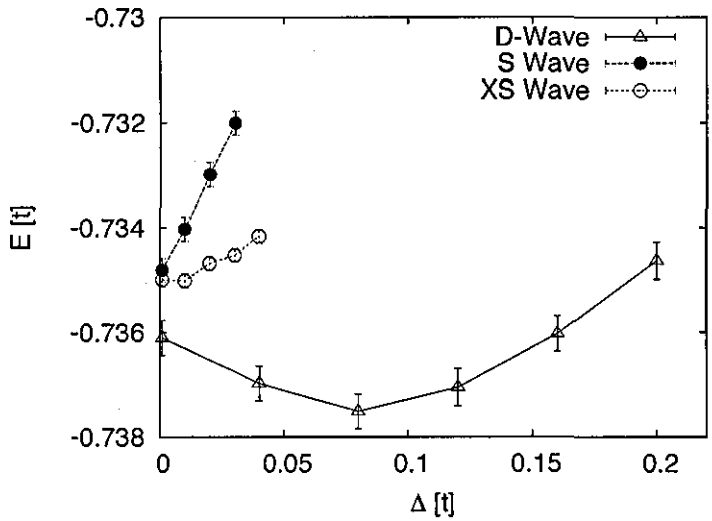

Figure 3.12: $E(\Delta)$ for the 10x10 site 2D system and 84 electrons with the superconducting wave-function. The minimum energy, $E = (-0.7375 \pm 0.0003)$ is found at $\Delta = 0.08$ with $g = 0.31$ and $\mu = -0.44$ for a d-wave order parameter.

state [24]. This implies that any theory for the high temperature superconductors must go beyond the Hubbard model.

Chapter 4

Superconductivity in the Hubbard-Fröhlich Model

In this chapter we present our results for the Hubbard-Fröhlich model. We use the VMC technique, discussed in chapter(3), to minimise the energy of the Hubbard-Fröhlich Hamiltonian, derived in section 4.2. Our main focus is on the optimally hole doped ($\delta \approx 16\%$) system where, experimentally, the highest transition temperatures have been recorded. In addition we present some results for other doping levels. The variational energies are also compared with those of static configurations to ensure the superconducting state is stable against the formation of immobile clusters.

Our results, for optimal doping, are presented in Ref [75] where we find that relatively small values of the EPI lead to sizeable increases in the condensation energy for a d-wave order parameter. By setting $U = \infty$, so the exchange term ($J = -4t^2/U = 0$) disappears, we find that the EPI alone is enough to induce a d-wave superconducting state. These results provide evidence that it is possible to account for high temperature superconductivity by combining strongly correlated electrons with an electron-phonon interaction.

4.1 Introduction

It is now over 20 years since the discovery of the first high temperature superconductor [11] and yet, despite intensive effort, the origin of the superconductivity remains fundamentally unknown, with no widely accepted theory. The lack of agreement on the relevant physics for the superconducting state in the cuprates and the recent discovery of a new class of superconducting materials with high transition temperatures, based on iron alloys [76], has re-emphasised the need to understand the superconducting mechanism in quasi-two-dimensional solids.

Using the local density approximation (LDA), it is frequently predicted that the EPI is negligible and too weak to account for the kink in the quasiparticle energy spectrum found with ARPES [77]. Because of this, many in the condensed matter community believe that, unlike in conventional superconductors, the EPI is unimportant for high temperature superconductors, see for example Ref [78]. Coupled with the Mott-Hubbard physics displayed by the undoped parent compounds, this has led a large number of researchers to hold the view that the simple repulsive Hubbard model would have the essential physics to account for the superconducting and non-Fermi-liquid normal states of cuprates. The idea behind this, originally proposed by Anderson [19], is that mobile hole pairs are created via a strong on-site repulsion, U. Results by Paramekanti *et al.* [20] and Yamaji *et al.* [21], using a variational Monte Carlo (VMC) simulation with a (projected) BCS-type trial wave function, appear to back this up. Also, using the VMC method, with a trial function that promotes virtual hopping processes, Yokoyama *et al* [79] found that superconductivity was present in a wide range of U. In addition work by Sorella *et al* using a Green Function MC technique for the $t - t' - J$ model [22] and earlier work using a combination of the VMC and Lanczos method [80] are also in agreement with these findings. Further support for superconductivity within the Hubbard model was provided by DMFT and DCA results; for a review see Ref. [81].

However recent studies by Aimi and Imada [24], using a Gaussian-Basis Monte Carlo

(GBMC) algorithm [82] indicate that the Hubbard model does not account for high-temperature superconductivity. These results state that errors, due to the small clusters causing finite-size effects, in the numerical studies mentioned in the previous paragraph lead to an overestimation of the condensation energies. Imada's remarkable result is not unique and previous numerical studies using the auxiliary-field quantum Monte Carlo [26] and constrained-path Monte-Carlo [27, 28] methods, all find no evidence for high temperature superconductivity in the Hubbard model. Furthermore, the validity of the Lanczos extrapolation used by Sorella *et al* [80] was questioned by Lee *et al* [83] who suggest that the robustness of the superconductivity was overestimated.

While there is still an on going debate about the presence of high temperature superconductivity in the Hubbard model, there is compelling evidence, from a number of experiments, for a significant EPI. The experimental evidence, described in more detail in section(1.2.2), includes; isotope effects [29, 30, 31], various high resolution ARPES studies [32, 33, 34, 35] and results finding polaronic charge carriers [36, 37, 38, 39]. Earlier numerical studies have shown that d-wave order can exist in EPI models [84] and other work has demonstrated that mobile bipolarons can exist [85, 86]. In this chapter we demonstrate that even a relatively weak long-range Fröhlich EPI [87] when combined with a strong Hubbard U leads to a substantial increase of the condensation energy in doped Mott-Hubbard insulators and/or strongly-correlated metals. In addition we find that the superconductivity persists even with an infinite Hubbard repulsion.

4.2 The Hubbard-Fröhlich model

The form of the electron-phonon Hamiltonian, discussed previously in section 2.4, is not suitable for our VMC algorithm in which only electrons are modelled. To perform the VMC simulation it is best to reduce the electron-phonon interaction to an effective

electron-electron interaction. Following Ref [88], the Lang-Firsov transformation is made to reduce a Coulomb-Fröhlich (CFM) model to an extended Hubbard model.

4.2.1 The canonical transformation

Canonical transformations can be used to transform from one set of eigenstates of a Hamiltonian to another set of eigenstates of a new Hamiltonian. Here we give a brief discussion of the canonical transformation for furtther details see Ref [15]. For a multi-particle set of eigenstates $|n\rangle$ the time independent Schrödinger equation is:

$$H|n\rangle = E_n|n\rangle. \tag{4.1}$$

Applying a unitary transformation to the eigenstates leads to a new set of eigenstates $|\tilde{n}\rangle = U|n\rangle$ leaving the eigenvalues unchanged. The new Hamiltonian is defined by $\tilde{H} = U^\dagger H U$ so that:

$$\tilde{H}|\tilde{n}\rangle = E_n|\tilde{n}\rangle. \tag{4.2}$$

For the new set of eigenstates to be orthonormal, $\langle n|n'\rangle = \langle\tilde{n}|U^\dagger U|\tilde{n}'\rangle = \delta_{n,n'}$ it is required that $U^\dagger = U^{-1}$. Here we use the Lang-Firsov transformation [89] in which the unitary transform is given by:

$$U = e^{-S} \tag{4.3}$$

where

$$S = \sum_{\mathbf{q},\mathbf{i}} \hat{n}_i[V_i^*(\boldsymbol{q})a_{\mathbf{q}}^\dagger - H.c.] \tag{4.4}$$

The transforms for the electron and phonon operators required in this particular problem are:

$$\begin{aligned} \tilde{c}_i &= e^S c_i e^{-S} \\ \tilde{a}_{\boldsymbol{q}} &= e^S a_{\mathbf{q}} e^{-S} \end{aligned} \tag{4.5}$$

By scaling all the matrix elements, $V_i^*(\boldsymbol{q})$, by the same amount $S \rightarrow \eta S$ and differentiating the transformed operators with respect to η the new operators can be simplified.

Differentiation of the operators results in the following equations:

$$\begin{aligned} \frac{\partial \tilde{c}_i}{\partial \eta} &= \sum_{\mathbf{q},\nu} e^{\eta S}[\hat{n}_i, c_i][V_i^*(\boldsymbol{q})a_{\mathbf{q}}^\dagger - V_i(\boldsymbol{q})a_{\boldsymbol{q}}]e^{-\eta S} \\ \frac{\partial \tilde{a}_{\mathbf{q}}}{\partial \eta} &= \sum_i e^{\eta S}\hat{n}_i V_i^*(\boldsymbol{q})[a_{\boldsymbol{q}}^\dagger, a_{\boldsymbol{q}}]e^{-\eta S}. \end{aligned} \tag{4.6}$$

By making use of the commutation relations $[\hat{n}_i, c_i] = -c_i$, $[a_{\boldsymbol{q}}^\dagger, a_{\boldsymbol{q}}] = -1$ and $[\hat{n}_i, S] = 0$ the differentials become:

$$\begin{aligned} \frac{\partial \tilde{c}_i}{\partial \eta} &= -\tilde{c}_i \sum_{\mathbf{q}} [V_i^*(\boldsymbol{q})a_{\mathbf{q}}^\dagger - V_i(\boldsymbol{q})a_{\boldsymbol{q}}] \\ \frac{\partial \tilde{a}_{\mathbf{q}}}{\partial \eta} &= -\sum_i \hat{n}_i V_i^*(\boldsymbol{q}) \end{aligned} \tag{4.7}$$

Applying the boundary conditions $\tilde{a}_{\mathbf{q}} = a_{\mathbf{q}}$ and $\tilde{c}_i = c_i$ when $\eta = 0$ the solutions to the differentials are:

$$\begin{aligned} \tilde{c}_i &= c_i e^{\eta \sum_{\mathbf{q}} [V_i(\boldsymbol{q})a_{\mathbf{q}} - V_i^*(\boldsymbol{q})a_{\mathbf{q}}^\dagger]} \\ \tilde{a}_{\boldsymbol{q}} &= a_{\mathbf{q}\nu} - \eta \sum_i \hat{n}_i V_i^*(\boldsymbol{q}). \end{aligned} \tag{4.8}$$

4.2.2 Applicability of the canonical transformation

The EPI radius determines both the size of the charge carrier mass renormalization and the range in which the weak and strong-coupling expansions are valid. Using the Holstein model a very large effective charge carrier mass is predicted which leads to immobile pairs. However the carrier mass calculated with a continuous-time QMC [90] algorithm for a Fröhlich EPI in the relevant region of $\hbar\omega/t$ ratio was found to be several orders of magnitude smaller. The Lang-Firsov transformation is exact but the subsequent averaging over the phonons is approximate; It is found that the carrier mass determined by experiment is well characterised by an exponential term very similar to the exponent from the Lang-Firsov transformation for any value of the EPI, so its application here is valid.

4.2.3 Application of the canonical transformation

For the purposes of this thesis the full Coulomb interaction is not required so the CFM is simplified slightly to the Hubbard-Fröhlich model (HFM). Our HFM contains the usual nearest-neighbour electron hopping, t_{ij}, and electron-electron on-site repulsive correlations, U, from the Hubbard model. We then add two terms to the standard Hubbard model; a term to describe lattice ions with mass, M, vibrating with frequency, ω, and a term to describe the long-range effect of the lattice vibrations on the electrons. The HFM then takes the form of;

$$\hat{H}_{HFM} = \sum_{ij} t_{ij}(\tilde{c}^{\dagger}_{i\uparrow}\tilde{c}_{j\uparrow}+\tilde{c}^{\dagger}_{i\downarrow}\tilde{c}_{j\downarrow})+U\sum_{i}\hat{n}_{i\uparrow}\hat{n}_{i\downarrow}+\sum_{m}\left[\frac{\hat{P}^2_m}{2M}+\frac{\xi^2_m M\omega^2}{2}\right]-\sum_{mn\sigma} f_m(n)\tilde{c}^{\dagger}_{n\sigma}\tilde{c}_{n\sigma}\xi_m \tag{4.9}$$

Here $c^{\dagger}_{\mathbf{n}\sigma}$ and $c_{\mathbf{n}\sigma}$are the usual electron creation and annihilation operators, $\hat{P}_{\mathbf{m}} = -i\hbar\partial/\partial\xi_{\mathbf{m}}$ is the quantum momentum operator for an ion at site $\mathbf{m}$ with a displacement $\xi_{\mathbf{m}}$ and $f_{\mathbf{m}}(\mathbf{n})$ is a force function to describe the long-range Fröhlich type interaction. The force function is used to describe the interaction of an ion on site $\boldsymbol{m}$ and electron on site $\boldsymbol{n}$ and given by:

$$f_m(n) = \frac{\kappa}{[(m-n)^2+1]^{3/2}} e^{-\frac{|m-n|}{R_{sc}}} \tag{4.10}$$

where R_{sc} is the screening length. In the results presented here we use $R_{sc} = \infty$ so the exponential term can be removed.

Using optical data for cuprate superconductors it is estimated that the Fröhlich EPI, Eq.(4.10), is of the order of 1eV [87] and therefore of a comparable size to the hopping integral. Despite such a substantial EPI it is still ignored in the Hubbard U and t–J, RVB models of high temperature superconductors [78]. As with the coulomb interaction the EPI in-plane is highly screened by the mobile electrons. Thus, here, the force function describes the interaction between electrons and phonons polarised in the c-axis where screening is much smaller due to the high out-of-plane resistivity.

From the discussion on electron-phonon interactions in section 2.4 it is known that the

atomic part of the Hamiltonian in real space is of the following form:

$$\hat{H}_{e-ph} = -\omega \sum_{ij} g_{ij} \tilde{c}_i^\dagger \tilde{c}_i (\tilde{a}_j + \tilde{a}_j^\dagger) + \omega \sum_j (\tilde{a}_j^\dagger \tilde{a}_j + \frac{1}{2}) \tag{4.11}$$

For simplicity the force function has been replaced with a dimensionless interaction proportional to the force

$$g_{ij} = \frac{f_{ij}}{\omega\sqrt{2M\omega}}. \tag{4.12}$$

The Lang-Firsov transformation makes the following new operators, Eq(4.8) with $\eta = 1$:

$$\begin{aligned} \tilde{a}_j^\dagger &= a_j^\dagger + \textstyle\sum_i g_{ij} n_i \qquad & \tilde{c}_i^\dagger &= c_i^\dagger \exp\Big[\sum_j g_{ij}(a_j^\dagger - a_j)\Big] \\ \tilde{a}_j &= a_j + \textstyle\sum_i g_{ij} n_i \qquad & \tilde{c}_i &= c_i \exp\Big[-\sum_j g_{ij}(a_j^\dagger - a_j)\Big]. \end{aligned} \tag{4.13}$$

Since the exponential terms from the electron operators cancel, applying the transformation to the Hamiltonian leads to:

$$\hat{H}_{e-ph} = -\omega \sum_{ij} g_{ij} c_i^\dagger c_i (a_j + a_j^\dagger + \sum_{i'} 2 g_{i'j} n_{i'}) + \omega \sum_j \Big[(a_j^\dagger + \sum_i g_{ij} n_i)(a_j + \sum_{i'} g_{i'j} n_{i'}) + \frac{1}{2}\Big] \tag{4.14}$$

It is easy to see the terms with both electron and phonon operators cancel and the Hamiltonian reduces to:

$$\hat{H}_{e-ph} = -\omega \sum_{ii'} n_i n_{i'} \sum_j g_{ij} g_{i'j} + \omega \sum_j (a_j^\dagger a_j + \frac{1}{2}). \tag{4.15}$$

Substitution of the Lang-Firsov operators into the electronic part of the Hamiltonian gives:

$$\begin{aligned} \hat{H}_{tb} &= \sum_{ii'} t_{ii'} \exp\Big[\sum_j g_{ij}(a_j^\dagger - a_j) - g_{i'j}(a_j^\dagger - a_j)\Big] c_I^\dagger c_{i'} \\ &= \sum_{ii'} t_{ii'} \exp\Big[-\sum_j (g_{ij} - g_{i'j}) a_j + \sum_j (g_{ij} - g_{i'j}) a_j^\dagger\Big] c_I^\dagger c_{i'} \end{aligned} \tag{4.16}$$

where we have made the of the identity, $e^A e^B e^{-[A,B]/2} = e^{A+B}$, to combine the exponentials. To simplify this expression further further we make use of the identity again. Let

$A = -\sum_j (g_{ij} - g_{i'j}) a_j$ and $B = \sum_j (g_{ij} - g_{i'j}) a_j^\dagger$, remembering the commutation relation for Bosons $a_i^\dagger a_j - a_j a_i^\dagger = \delta_{ij}$ so that the commutator is $[A, B] = -\sum_j (g_{ij} - g_{i'j})^2$. Expanding the commutator $[A, B] = -\sum_j g_{ij}^2 + g_{i'j}^2 - 2 g_{ij} g_{i'j}$. Introducing the function:

$$\Phi(\mathbf{n} - \mathbf{n}') = \sum_{\mathbf{m}} f_{i,m} f_{j,m}, \tag{4.17}$$

that defines the interaction between two electrons i and j, allows the renormalized hopping integral to be defined as:

$$\tilde{t}_{ii'} = t_{ii'} \exp\Big[-\frac{\lambda W}{\omega} \Big(1 - \frac{\Phi(\mathbf{i}, \mathbf{i})}{\Phi(0,0)} \Big) \Big] \exp\Big[\sum_j (g_{ij} - g_{i'j}) a_j^\dagger \Big] \exp\Big[-\sum_j (g_{ij} - g_{i'j}) a_j \Big] \tag{4.18}$$

where we have defined $\lambda = \Phi_{0,0}/2M\omega^2$. The last two exponential terms are 1, when they are averaged over phonons at T=0, so that for our purposes the hopping integral becomes:

$$\tilde{t}_{ii'} = t_{ii'} \exp\Big[-\frac{\lambda W}{\omega} \Big(1 - \frac{\Phi(\mathbf{i}, \mathbf{i})}{\Phi(0,0)} \Big) \Big]. \tag{4.19}$$

The exponential terms from the transformation for the Hubbard repulsion cancel as the electrons are on the same site but it is renormalized due to the polaron energy shift, $\tilde{U} = U - 2E_p$ where $E_p = 1/2M\omega^2 \sum_j f_{0j}^2 = \Phi(0,0)/2M\omega^2$. Combining the above terms the Hubbard-Fröhlich Hamiltonian is obtained:

$$\tilde{H} = \sum_{\mathbf{n} \neq \mathbf{n}', \sigma} \tilde{t} c_{\mathbf{n}'\sigma}^\dagger c_{\mathbf{n}\sigma} + \tilde{U} \sum_{\mathbf{n}} \hat{n}_{\mathbf{n}\uparrow} \hat{n}_{\mathbf{n}\downarrow} - \lambda W \sum_{\mathbf{n} \neq \mathbf{n}', \sigma\sigma'} \Phi(\mathbf{n} - \mathbf{n}') \hat{n}_{\mathbf{n}'\sigma'} \hat{n}_{\mathbf{n}\sigma}. \tag{4.20}$$

Here the renormalized hopping integral is given by $\tilde{t} = t \exp[-g^2(\mathbf{n})]$, with $g^2(\mathbf{n}) = [E_p - \lambda W \Phi(\mathbf{n})]/\hbar\omega$, $\Phi(\mathbf{n}) = \kappa^{-2} \sum_{\mathbf{m}} f_{\mathbf{m}}(\mathbf{0}) f_{\mathbf{m}}(\mathbf{n})$, $\tilde{U} = U - 2E_p$, $W = z\tilde{t}(a)$ is the renormalized half-bandwidth, z is the co-ordination number and $\lambda = \kappa^2/2M\omega^2 W$ is proportional to the conventional BCS electron-phonon coupling constant. Because it is proportional to the single-particle density of states (DOS), which is effected by the presence of a van-Hove singularity and the increase of the carrier mass due to electron correlations, our λ may be larger than that of the BCS theory. The polaronic shift, $E_p = (\kappa^2/2M\omega^2)\Phi(\mathbf{0})$, of atomic levels is included in the chemical potential. In the following only nearest-neighbour hops are allowed. The results by Bonča and Trugman

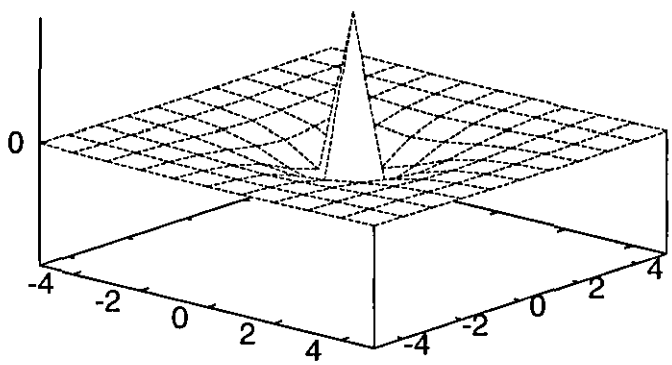

Figure 4.1: The interaction between two electrons as a function of relative lattice position

[86] state that 94% of the EPI energy in Eq.(4.10) comes from the first two sites , so that taking $R_{sc} = \infty$ in our simulations, to eliminate the dependence of the force function on the exponent, has little effect. In fig(4.1) we plot, schematically, the effective inter-electron interaction against the electron separation; when the electrons are on the same site this is a repulsive interaction due to the Hubbard U, the EPI causes an attraction, that diminishes rapidly, between electrons on different sites. Note that the EPI also causes an attraction between electrons on the same site but the Hubbard U dominates.

4.2.4 Studying the Hubbard-Fröhlich model

For a strong EPI, $\lambda \gg 1$, the perturbation theory can be used, expanding in terms of $1/\lambda$, to reduce the many polaron problem to a charged Bose-gas of small mobile bipolarons [87]. In the intermediate and weak coupling regime, $\lambda \lesssim 1$ with large $\tilde{U}$, as in the current context, the variational method can be applied. Here we use a standard VMC method as for example in Ref. [20] to minimise the energy $\langle\Psi|\tilde{H}|\Psi\rangle/\langle\Psi|\Psi\rangle$ of the HFM. The differnece is that our Hubbard-Fröhlich Hamiltonian requires we make an additional measurement of the long-range attraction in the extended Hubbard Hamiltonian, Eq.(4.20).

The superconducting trial function

A BCS type trial wave-function, as discussed in detail in section 3.5.1 is used, which has the form:

$$|\Psi_T\rangle = P_N P_G \prod_{\mathbf{k}} (u_{\mathbf{k}} + v_{\mathbf{k}} c^{\dagger}_{\mathbf{k}\uparrow} c^{\dagger}_{-\mathbf{k}\downarrow})|0\rangle, \tag{4.21}$$

where $P_N = \delta_{\sum_i \hat{n}_{i,N}}$ projects onto a fixed particle number state and $P_G = \prod_{\mathbf{n}}[1-(1-g)\hat{n}_{\mathbf{n}\uparrow}\hat{n}_{\mathbf{n}\downarrow}]$, $0 \leq g \leq 1$, suppresses double occupancy [21]. Our variational parameters are g and the chemical potential, μ, that enters through the kinetic energy, $\xi_{\mathbf{k}} \equiv \tilde{t}(\cos k_x + \cos k_y) - \mu$, via $u^2_{\mathbf{k}} = (1 + \xi_{\mathbf{k}}/\sqrt{\xi^2_{\mathbf{k}} + \Delta^2_{\mathbf{k}}})/2$ and $v^2_{\mathbf{k}} = (1 - \xi_{\mathbf{k}}/\sqrt{\xi^2_{\mathbf{k}} + \Delta^2_{\mathbf{k}}})/2$.

4.3 Results

We now present our results for the HFM. Due to the quasi-2D nature of the superconductivity in the cuprates we restrict our results to a 2D lattice, although the method is applicable to 1D and 3D lattices as well. We obtain our results by varying the parameters to minimise the total energy, of the Hubbard Fröhlich Hamiltonian for values of the electron density ρ, $\tilde{U}$, superconducting order parameter $\Delta_{\mathbf{k}}$ and λ keeping $\tilde{t} = 1$

and $a = 1$. For a certain electron density and order parameter Δ the minimum energy is then found by running simulations within the 2d parameter space that consists of the variational parameters g and μ. Once the minimum energies for each Δ have been found then the corresponding condensation energies can be computed.

4.3.1 Optimal Doping

Here we refer to optimal doping as the level of doping found experimentally to produce the highest transition temperature, it does not indicate optimal doping in our results. We place 42 spin-up and 42 spin-down electrons on a 10×10 2D square lattice, keeping the electron density fixed at $\rho = 0.84$ in this section, to simulate optimal doping and allow direct comparison with Yamaji's results [21]. Two cases are investigated: a) an on-site repulsion $\tilde{U} = 8$, and b) an infinite $\tilde{U}$ is used to see if the attraction induced by EPI, alone, is enough for high temperature superconductivity. The results for $U = 8$ and $\lambda = 0$ are used for comparison with the results of Ref. [21]. It should be noted that here the condensation energy of electron pairs is computed which is not a direct indication of the transition temperature.

We examine the d-wave $\Delta_{\mathbf{k}} = \Delta(\cos k_x - \cos k_y)$, extended s-wave $\Delta_{\mathbf{k}} = \Delta(\cos k_x + \cos k_y)$ and s-wave $\Delta_{\mathbf{k}} = \Delta$ order parameters. For reasons detailed in chapter 3, periodic boundary conditions in one direction and anti-periodic boundary conditions in the other are used. The value of λ is varied to study the effect of increasing EPI and we find the value of Δ at which the minimum energy occurs. We also measure the energy of clustered states to ensure our results are stable against the formation of immobile clusters. In our results all energies quoted are *per electron*; note that Yamaji *et al.* [21] use energy per site. In the following results, all energies are quoted in units of $\tilde{t}$, the renormalized hopping integral.

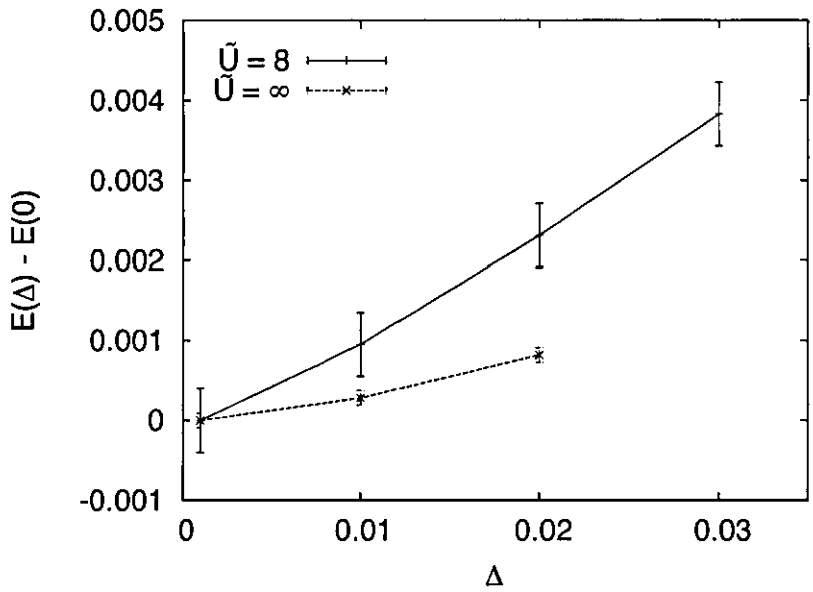

Figure 4.2: Condensation energy per electron (in units of $\tilde{t}$) versus the amplitude of the superconducting s-wave order-parameter (top) for $\tilde{U} = \infty$ and $\tilde{U} = 8$, showing no s-wave ground state for λ up to 0.075.

S-wave order parameter

Here we present our results for the HFM using an s-wave order parameter. After determining the minimum energies $E(\Delta)$ we plot these energies relative to the the normal state energy $E(0)$. Firstly we examine the $\tilde{U} = 8$ and find no s-wave state for values up to $\lambda = 0.075$, fig(4.2). When the exchange term is zero with $\tilde{U} = \infty$ again no s-wave state is found, fig(4.2). In both cases a graph of energy against Δ produces a curve with a positive gradient. We conclude that the addition of the EPI does not lead to a superconducting state so that neither the HFM or HM, see fig(3.12), have s-wave superconductivity.

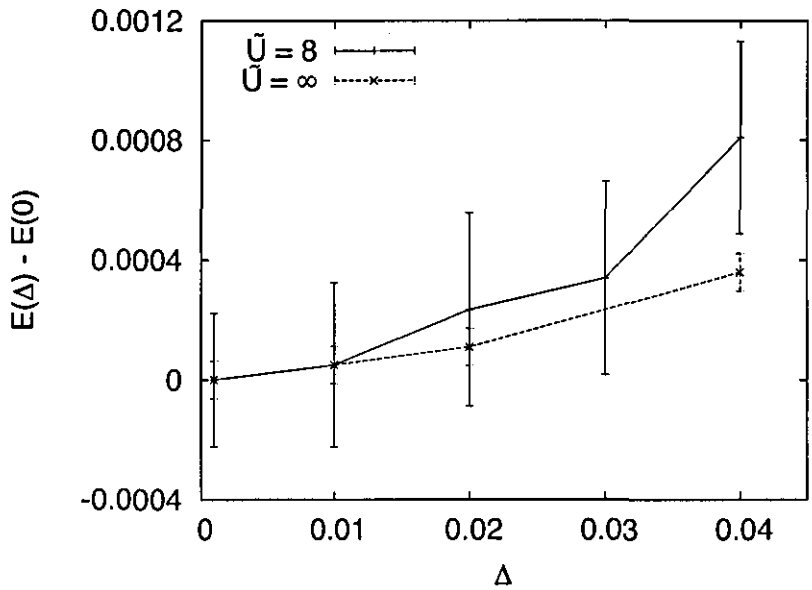

Figure 4.3: The condensation energy versus the amplitude of the extended s-wave order-parameter (bottom) for $\tilde{U} = \infty$ and $\tilde{U} = 8$, showing no extended s-wave ground state.

Extended s-wave order parameter

We now examine the same systems for the extended s-wave order parameter. For the $\tilde{U} = 8$ case again no superconducting state is found up to $\lambda = 0.075$, fig(4.3). With $\tilde{U} = \infty$ we do not find an extended s-wave superconductor, fig(4.3). Again we conclude, from the positive gradients, that the addition of the EPI to the Hubbard model does not induce an extended s-wave, superconducting, ground state.

D-wave order parameter

This section details the results for the d-wave order parameter on the HFM with optimal filling. We find that increasing λ leads to an increase in the condensation energy $E(0) - E(\Delta)$ for both $\tilde{U} = 8$ and $\tilde{U} = \infty$.

For the $\lambda = 0$ and $\tilde{U} = 8$ case shown in Fig.4.4, we recover Yamaji's result [21] with

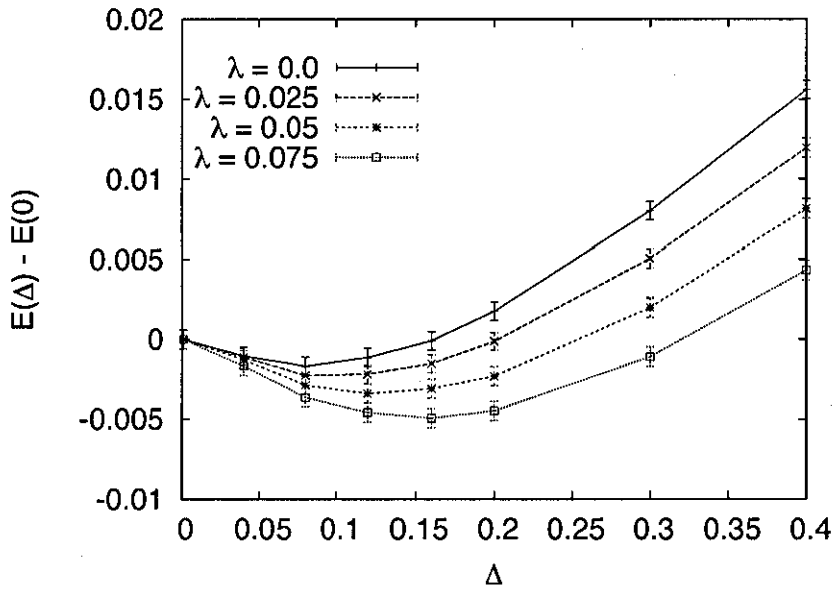

Figure 4.4: The energy, $E(\Delta)$, per electron relative to the normal state energy (in units of $\tilde{t}$) versus the amplitude of the superconducting d-wave order-parameter for $\tilde{U} = 8$, with different EPI coupling, λ.

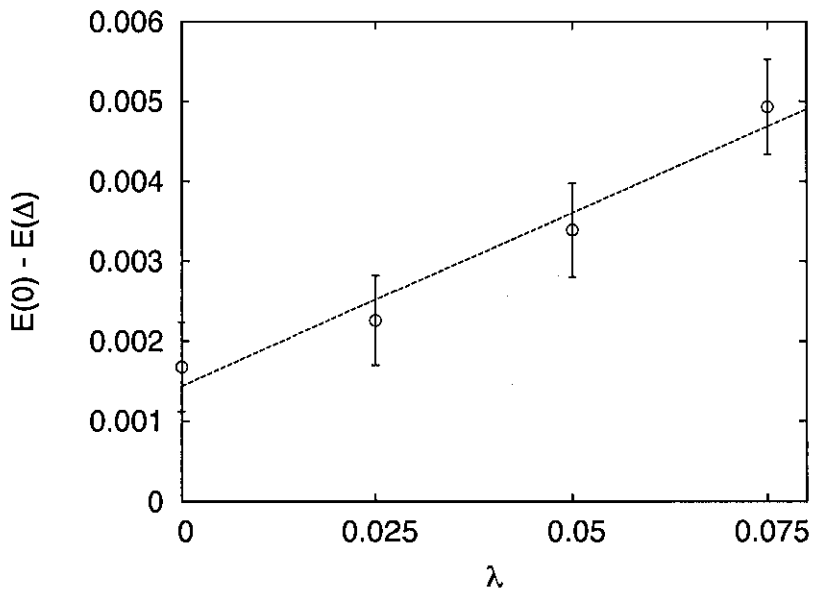

Figure 4.5: Condensation energy, $E(0) - E(\Delta)$, against λ with $\tilde{U} = 8$ with a line of best fit.

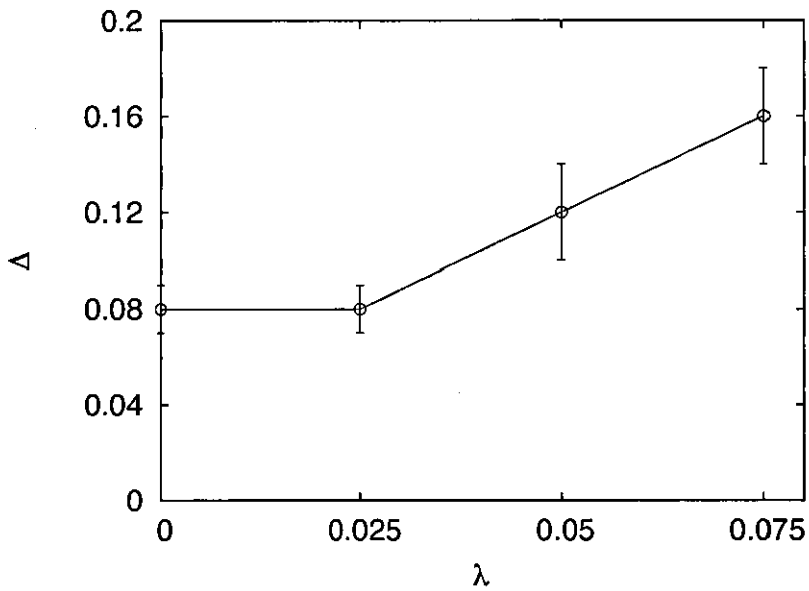

Figure 4.6: The value of the order parameter, Δ, at which the minimum energy occurs against λ with $\tilde{U} = 8$

a minimum at $\Delta \approx 0.08$ and energy per electron of (-0.8780 ± 0.0004), the normal state energy is (-0.8763 ± 0.0004). It can clearly be seen that the effect of increasing the EPI is to increase the depth of the minimum and therefore the stability of the superconducting state. Our minimum energy per electron is (-4.4012 ± 0.0004) at $\Delta = 0.16$ and $\lambda = 0.075$ and our normal state energy, with $\lambda = 0.075$, is (-4.3963 ± 0.0004). The maximum condensation energy gain, $E(0) - E(\Delta)$, with $\lambda = 0$ is (0.0017 ± 0.0006) and (0.0049 ± 0.0006) per electron with $\lambda = 0.075$.

To clarify the influence of the EPI we also plot the condensation energy, $E(0) - E(\Delta)$ fig(4.5) against λ. The effect of increasing the strength of the EPI is to increase the condensation energy, the energy required to break paired electrons, thus increasing the stability of the d-wave superconductivity. A straight line fit, with a gradient of 0.043 ± 0.006 and intercept at 0.0014 ± 0.0003 has also been included in fig(4.5) that indicates a possible linear dependance of the condensation energy on λ. For a more definite relationship between the condensation energy and EPI more data is required

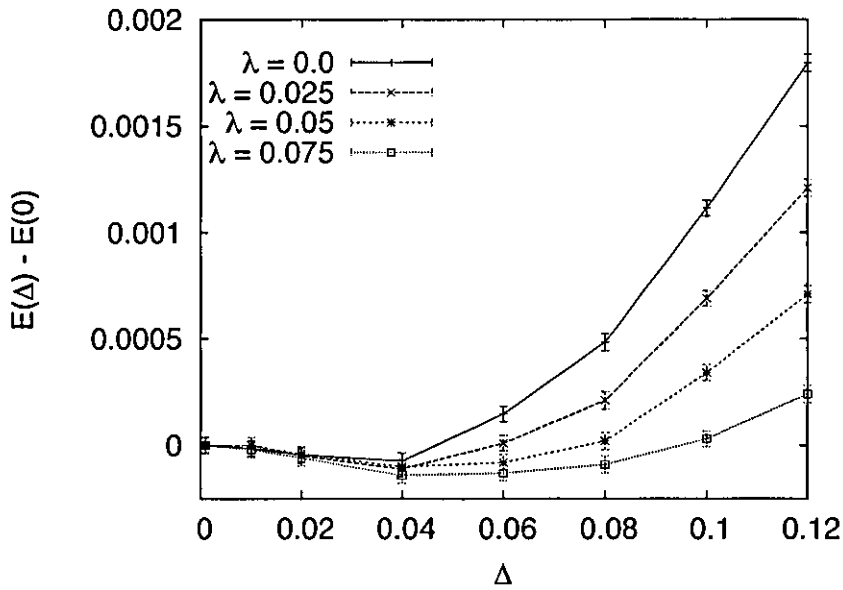

Figure 4.7: The energy, $E(\Delta)$, per electron relative to the normal state energy (in units of $\tilde{t}$) versus the amplitude of the superconducting d-wave order-parameter for $\tilde{U} = \infty$, with different EPI coupling, λ.

over a wider range of EPI strengths. In addition we plot the minimised order parameter Δ against λ. We find that the order parameter also increases with the EPI. A smoother curve of Δ against λ could be achieved by sampling with a smaller Δ step size; as it is there is not enough data to determine a relationship.

Next we examine the Hubbard-Fröhlich with $U = \infty$ and find an unexpected result. With no EPI this is equivalent to a t-J model with no anti-ferromagnetic exchange, $|J| = 4t^2/U = 0$, to drive a superconducting state. In this case the trial function used in Ref [79], which promotes virtual hoping processes, will have no effect and will not qualitatively change our result. Fig.4.7 shows an increasing condensation energy gain with λ for $\tilde{U} = \infty$: the condensation energy gain is (0.00014 ± 0.00004) per electron at $\Delta = 0.04$ for $\lambda = 0.075$. While this energy gain is not large enough to guarantee stability against other trial wave functions and finite size effects, it does suggest a d-wave superconducting state exists for $\tilde{U} = \infty$ with a large enough λ. This implies

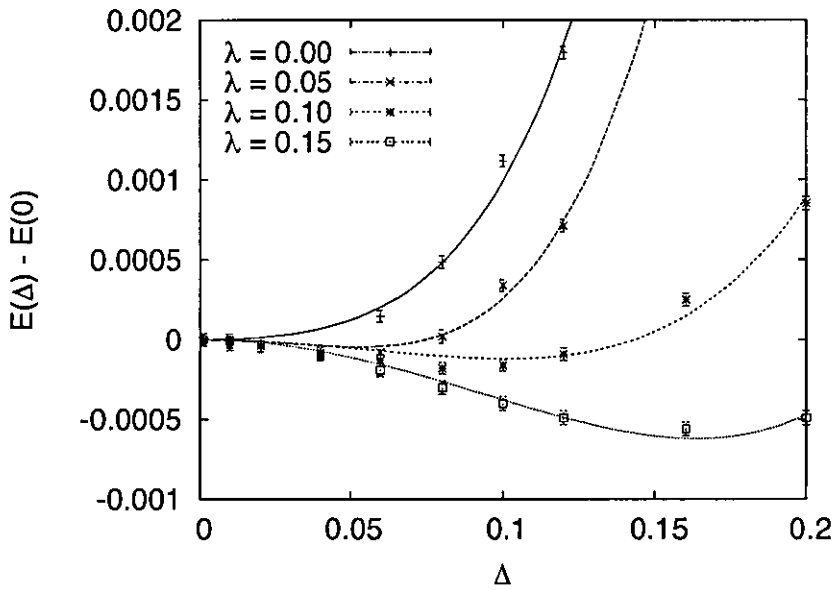

Figure 4.8: The energy, $E(\Delta)$, per electron relative to the normal state energy (in units of $\tilde{t}$) versus the amplitude of the superconducting d-wave order-parameter for $\tilde{U} = 8$, with different EPI coupling, λ.

a d-wave superconducting state can be formed without spin fluctuations. In order to achieve more significant condensation energies stronger EPI have been studied.

In fig(4.8) we plot the condensation energy against the amplitude of the order parameter for stronger EPI. With $\lambda = 0.15$ the minimum energy is found to be -7.5517 ± 0.00003 at $\Delta = 0.16$. From this we calculate a maximum condensation energy of 0.00056 ± 0.00004. From this data we can conclude that the inclusion of the EPI allows the formation of a d-wave superconducting state without the need for spin fluctuation.

Fig(4.8) also includes curves of the form $ax^2 + bx^4$ to parameterise the data. The coefficients a and b have been used to analytically determine the minimum energies. As expected, the $\lambda = 0$ curve shows no superconducting order. The analytic results are used to examine the dependence of the condensation energy, fig(4.9), and Δ, fig(4.10) on the strength of the EPI. With the inclusion of stronger electron-phonon interactions, up to $\lambda = 0.015$, it is clear that the condensation energy increases with a non-linear

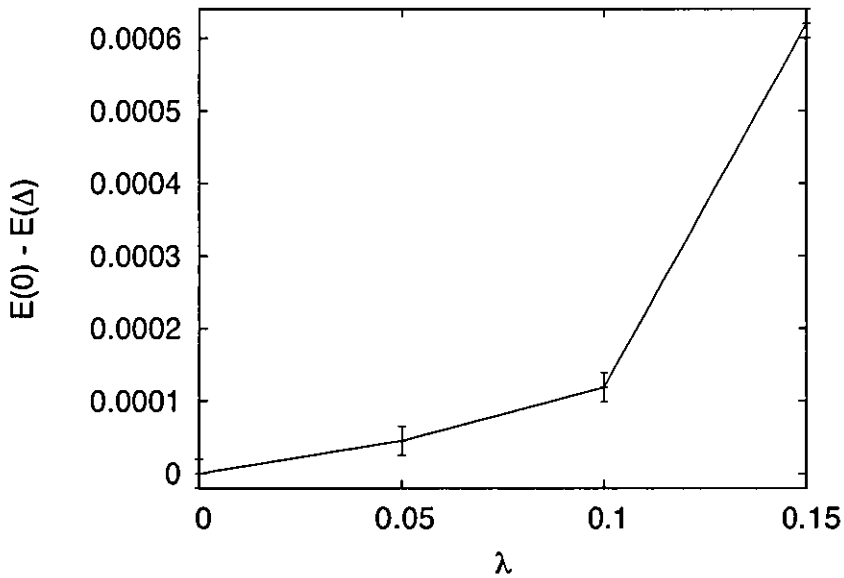

Figure 4.9: Condensation energy, $E(0) - E(\Delta)$, against λ with $\tilde{U} = \infty$.

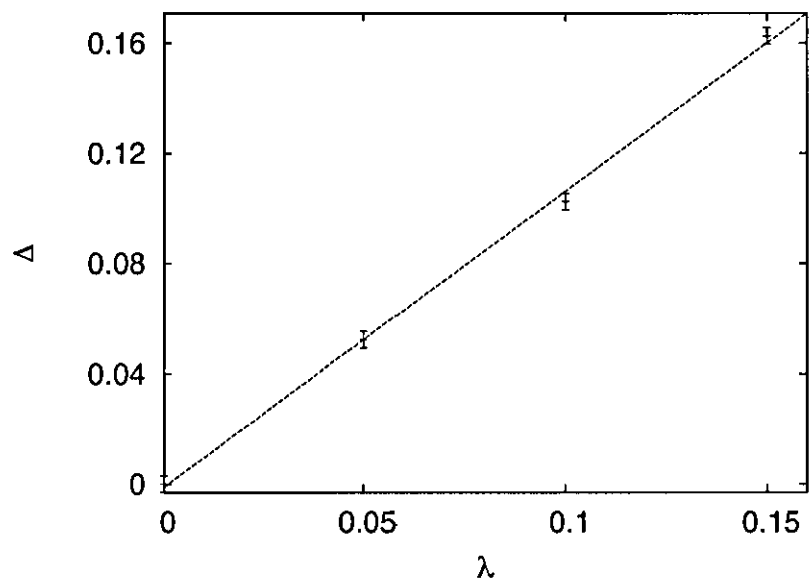

Figure 4.10: The value of the order parameter, Δ, at which the minimum energy occurs against λ with $\tilde{U} = \infty$

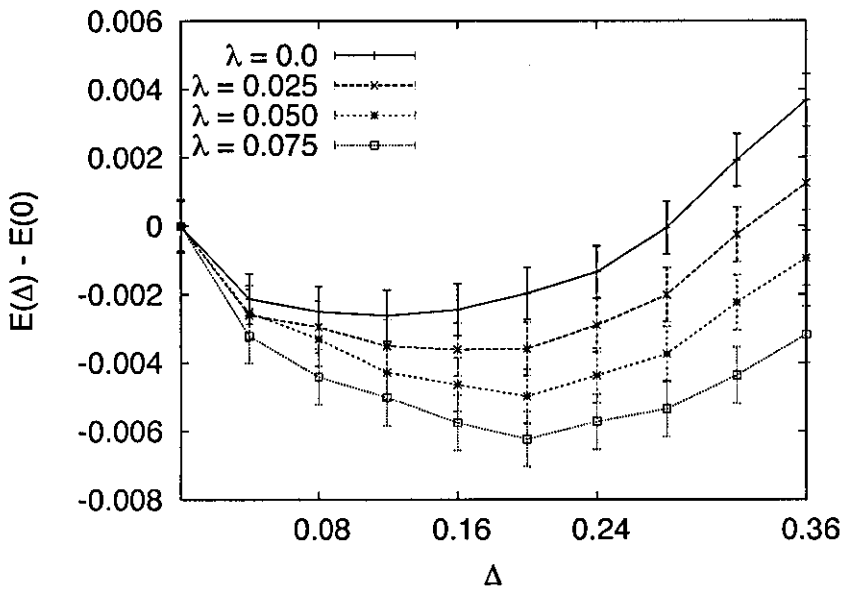

Figure 4.11: The energy, $E(\Delta)$, per electron relative to the normal state energy (in units of $\tilde{t}$) versus the amplitude of the superconducting d-wave order-parameter for $\tilde{U} = 8$ and hole density $x = 0.1$, with different EPI coupling, λ.

dependence on λ. Fitting a quadratic or higher order polynomial with so few data points was considered inappropriate. From fig(4.10) it is seen that in this range the effect of increasing λ is to increase the amplitude of the superconducting order parameter; this is further evidence supporting our conclusion that including an EPI stabilises the superconducting state. A straight line with gradient 1.08 ± 0.03 and intercept -0.001 ± 0.003 has been included in fig(4.10).

4.3.2 The under doped regime

We now examine the under doped regime where less holes are injected so the electron density is higher. The simulations were performed with $\tilde{U} = 8$, $\lambda = 0.0, 0.025, 0.05, 0.075$ with 90 electrons on a 10x10 lattice to model a hole density of 10%. For this doping level only the d-wave order parameter is examined.

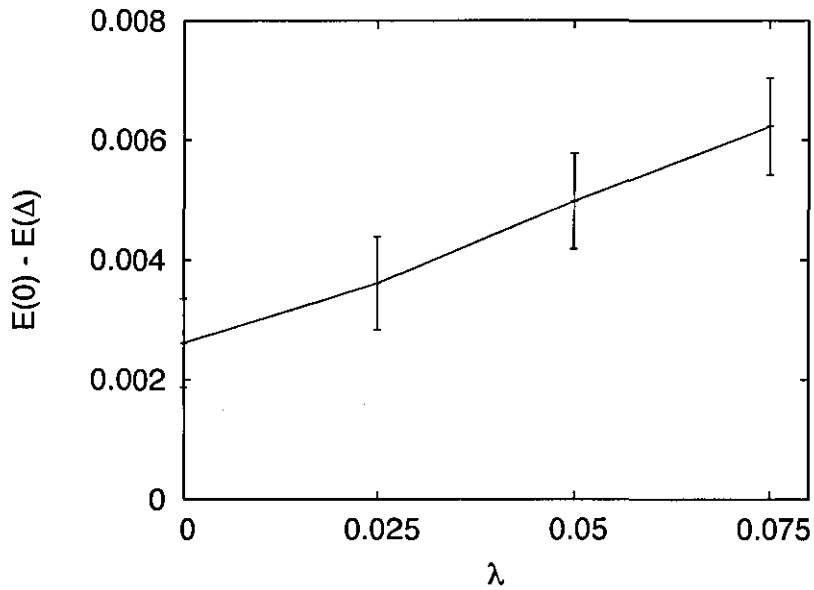

Figure 4.12: The condensation energy, $E(0) - E(\Delta)$, against λ for the under-doped lattice.

From fig(4.11) it can be seen that the EPI increases the condensation energy. With no EPI there is a condensation energy of 0.0028 ± 0.0007. When the EPI is included our lowest energy was -4.4553 ± 0.0006 for $\lambda = 0.075$ at $\Delta = 0.2$ and results in a condensation energy of -0.0062 ± 0.0008. Here the error bars are large and further data gathering is recommended for future work.

The effects of increasing λ on the condensation energy and order parameter are examined in figures 4.12 and 4.13. Plotting the maximum condensation energies against λ, fig(4.12), shows that the condensation energy increases with the the strength of the EPI. In fig(4.13) it can be seen that increasing the strength of the EPI increases the size of the order parameter Δ.

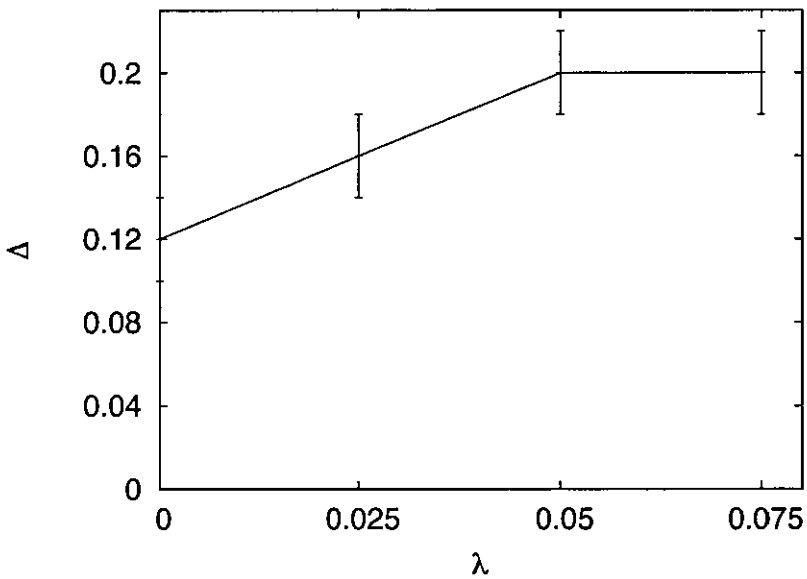

Figure 4.13: Δ against λ for the under-doped lattice.

4.3.3 The over-doped regime

In this section results for the over doped regime are presented i.e a lower electron density. We repeat our simulations using the same values, $\tilde{U} = 8$ and $\lambda = 0.0, 0.025, 0.05, 0.075$ but adjust the number of electrons to 78 so the hole density is 22%. As with the under-doped lattice only the d-wave order-parameter results are presented.

For this hole density again it is found that the EPI enhances the condensation energy, see fig(4.14). With no EPI the condensation energy is 0.0006 ± 0.0007 indicating longer simulations are required to reduce errors and enable clear conclusions to be drawn. With $\lambda = 0.075$ the condensation energy is much larger, 0.0030 ± 0.0007, so that the error bars are not significant and it is clear that the EPI enhances the condensation energy. The condensation energies here are smaller than those found for optimal doping indicating a lower transition temperature which is consistent with the schematic phase diagram fig(1.3).

Examining theses results further by plotting the condensation energy against λ in

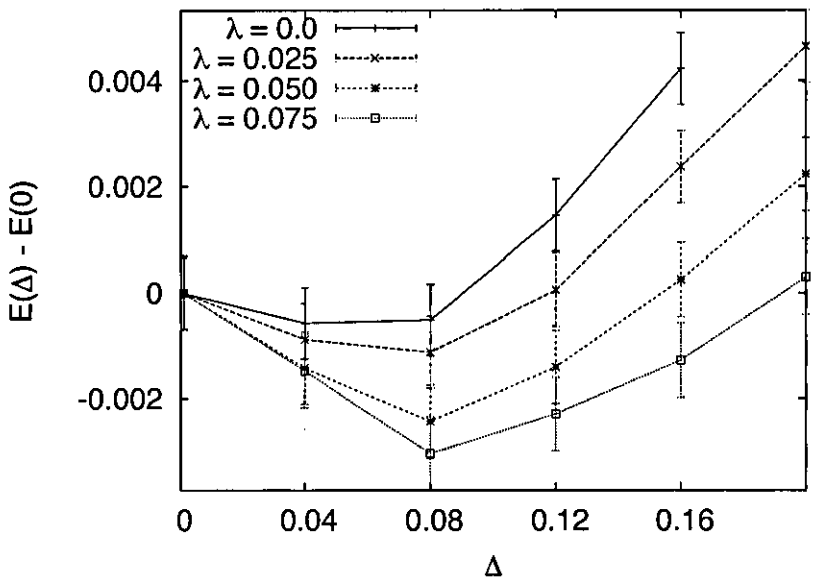

Figure 4.14: The energy, $E(\Delta)$, per electron relative to the normal state energy (in units of $\tilde{t}$) versus the amplitude of the superconducting d-wave order-parameter for $\tilde{U} = 8$, with different EPI coupling, λ.

fig(4.15) it is found that the enhancement of the condensation induced by the EPI is again present for this doping level. The plot of Δ against λ, fig(4.16) indicates that increasing the EPI strength increases the amplitude of the superconducting order parameter though the error bars are large and more results for other values Δ are required.

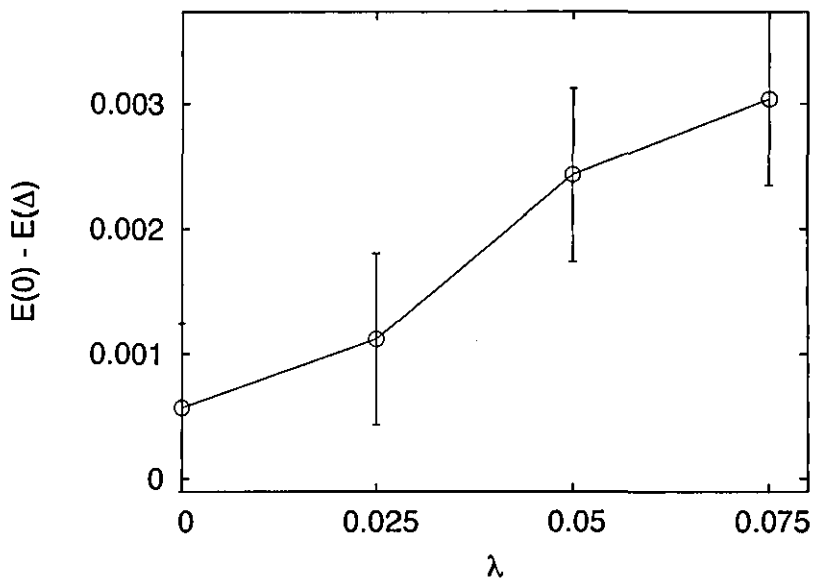

Figure 4.15: The condensation energy, $E(0) - E(\Delta)$, against λ for the over-doped lattice.

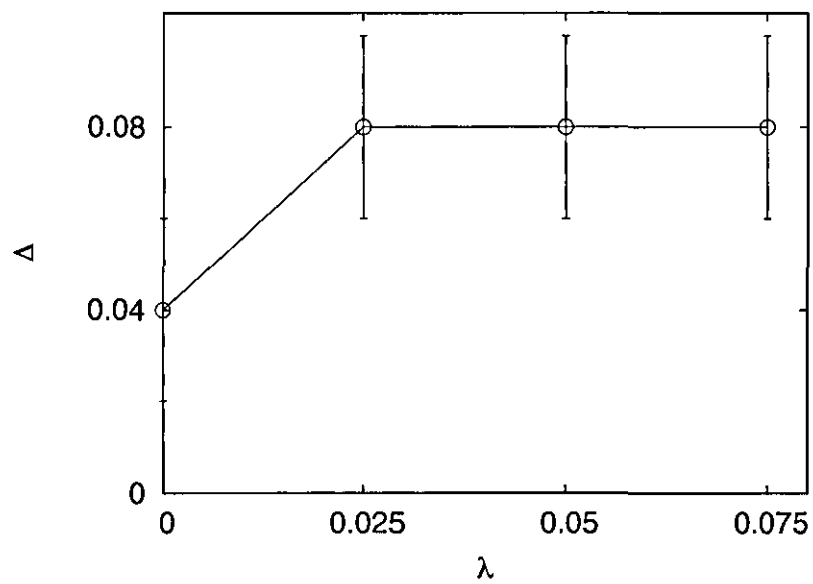

Figure 4.16: Δ against λ for the over-doped lattice.

4.3.4 Phase diagram

Here we plot the maximum condensation energies and amplitude of the superconducting order parameter, for values of λ up to 0.075, against the doping level, see fig(4.17) and fig(4.18) respectively. We use the definition $x = 1 - \rho$, where $\rho = n_e/n_s$ i.e the number of electrons divided by the number of sites. With the data available we are unable to reproduce the superconducting dome. On the over-doped side we find a reduction in both the condensation energy and order parameter which may indicate a reduction in the transition temperature as is expected, see fig(1.2). The accuracy of the data is insufficient to predict a value at which the superconductivity would disappear.

When under-doped we find larger condensation energies and order parameters which appears to disagree with the experimental phase diagrams. However the relationship between the condensation energy and transition temperature is not well understood and the larger condensation energies found do not necessarily indicate larger transition temperatures. In fact this may be accounted for by heavy pre-formed immobile pairs with a large binding energy and therefore could be an explanation of the pseudogap and therefore consistent with the phase diagram [15].

4.3.5 Static configurations

In this section we examine the energies of various static configurations. If a static energy has a lower energy than the energy calculated with the VMC simulation, then the static configuration would be the ground state. We placed 84 electrons on a 10x10 square lattice in various configurations, with no double occupancy setting $U = \infty$. In this case only the last term of the HFM contributes, we calculate:

$$E_{Static} = -W \sum_{\mathbf{n} \neq \mathbf{n}', \sigma\sigma'} \Phi(\mathbf{n} - \mathbf{n}') \hat{n}_{\mathbf{n}'\sigma'} \hat{n}_{\mathbf{n}\sigma} \tag{4.22}$$

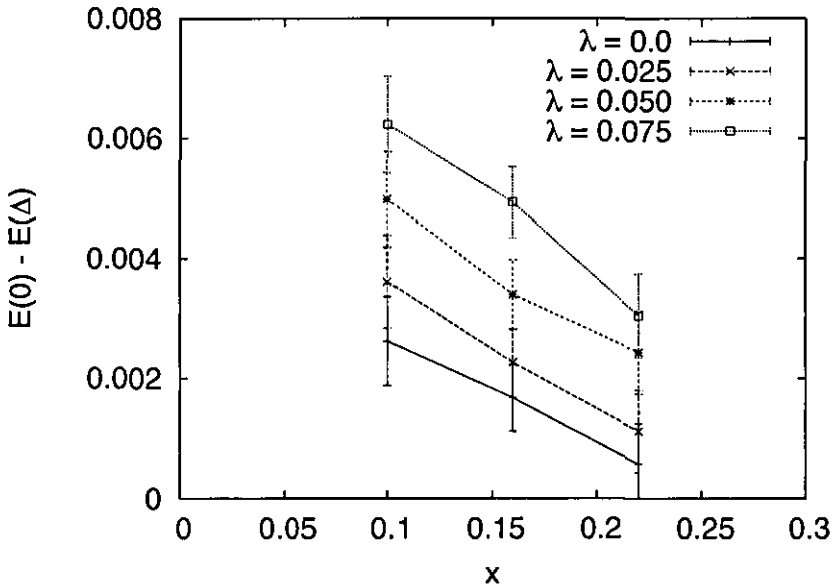

Figure 4.17: The condensation energy as a function of the doping level x.

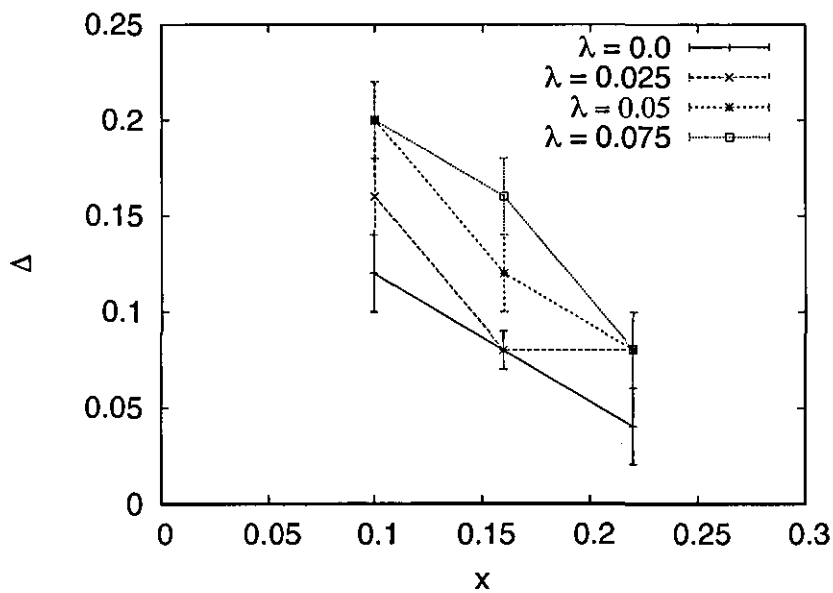

Figure 4.18: The amplitude of the d-wave superconducting order parameter as a function of the doping level x.

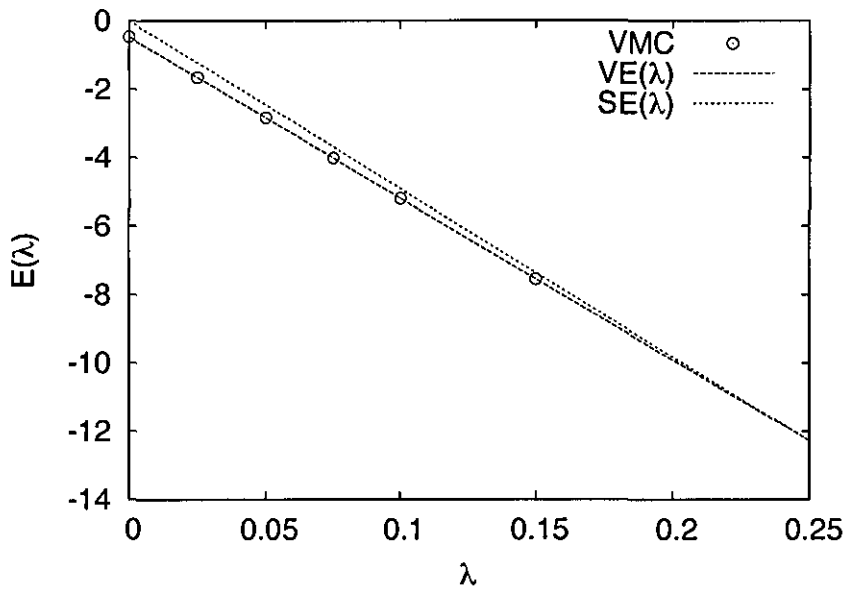

Figure 4.19: Energy of the static configurations as a function of $SE(\lambda)$ and a straight line fit of the variational energy $VE(\lambda)$ for $\tilde{u} = \infty$.

so that the static energy as a function of λ can be found fig(4.19). The lowest static energy for $\lambda = 0.075$ is -3.6824 per electron, with the electrons in a circular configuration, so that the $U = 8$ system is stable against the formation of immobile clusters. With $\lambda = 0.15$ the static energy is -7.3648 so that our $\tilde{U} = \infty$ superconducting state is also stable against cluster formation. It is found that the straight line fit of $E(\lambda)$, for $\tilde{U} = \infty$,intersects the line for the static configurations at $\lambda = 0.246 \pm 0.001$ where the formation of clusters would occur. For smaller values of the Hubbard repulsion the formation of clusters would occur at larger values of λ.

The static energy was also examined with a hole density of 10% were clusters are more readily formed. In this regime the lowest static energy was found to be -3.9631 for $\lambda = 0.075$ our system is stable against cluster formation. The difference between the VMC and static energies is smaller than in the optimally doped lattice and cluster will form at a weaker EPI. In the over-doped case clusters are less likely and will form at larger values of λ so again, for the EPI strengths studied here, clusters will not be

formed.

4.4 Conclusions

There is substantial evidence [24, 26, 27, 28] indicating that the Hubbard U and t–J models do not lead to high enough transition temperatures to be considered valid models of the cuprate superconductors. Some studies using the LDA method indicate that phonons are also unable to explain the high transition temperatures [77]. However it is clear these calculations are flawed, wrongly resulting in a metallic rather than insulating state for the undoped compounds, as they underestimate the electron correlations and should not be relied upon. The metallic nature of these states, predicted with the LD approximation, will cause an overestimation of the screening effects and therefore underestimate the long range EPI. With the addition of the on-site repulsion, in the LDA+U approach, the system becomes a Mott insulator reducing the screening in the c-axis, as predicted by Alexandrov [87], Mott [40] and Bauer [91]), and strengthening the EPI.

Our theoretical results, along with various experiments, see for example [29, 32, 36, 37, 44, 92, 39], indicate the need to include the *Fröhlich* EPI as well as strongly correlated electrons for a theory of the high superconductors as was initially proposed by Alexandrov and Mott [40]. In the Holstein model even a moderate EPI can cause charge carriers to be self-trapped and an insulating state[93]. When the Fröhlich EPI is considered this is not the case; a strong EPI has been shown small, light and mobile bipolarons can exist[87, 94, 85].

Here we have shown, using the VMC method, that even a relatively weak Fröhlich EPI is sufficient to induce a d-wave superconducting state with substantial condensation energy in a doped Mott-Hubbard insulator and/or strongly-correlated metals. While the exact energy gain may be overestimated, due to finite size scaling errors, our results

clearly demonstrate that increasing the EPI strength increases the condensation energy. The superconducting energies are lower than the static energies in a wide region of λ so that our superconducting state is stable against the formation of clusters. In addition the increase in condensation energy is large so that our superconducting state is likely to be robust against other choices of trial function. As a result we conclude that a combination of strong electron-electron correlations with long range electron-phonon interactions is a mechanism for high temperature superconductivity in the cuprates.

Chapter 5

Ferromagnetism and Superconductivity

In this chapter we examine the coexistence of ferromagnetism and superconductivity. These are two competing states with ferromagnetism favouring aligned spins and superconductivity favouring paired electrons with opposite spins. Therefore a perfect ferromagnet, in which all spins are aligned, cannot be a singlet superconductor.

Departing from the previous chapters based on numerical solutions here we use an analytical method. More precisely we use Greens Functions (GFs) to examine the Fulde-Ferrell-Larkin-Ovchinnikov state. We find some extra branches in the energy spectrum and a new expression for the finite momentum pairing amplitude.

5.1 Coexistence of ferromagnetism and superconductivity with zero momentum pairs

In the normal superconducting state electron pairs are created near the Fermi surface with equal but opposite momentum; these pairs therefore have a net zero momentum. Examining Fig(5.1) it can be seen that at the Fermi surface electron pairs with equal and opposite momentum do not exist in the ferromagnetic system. Thus it is generally thought that singlet superconductivity is inhibited by the presence of ferromagnetism though experimentally this is not necessarily the case [95].

Intuitively, it is predicted that increasing the ferromagnetic exchange energy should, at some value, cause the Cooper pairs, along with the superconductivity, to be destroyed [95]. This is not the case and it is has been found that it is possible for the ferromagnetic and superconducting states to coexist with an inhomogeneous order parameter. The idea of coexisting ferromagnetic and superconducting states with, finite momentum electron pairs and an oscillating order parameter, was originally proposed independently by Fulde and Ferrell [45] and Larkin and Ovchinnikov [46]. Such a state is often referred to as the Fulde-Ferrell-Larkin-Ovchinnikov (FFLO) state. Recently there has been revived interest in the area with the discovery of superconductivity in ferromagnetic metallic compounds UGe_2 [41], $ZrZn_2$ [42], URhGe [43] and $RuSr_2RECu_2O_8$ [44].

5.1.1 Analysis of the coexistence of ferromagnetism and superconductivity with zero momentum pairs

Theoretical work looking at the interplay of the two states, assuming that the electron pairs have zero-momentum, has been carried out by Cuoco *et al* [96, 97]. To do so a BCS type Hamiltonian (for detail see section 2.5), with a spin dependent electron

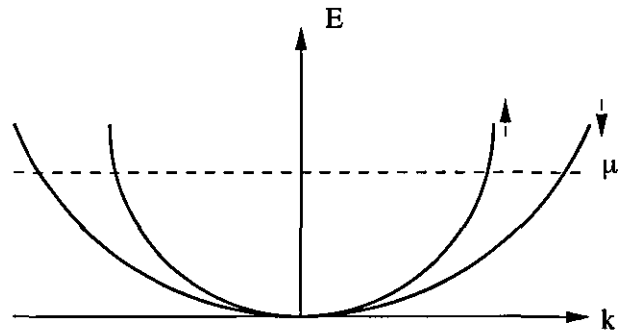

Figure 5.1: Energy spectrum for the ferromagnetic superconducting state.

mass [96], is written:

$$H = \sum_k \xi_k [2w_\uparrow c^\dagger_{k\uparrow} c_{k\uparrow} + 2w_\downarrow c^\dagger_{-k\downarrow} c_{-k\downarrow}] + \Delta_k c^\dagger_{k\uparrow} c^\dagger_{-k\downarrow} + \Delta^*_k c_{-k\downarrow} c_{k\uparrow} - \mu \sum_{k\sigma} c^\dagger_{k\sigma} c_{k\sigma} \quad (5.1)$$

where w_σ determines the mass re-normalisation of the spin σ electrons. The difference between the spin-up and spin-down electron mass leads to different numbers of up and down electrons and hence ferromagnetism, see Fig(5.1). In other theoretical work, see for example Ref [95], a Hubbard Hamiltonian has been used as the basis for the analysis of the coexisting ferromagnetic and superconducting states.

The ferromagnetic BCS Hamiltonian can be solved, like the standard BCS Hamiltonian, using a Bogoliubov transformation of the form:

$$\begin{aligned} \alpha_k &= u_k c_{k\uparrow} - v_k c^\dagger_{-k\downarrow} \qquad & \alpha^\dagger_k &= u_k c^\dagger_{k\uparrow} - v_k c_{-k\downarrow} \\ \beta_k &= u_k c_{-k\downarrow} + v_k c^\dagger_{k\uparrow} \qquad & \beta^\dagger_k &= u_k c^\dagger_{-k\downarrow} + v_k c_{k\uparrow} \end{aligned} \quad (5.2)$$

Applying the transformation reduces the Hamiltonian to the following diagonal form, the details of the derivation are shown in appendix A.1:

$$H = \sum_{\mathbf{k}} (E^\alpha_{\mathbf{k}} \alpha^\dagger_{\mathbf{k}} \alpha_{\mathbf{k}} + E^\beta_{\mathbf{k}} \beta^\dagger_{\mathbf{k}} \beta_{\mathbf{k}}) + \sum_{\mathbf{k}} [-E^\beta_{\mathbf{k}} + (2w_\downarrow \epsilon_{\mathbf{k}} - \mu)] + \frac{\Delta^2}{g} \quad (5.3)$$

where the quasi-particle energies, according to Ref [96], are given by:

$$E^{\alpha,\beta}_{\mathbf{k}} = \pm a\epsilon_{\mathbf{k}} + \sqrt{(b\epsilon_{\mathbf{k}} - \mu)^2 + \Delta^2} \quad (5.4)$$

with the definitions: $b = w_\uparrow + w_\downarrow$ and $a = w_\uparrow - w_\downarrow$.

Cuoco *et al* [96] then derived the following equation for the pairing amplitude, $\Delta = g\sum_{\mathbf{k}}\langle c^\dagger_{\mathbf{k}} c_{\mathbf{k}}\rangle$, is derived:

$$\Delta = \frac{g\Delta}{2}\sum_{\mathbf{k}} \frac{1 - n^\alpha_{\mathbf{k}} - n^\beta_{\mathbf{k}}}{\sqrt{(b\epsilon_{\mathbf{k}} - \mu)^2 + \Delta^2}} \tag{5.5}$$

where and $n^{\alpha,\beta}_{\mathbf{k}}$ are the occupation numbers of the new quasi-particles.

5.1.2 Energy spectrum

Examining the mathematics in appendix A.1 carefully it can be seen that the quasi-particle energies given in ref [96] contain an error; the negative part of the square root has been omitted. So, in fact, the quasi-particle energies are given by:

$$\begin{aligned} E^\pm_\alpha &= \xi a \pm \sqrt{\Delta^2 + (\xi b - \mu)^2} \\ E^\pm_\beta &= -\xi a \pm \sqrt{\Delta^2 + (\xi b - \mu)^2} \end{aligned} \tag{5.6}$$

If these excitation energies are to be physically significant they must be positive. By examining all four branches of the energy spectrum, varying a, b, μ and Δ, it can be seen in some cases the negative root can lead to positive energies; one such case is shown in Fig(5.2). In Fig(5.2) it can be seen that, for values of k around zero, a positive value for E^-_β can be found and without the negative root the energy dispersion would be incomplete. This means that there is an omission in the energy spectrum given in Ref [96]. For this reason it was decided that the Hamiltonian needs to be re-evaluated using another method. Here we study the coexistence of ferromagnetism and superconductivity using Green functions.

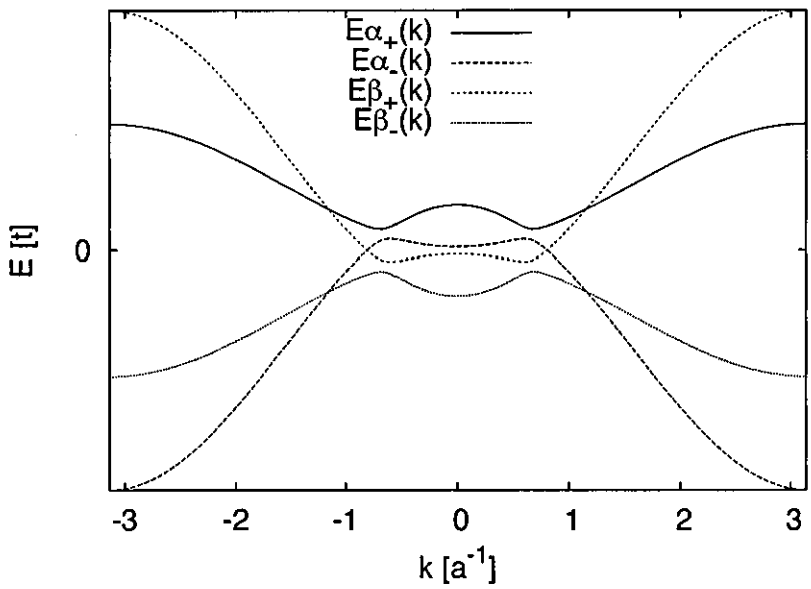

Figure 5.2: Sample energy spectrum of the α and β excitations, including all four branches, demonstrating that, under certain conditions, the negative root can lead to positive energies

5.2 Introduction to Green Functions

Green functions offer a more elegant approach to solving many body problems and are applied here. The idea behind the approach is that often it is not necessary to know all the eigenstates and eigenfunctions of a Hamiltonian but rather how it responds to perturbations [98]. The zero temperature Green function for an electron is defined as [52]:

$$G(\lambda, t-t') = -i\langle|TC_\lambda(t)C_\lambda^\dagger(t')|\rangle \tag{5.7}$$

where the Heisenberg representation is used to write the time dependent creation and annihilation operators as:

$$C_\lambda(t) = e^{iHt}C_\lambda e^{-iHt} \qquad C_\lambda^\dagger(t) = e^{iHt}C_\lambda^\dagger e^{-iHt} \tag{5.8}$$

and the time ordering operator, for fermions, has been introduced as:

$$T_t\hat{A}(t)\hat{b}(t') = \theta(t-t')\hat{A}(t)\hat{B}(t') - \theta(t'-t)\hat{B}(t')\hat{A}(t). \tag{5.9}$$

Here the step function is defined as $\theta(x) = 1$ for $x > 0$, $\theta(x) = 0$ for $x < 0$ and $\theta(x) = 1/2$ for $x = 0$.

5.2.1 BCS theory with Green Functions at finite temperature

As an introduction to the finite temperature Greens function [98] techniques, used later to study the competing ferromagnetic and superconducting states, here we re-derive the BCS equations using finite temperature Green functions (GF). To begin with the BCS Hamiltonian is rewritten in terms of field operators [9], $\Psi_s(\mathbf{r}) = \sum_{\mathbf{k}} c_{\mathbf{k}s} \exp[i\mathbf{k}.\mathbf{r}]$ [52] as:

$$\tilde{H} = \int dr[\sum_s \Psi_s^\dagger(r)\hat{h}_s(r)\Psi_s(r) + \Delta(r)\Psi_\uparrow^\dagger(r)\Psi_\downarrow^\dagger(r) + \Delta^*(r)\Psi_\downarrow(r)\Psi_\uparrow(r)] \qquad (5.10)$$

where $\hat{h}(\mathbf{r}) = -[\nabla + ie\mathbf{A}(\mathbf{r})]^2/2m + U(\mathbf{r}) - \mu$ and $\Delta(\mathbf{r}) = -2E_p\langle\langle\Psi_\downarrow(\mathbf{r})\Psi_\uparrow(\mathbf{r})\rangle\rangle$

Following the derivation described in reference [15], the Greens function at finite temperature is then defined with the same form as the zero temperature GF by:

$$\mathscr{G}(\boldsymbol{r}, \boldsymbol{r}', \tau_1\tau_2) = -\langle\langle T_\tau\psi_s(\boldsymbol{r}, \tau_1)\bar{\psi}_s(\boldsymbol{r}', \tau_2)\rangle\rangle \qquad (5.11)$$

where 'thermodynamic time' $\tau = it$ has been used in the Heisenberg operators to form Matsubara operators [99]:

$$\psi_s(\boldsymbol{r}, \tau) = e^{H\tau}\Psi_s(\boldsymbol{r})e^{-H\tau} \qquad \bar{\psi}_s(\boldsymbol{r}, \tau) = e^{H\tau}\Psi_s^\dagger(\boldsymbol{r})e^{-H\tau} \qquad (5.12)$$

Note that these operators are no longer hermitian conjugates [100]. The Gor'kov finite temperature GF is then:

$$\mathscr{F}^+(\boldsymbol{r}, \boldsymbol{r}', \tau_1, \tau_2) = -\langle\langle T_\tau\bar{\psi}_\downarrow(\boldsymbol{r}, \tau_1)\bar{\psi}_\uparrow(\boldsymbol{r}', \tau_2)\rangle\rangle \qquad (5.13)$$

The thermodynamic times are real and defined in the interval $0 < \tau_1, \tau_2 < 1/T$. In fact the GFs only depend on the difference $\tau = \tau_1 - \tau_2$. Replacing τ by a negative $\tilde{\tau}$, $\tau = \tilde{\tau} + \frac{1}{T}$ the result that $\mathscr{G}(\boldsymbol{r}, \boldsymbol{r}', \tilde{\tau} + \frac{1}{T}) = -\mathscr{G}(\boldsymbol{r}, \boldsymbol{r}', \tilde{\tau})$ is found (for details see [15]).

The next stage is to take Fourier transforms of the GFs. A function, $F(\tau)$, can be transformed using the Fourier expansion:

$$F(\tau) = T \sum_{n=-\infty}^{\infty} f_n e^{-i\pi n T\tau} \tag{5.14}$$

with the Fourier coefficients, f_n, defined by

$$f_n = \frac{1}{2} \int_{-\frac{1}{T}}^{\frac{1}{T}} d\tau F(\tau) e^{i\pi n T\tau}. \tag{5.15}$$

Noting that $F(\tau) = -F(\tau + \frac{1}{T})$, the Fourier coefficients are written:

$$f_n = \frac{1}{2}(1 - e^{i\pi n}) \int_0^{\frac{1}{T}} d\tau F(\tau) e^{i\pi n T\tau}. \tag{5.16}$$

So expanding the GFs with the Fourier transforms the equations below are found:

$$\begin{aligned} \mathscr{G}(\boldsymbol{r}, \boldsymbol{r}', \tau) &= T \sum_{\omega_n} \mathscr{G}(\boldsymbol{k}, \omega_n) e^{i\boldsymbol{k}.(\boldsymbol{r}-\boldsymbol{r}') - i\omega_n \tau} \\ \mathscr{F}^+(\boldsymbol{r}, \boldsymbol{r}', \tau) &= T \sum_{\omega_n} \mathscr{F}^+(\boldsymbol{k}, \omega_n) e^{i\boldsymbol{k}.(\boldsymbol{r}-\boldsymbol{r}') - i\omega_n \tau} \end{aligned} \tag{5.17}$$

Differentiating the Mastubara operators Eq(5.12) the following equations of motion are found:

$$\frac{\partial \Psi_s(\boldsymbol{r}, \tau)}{\partial \tau} = H e^{H\tau} \Psi_s(\boldsymbol{r}) e^{-H\tau} - e^{H\tau} \Psi_s(\boldsymbol{r}) H e^{-H\tau} = [H, \Psi_s(\boldsymbol{r}, \tau)] \tag{5.18}$$

For the BCS Hamiltonian, the equations of motion are given by:

$$\begin{aligned} \frac{\partial \Psi_\uparrow(\boldsymbol{r}, \tau)}{\partial \tau} = &\int d\boldsymbol{r} [\sum_s \Psi_s^\dagger(\boldsymbol{r}) \hat{h}(\boldsymbol{r}) \Psi_s(\boldsymbol{r}) + \Delta(\boldsymbol{r}) \Psi_\uparrow^\dagger(\boldsymbol{r}) \Psi_\downarrow^\dagger(\boldsymbol{r}) + \Delta^*(\boldsymbol{r}) \Psi_\downarrow(\boldsymbol{r}) \Psi_\uparrow(\boldsymbol{r})] \Psi_\uparrow(\boldsymbol{r}, \tau) \\ &- \Psi_\uparrow(\boldsymbol{r}, \tau) \int d\boldsymbol{r} [\sum_s \Psi_s^\dagger(\boldsymbol{r}) \hat{h}(\boldsymbol{r}) \Psi_s(\boldsymbol{r}) + \Delta(\boldsymbol{r}) \Psi_\uparrow^\dagger(\boldsymbol{r}) \Psi_\downarrow^\dagger(\boldsymbol{r}) + \Delta^*(\boldsymbol{r}) \Psi_\downarrow(\boldsymbol{r}) \Psi_\uparrow(\boldsymbol{r})] \end{aligned}$$

Applying the anti-commutation relations the equations of motion are reduced to:

$$\begin{aligned} -\frac{\partial \psi_\uparrow(\boldsymbol{r}, \tau)}{\partial \tau} &= \hat{h}(\boldsymbol{r}) \psi_\uparrow(\boldsymbol{r}, \tau) + \Delta(\boldsymbol{r}) \bar{\psi}_\downarrow(\boldsymbol{r}, \tau) \\ \frac{\partial \bar{\psi}_\uparrow(\boldsymbol{r}, \tau)}{\partial \tau} &= \hat{h}^*(\boldsymbol{r}) \bar{\psi}_\downarrow(\boldsymbol{r}, \tau) - \Delta^*(\boldsymbol{r}) \psi_\uparrow(\boldsymbol{r}, \tau) \end{aligned} \tag{5.19}$$

Then taking the derivative of the GFs, assuming $\tau > 0$, it is found that:

$$-\frac{\partial \mathscr{G}(\boldsymbol{r},\boldsymbol{r}',\tau)}{\partial \tau} = \bar{\psi}_s(\boldsymbol{r}',\tau_2)\frac{\partial \psi_s(\boldsymbol{r},\tau_1)}{\partial \tau} + \psi_s(\boldsymbol{r}',\tau_1)\frac{\partial \bar{\psi}_s(\boldsymbol{r},\tau_2)}{\partial \tau}. \tag{5.20}$$

Subsequent substitution of the equations of motion and application of the anti-commutation relations yields:

$$\begin{aligned} -\frac{\partial \mathscr{G}(\boldsymbol{r},\boldsymbol{r}',\tau)}{\partial \tau} &= \delta(\tau)\delta(\boldsymbol{r}-\boldsymbol{r}') + \hat{h}(\boldsymbol{r})\mathscr{G}(\boldsymbol{r},\boldsymbol{r}',\tau) + \Delta(\boldsymbol{r})\mathscr{F}^{+}(\boldsymbol{r},\boldsymbol{r}',\tau) \\ \frac{\partial \mathscr{F}^{+}(\boldsymbol{r},\boldsymbol{r}',\tau)}{\partial \tau} &= \hat{h}^{*}(\boldsymbol{r})\mathscr{F}^{+}(\boldsymbol{r},\boldsymbol{r}',\tau) - \Delta^{*}(\boldsymbol{r})\mathscr{G}(\boldsymbol{r},\boldsymbol{r}',\tau) \end{aligned} \tag{5.21}$$

Taking the Fourier transform of the differentiated GFs we get:

$$\begin{aligned} i\omega\mathscr{G}(\boldsymbol{k},\omega) &= 1 + \xi_k\mathscr{G}(\boldsymbol{k},\omega) + \Delta\mathscr{F}^{+}(\boldsymbol{k},\omega) \\ -i\omega\mathscr{F}(\boldsymbol{k},\omega) &= \xi_k\mathscr{F}(\boldsymbol{k},\omega) - \Delta\mathscr{G}(\boldsymbol{k},\omega) \end{aligned} \tag{5.22}$$

to which the solutions are:

$$\begin{aligned} \mathscr{G}(\boldsymbol{k},\omega_n)) &= -\frac{i\omega_n + \xi_k}{\omega_n^2 + \epsilon^2} \\ \mathscr{F}^{+}(\boldsymbol{k},\omega_n) &= -\frac{\Delta^*}{\omega_n^2 + \epsilon^2} \end{aligned} \tag{5.23}$$

where we have defined $\epsilon^2 = \xi_k^2 + \Delta^2$ as usual. The order parameter is then given by:

$$\Delta^* = -2E_pT\sum_k\sum_{\omega_n}\mathscr{F}^{+}(\boldsymbol{k},\omega_n) = 2E_pT\sum_k\sum_{\omega_n}\frac{\Delta^*}{\omega_n^2+\epsilon^2}. \tag{5.24}$$

Using the definition of the Matsubara frequencies $\omega_n = \pi T(2n+1)$ and the identity:

$$\frac{\tanh x}{x} = \sum_{n=-\infty}^{\infty}\frac{1}{x^2[\pi(n+\frac{1}{2})]^2} \tag{5.25}$$

the usual BCS result Eq(2.97) is recovered:

$$1 = \frac{\lambda}{2}\int\frac{d\xi}{\sqrt{\xi^2+\Delta(T)^2}}\tanh\frac{\sqrt{\xi^2+\Delta(T)^2}}{2T}. \tag{5.26}$$

5.3 Analysis of the coexistence of ferromagnetism and superconductivity with finite momentum pairs

We now apply the GF method to the ferromagnetic superconducting system with an inhomogeneous pairing amplitude. In terms of Heisenberg operators the Ferromagnetic BCS Hamiltonian Eq(5.1) is:

$$\tilde{H}_F = \int dr[\Psi_\uparrow^\dagger(r)\hat{h}_\uparrow(r)\Psi_\uparrow(r)+\Psi_\downarrow^\dagger(r)\hat{h}_\downarrow(r)\Psi_\downarrow(r)+\Delta(r)\Psi_\uparrow^\dagger(r)\Psi_\downarrow^\dagger(r)+\Delta^*(r)\Psi_\downarrow(r)\Psi_\uparrow(r)] \tag{5.27}$$

with $\Delta = \Delta_0 e^{i\mathbf{q}\mathbf{r}}$ allowing oscillations of the order parameter. With the ferromagnetic Hamiltonian the equations of motion now take the following form:

$$\begin{aligned} \frac{\partial\Psi_\uparrow(\boldsymbol{r},\tau)}{\partial\tau} &= -\hat{h}_\uparrow(\boldsymbol{r})\Psi_\uparrow(\boldsymbol{r},\tau) - \Delta(\boldsymbol{r})\Psi_\downarrow^\dagger(\boldsymbol{r},\tau) \\ \frac{\partial\Psi_\downarrow^\dagger(\boldsymbol{r},\tau)}{\partial t} &= \hat{h}_\downarrow^*(\boldsymbol{r},\tau)\Psi_\downarrow^\dagger(\boldsymbol{r},\tau) - \Delta^*(\boldsymbol{r})\Psi_\uparrow(\boldsymbol{r},\tau) \end{aligned} \tag{5.28}$$

So that the differentials of the GFs are now given by:

$$\begin{aligned} \frac{\partial\mathscr{G}_\uparrow(\boldsymbol{r},\boldsymbol{r}',\tau)}{\partial\tau} &= -\delta(\boldsymbol{r}-\boldsymbol{r}') - \hat{h}_\uparrow(\boldsymbol{r})\mathscr{G}_\uparrow(\boldsymbol{r},\boldsymbol{r}',\tau) - \Delta_0 e^{i\boldsymbol{q}\boldsymbol{r}}\mathscr{F}_{\downarrow\uparrow}^+(\boldsymbol{r},\boldsymbol{r}',\tau) \\ \frac{\partial\mathscr{G}_\downarrow(\boldsymbol{r},\boldsymbol{r}',\tau)}{\partial\tau} &= -\delta(\boldsymbol{r}-\boldsymbol{r}') - \hat{h}_\downarrow(\boldsymbol{r})\mathscr{G}_\downarrow(\boldsymbol{r},\boldsymbol{r}',\tau) - \Delta_0 e^{i\boldsymbol{q}\boldsymbol{r}}\mathscr{F}_{\uparrow\downarrow}^+(\boldsymbol{r},\boldsymbol{r}',\tau) \end{aligned} \tag{5.29}$$

and the differentials of the Gor'kov GFs now:

$$\begin{aligned} \frac{\partial\mathscr{F}_{\downarrow\uparrow}^+(\boldsymbol{r},\boldsymbol{r}',\tau)}{\partial\tau} &= \hat{h}_\downarrow^*(\boldsymbol{r})\mathscr{F}_{\downarrow\uparrow}^+(\boldsymbol{r},\boldsymbol{r}',\tau) - \Delta_0 e^{-i\boldsymbol{q}\boldsymbol{r}}\mathscr{G}_\uparrow(\boldsymbol{r},\boldsymbol{r}',\tau) \\ \frac{\partial\mathscr{F}_{\uparrow\downarrow}^+(\boldsymbol{r},\boldsymbol{r}',\tau)}{\partial\tau} &= \hat{h}_\uparrow^*(\boldsymbol{r})\mathscr{F}_{\uparrow\downarrow}^+(\boldsymbol{r},\boldsymbol{r}',\tau) - \Delta_0 e^{-i\boldsymbol{q}\boldsymbol{r}}\mathscr{G}_\downarrow(\boldsymbol{r},\boldsymbol{r}',\tau). \end{aligned} \tag{5.30}$$

As before the Fourier transforms of the GFs are now given by;

$$\begin{aligned} \mathscr{G}(\boldsymbol{r},\boldsymbol{r}',\tau) &= T\sum_{\boldsymbol{k}\boldsymbol{k}'\omega_n}\mathscr{G}(\boldsymbol{k},\boldsymbol{k}',\omega_n)e^{i(\boldsymbol{k}.\boldsymbol{r}+\boldsymbol{k}'\boldsymbol{r}')-i\omega_n\tau} \\ \mathscr{F}^+(\boldsymbol{r},\boldsymbol{r}',\tau) &= T\sum_{\boldsymbol{k}\boldsymbol{k}'\omega_n}\mathscr{F}^+(\boldsymbol{k},\boldsymbol{k}',\omega_n)e^{i(\boldsymbol{k}.\boldsymbol{r}+\boldsymbol{k}'\boldsymbol{r}')-i\omega_n\tau}. \end{aligned} \tag{5.31}$$

Taking the Fourier transformations of the GFs, then multiplying through by the factor, $e^{-i(\boldsymbol{p}.\boldsymbol{r}+\boldsymbol{p}'\boldsymbol{r}')+i\omega_n'\tau}$, and integrating over $\int d\boldsymbol{r}\int d\boldsymbol{r}'\int d\tau$, leads to the following set of equations (see A.2 for details):

$$\begin{aligned}
-i\omega_n\mathscr{G}_\uparrow(\boldsymbol{k},\boldsymbol{k}',\omega_n) &= -\delta_{kk'}-\xi_\uparrow\mathscr{G}_\uparrow(\boldsymbol{k},\boldsymbol{k}',\omega_n)-\Delta_0\mathscr{F}^+_{\downarrow\uparrow}(\boldsymbol{k}-\boldsymbol{q},\boldsymbol{k}',\omega_n) \quad (5.32)\\
-i\omega_n\mathscr{G}_\downarrow(\boldsymbol{k},\boldsymbol{k}',\omega_n) &= -\delta_{kk'}-\xi_\downarrow\mathscr{G}_\downarrow(\boldsymbol{k},\boldsymbol{k}',\omega_n)-\Delta_0\mathscr{F}^+_{\uparrow\downarrow}(\boldsymbol{k}-\boldsymbol{q},\boldsymbol{k}',\omega_n)\\
-i\omega_n\mathscr{F}^+_{\downarrow\uparrow}(\boldsymbol{k},\boldsymbol{k}',\tau) &= \xi(k)_\downarrow\mathscr{F}^+_{\downarrow\uparrow}(\boldsymbol{k},\boldsymbol{k}',\tau)-\Delta_0\mathscr{G}_\uparrow(\boldsymbol{k}+\boldsymbol{q},\boldsymbol{k}',\tau)\\
-i\omega_n\mathscr{F}^+_{\uparrow\downarrow}(\boldsymbol{k},\boldsymbol{k}',\tau) &= \xi(k)_\uparrow\mathscr{F}^+_{\uparrow\downarrow}(\boldsymbol{k},\boldsymbol{k}',\tau)-\Delta_0\mathscr{G}_\downarrow(\boldsymbol{k}+\boldsymbol{q},\boldsymbol{k}',\tau).
\end{aligned}$$

The solutions to the set of equations (5.32) are therefore given by (for details see appendix):

$$\begin{aligned}
\mathscr{G}_\uparrow(\boldsymbol{k},\omega_n) &= \frac{i\omega_n+\xi(\boldsymbol{k}-\boldsymbol{q})_\downarrow}{(i\omega_n-\xi(k)_\uparrow)(i\omega_n+\xi(\boldsymbol{k}-\boldsymbol{q})_\downarrow)-\Delta_0^2} \quad (5.33)\\
\mathscr{F}^+_{\downarrow\uparrow}(\boldsymbol{k},\tau) &= \frac{\Delta_0}{(i\omega_n-\xi(k+q)_\uparrow)(i\omega_n+\xi(k)_\downarrow)-\Delta_0^2}.
\end{aligned}$$

These two solutions can be written in a more compact form using the following definitions for the quasi-particle energies:

$$\begin{aligned}
\epsilon_\alpha &= \frac{1}{2}(\xi(\mathbf{k}+\mathbf{q})_\uparrow-\xi(\mathbf{k})_\downarrow)+\epsilon \quad (5.34)\\
\epsilon_\beta &= -\frac{1}{2}(\xi(\mathbf{k}+\mathbf{q})_\uparrow-\xi(\mathbf{k})_\downarrow)+\epsilon\\
\epsilon=\sqrt{E^2+\Delta^2} \qquad E &= \frac{1}{2}(\xi(\mathbf{k}+\mathbf{q})_\uparrow+\xi(\mathbf{k})_\downarrow),
\end{aligned}$$

so that the GF and the Gorkov GF can now be written as (details are included in the appendix):

$$\begin{aligned}
\mathscr{G}_\uparrow(\boldsymbol{k},\omega_n) &= \frac{i\omega_n+\xi(\boldsymbol{k}-\boldsymbol{q})_\downarrow}{(i\omega_n-\epsilon_\alpha)(i\omega_n+\epsilon_\beta)} \quad (5.35)\\
\mathscr{F}^+_{\downarrow\uparrow}(\boldsymbol{k},\tau) &= \frac{\Delta_0}{(i\omega_n-\epsilon_\alpha)(i\omega_n+\epsilon_\beta)}
\end{aligned}$$

As before, with the zero-momentum pairs, the definition for the pairing amplitude is:

$$\Delta(\boldsymbol{q}) = gT\sum_{k\omega_n}\mathscr{F}^+_{\downarrow\uparrow}(\boldsymbol{k},\omega_n) \quad (5.36)$$

Substitution of the Gorkov GF Eq(5.35) into Eq(5.36) and making use of the identity Eq(5.25), leads to:

$$\Delta(q) = \sum_k \frac{g\Delta_0}{4\epsilon}[\tanh(\frac{\epsilon_\alpha}{2T}) + \tanh(\frac{\epsilon_\beta}{2T})]. \tag{5.37}$$

It is known that $1 - n_x = \tanh(\epsilon_x/2T)$ so the final form of the gap equation is:

$$\Delta(q) = \sum_k \frac{g\Delta_0[1 - n_\alpha - n_\beta]}{2\sqrt{\frac{1}{4}(\xi(k+q)_\uparrow + \xi(k)_\downarrow)^2 + \Delta^2}} \tag{5.38}$$

With $\mathbf{q} = \mathbf{0}$ this equation reduces to the gap equation, Eq(5.5), found by Cuoco et al [96].

5.4 Conclusions

A complete energy spectrum for a ferromagnetic BCS type Hamiltonian has been derived. We have derived a novel expression for the pairing amplitude of finite momentum electron pairs. To progress further this expression needs to be evaluated in the continuum limit. This has proved a difficult problem, beyond the scope of this thesis, and suggested as further work. As expected setting $\mathbf{q} = \mathbf{0}$ in Eq(5.38), for electron pairs with zero total momentum, the result by Cuoco et al [96] is recovered. We conclude that, despite an omission in the energy spectrum, the final result [96] is robust.

Chapter 6

Conclusions and Recommendations for Further Work

6.1 Conclusions

A VMC algorithm has been developed and tested against previous results that examined ground state energies the Hubbard model. Using the VMC method it is possible to examine various trial wave functions; Here we have used the free electron, anti-ferromagnetic and superconducting trial functions and accurately reproduced the results of various earlier studies.

An electron-phonon interaction has been added to the Hubbard model to form the Hubbard-Hröhlich model. The Lang-Firsiv transformation has then been applied to the HFM remove the phonon terms. Along with modifications to the VMC method, to measure the long range electron-electron attraction, this has allowed us to investigate the effects including an electron-phonon interaction in a strongly correlated electron system.

We have then used this VMC algorithm to demonstrate that the inclusion of the EPI

to the Hubbard model produces a substantial increase in the condensation energy. The condensation energy represents the energy required to break paired electrons so the larger condensation energies found here indicate an increase in the stability of the superconducting state.

The majority of our results are for an optimally doped, or close to optimally doped, system and detailed earlier in this thesis and in Ref [75]. In summary we find no s-wave or extended s-wave superconducting state in the HFM with either $\tilde{U} = 8$ or $\tilde{U} = \infty$. With a d-wave order parameter it is found that the EPI enhances the condensation energy considerably when $\tilde{U} = 8$; over the range $0 \leq \lambda \leq 0.075$ it was shown that the relationship between the condensation energy and the EPI can be approximated by a straight line with a positive gradient. For infinite on site repulsion we find that the condensation energy with a d-wave order parameter is again enhanced by the presence of an EPI; In this region the effect is smaller and larger values of λ must be used to produce a significant lowering of the energy.

In both the under and over-doped lattices it was found that the inclusion of the EPI enhances the condensation energy. With an under-doped lattice we found larger condensation energies, than those found in the optimally doped lattice, possibly due to the presence pre-formed pairs as seen in the phase diagram. When over doped we see smaller condensation energies suggesting lower transitions temperatures which is consistent with the phase diagram.

The coexistence of ferromagnetism and superconductivity was also examined. We re-derived the results by Cuoco *et al* [96] finding 2 new branches in the energy spectrum yet we find the same result for the expression for the pairing amplitude. In addition we allow pairs with finite momentum and derive the pairing amplitude for these states.

6.2 Further work

Further work on the coexistence of ferromagnetism and superconductivity with finite momentum pairs is suggested. Our work is incomplete and the expression for the pairing amplitude needs to be integrated. This is a difficult task: the expression has both angular and radial dependance. We have not been able to find a method to solve this numerically.

Using the current VMC algorithm and trial function it is possible to study the HFM further. A more comprehensive phase diagram can be produced. To do this the presence of s and extended s wave superconducting states at other doping levels should be investigated. Additional simulations, with the d-wave order parameter, at doping levels other than those presented here need to be carried out to produce more data points for the phase diagram. Larger EPI strengths can be investigated to better determine the relationship between the condensation energy and λ. To gain further understanding of the situation additional values of the Hubbard repulsion should also be investigated.

Our results give a clear qualitative picture of the effect the EPI though finite size errors may have led to an overestimation of the condensation energy. To gain a better quantitative insight the HFM could also be examined with other algorithms. In particular it would be useful to use the Gaussian basis MC method [82] to produce more accurate condensation energies. With the advance of computer technology it will be possible to study larger lattices to reduce any finite size errors. The VMC method could also be employed to examine the HFM with other trial functions, in particular a trial function that is defined for the normal state ($\Delta = 0$) would improve the reliability of the results. It should be pointed out that no qualitative change to the main result, that the inclusion of the EPI in the Hubbard model stabilises the superconducting state is expected.

Appendix A

Appendix

A.1 Derivation of the Zero Momentum pairing Ferromagnetic Superconducting state

Diagonalisation of the ferromagnetic BCS Hamiltonian proceeds as follows:

$$H = \sum_k \xi_k [2w_\uparrow c^\dagger_{k\uparrow} c_{k\uparrow} + 2w_\downarrow c^\dagger_{-k\downarrow} c_{-k\downarrow}] + \Delta_k c^\dagger_{k\uparrow} c^\dagger_{-k\downarrow} + \Delta^*_k c_{-k\downarrow} c_{k\uparrow} - \mu \sum_{k\sigma} c^\dagger_{k\sigma} c_{k\sigma} \quad \text{(A.1)}$$

The Bogoliubov particles are defined as:

$$\begin{aligned} \alpha_k &= u c_{k\uparrow} - v c^\dagger_{-k\downarrow} \qquad & \alpha^\dagger_k &= u c^\dagger_{k\uparrow} - v c_{-k\downarrow} \\ \beta_k &= u c_{-k\downarrow} + v c^\dagger_{k\uparrow} \qquad & \beta^\dagger_k &= u c^\dagger_{-k\downarrow} + v c_{k\uparrow} \end{aligned} \quad \text{(A.2)}$$

As α and β are fermions and must obey the same anticommutation rules.

$$\begin{aligned}\{\alpha_k^\dagger, \alpha_k\} = (uc_{k\uparrow} - vc_{-k\downarrow}^\dagger)(uc_{k\uparrow}^\dagger - vc_{-k\downarrow}) + (uc_{k\uparrow}^\dagger - vc_{-k\downarrow})(uc_{k\uparrow} - vc_{-k\downarrow}^\dagger) &= 1 \\ u^2(1 - c_{k\uparrow}^\dagger c_{k\uparrow}) + v^2 c_{-k\downarrow}^\dagger c_{-k\downarrow} + u^2 c_{k\uparrow}^\dagger c_{k\uparrow} + v^2(1 - c_{-k\downarrow}^\dagger c_{-k\downarrow}^\dagger) &= 1 \\ u^2 + v^2 &= 1\end{aligned}$$

The electron creation and annihilation operators are written as:

$$\begin{aligned} c_{k\uparrow} = u_k\alpha_k + v_k\beta_k^\dagger \qquad c_{k\uparrow}^\dagger = u_k\alpha_k^\dagger + v_k\beta_k \\ c_{-k\downarrow} = u_k\beta_k - v_k\alpha_k^\dagger \qquad c_{-k\downarrow}^\dagger = u_k\beta_k^\dagger - v_k\alpha_k \end{aligned} \tag{A.3}$$

Dropping the summation for simplicity and writing the Hamiltonian in terms of Bogoliubov operators:

$$\begin{aligned} H_k = \; & \xi_k[2w_\uparrow(u\alpha^\dagger + v\beta)(u\alpha + v\beta^\dagger) + 2w_\downarrow(u\beta^\dagger - v\alpha)(u\beta - v\alpha^\dagger)] + \\ & +\Delta(u\alpha^\dagger + v\beta)(u\beta^\dagger - v\alpha) + \Delta^*(u\beta - v\alpha^\dagger)(u\alpha + v\beta^\dagger) - \\ & -\mu[(u\alpha^\dagger + v\beta)(u\alpha + v\beta^\dagger) + (u\beta^\dagger - v\alpha)(u\beta - v\alpha^\dagger)] \end{aligned} \tag{A.4}$$

Expanding and gathering like terms together:

$$\begin{aligned} H_k = \; & \alpha^\dagger\alpha[\xi 2w_\uparrow u^2 - \xi 2w_\downarrow v^2 - 2\Delta uv - \mu(u^2 - v^2)] \\ & +\beta^\dagger\beta[\xi 2w_\downarrow u^2 - \xi 2w_\uparrow v^2 - 2\Delta uv - \mu(u^2 - v^2)] \\ & +\alpha^\dagger\beta^\dagger[\xi 2w_\uparrow uv + \xi 2w_\downarrow uv + \Delta(u^2 - v^2) - \mu 2uv] \\ & +\beta\alpha[\xi 2w_\uparrow uv + \xi 2w_\downarrow uv + \Delta(u^2 - v^2) - \mu 2uv] + \\ & +\xi 2w_\uparrow v^2 + \xi 2w_\downarrow v^2 + \Delta 2uv - \mu 2v^2 \end{aligned} \tag{A.5}$$

This is then diagonal if:

$$\xi 2w_{\uparrow}uv + \xi 2w_{\downarrow}uv + \Delta(u^2 - v^2) - \mu 2uv = 0 \tag{A.6}$$

is satisfied. Solving this equation with the condition $u^2 + v^2 = 1$ it is found that:

$$u^2 = \frac{1}{2}(1 + \frac{\xi b - \mu}{\sqrt{\Delta^2 + (\xi b - \mu)^2}}) \qquad v^2 = \frac{1}{2}(1 - \frac{\xi b - \mu}{\sqrt{\Delta^2 + (\xi b - \mu)^2}}) \qquad uv = \frac{1}{2}\sqrt{1 - x^2} \tag{A.7}$$

So that the quasi-particle energies are:

$$E_{\mathbf{k}}^{\alpha,\beta} = \pm a\epsilon \pm \sqrt{(b\epsilon_{\mathbf{k}} - \mu)^2 + \Delta^2} \tag{A.8}$$

A.2 Fourier Transformation of the Finite Momentum GFs

Here we show the details of the Fourier transform for the finite momentum pairing state. Taking the Fourier tranform of the left side of Eq(5.29):

$$-i\omega_n T \sum_{\boldsymbol{k}\boldsymbol{k}'\omega_n} \mathscr{G}_{\uparrow}(\boldsymbol{k}, \boldsymbol{k}', \omega_n) e^{i[\boldsymbol{k}.\boldsymbol{r} + \boldsymbol{k}'.\boldsymbol{r}' - \omega_n \tau]} \tag{A.9}$$

then the right side:

$$-\delta(\boldsymbol{r}-\boldsymbol{r}')-\xi_{\uparrow}T\sum_{\boldsymbol{k}\boldsymbol{k}'\omega_n}\mathscr{G}_{\uparrow}(\boldsymbol{k},\boldsymbol{k}',\omega_n)e^{i[\boldsymbol{k}.\boldsymbol{r}+\boldsymbol{k}'\boldsymbol{r}'-\omega_n\tau]} \tag{A.10}$$
$$-\Delta_0 T\sum_{\boldsymbol{k}\boldsymbol{k}'\omega_n}\mathscr{F}^{+}_{\downarrow\uparrow}(\boldsymbol{k},\boldsymbol{k}',\omega_n)e^{i[(\boldsymbol{k}+\boldsymbol{q}.)\boldsymbol{r}+\boldsymbol{k}'\boldsymbol{r}'-\omega_n\tau]}.$$

We then multiply through by the factor, $e^{-i(\boldsymbol{p}.\boldsymbol{r}+\boldsymbol{p}'\boldsymbol{r}')+i\omega'_n\tau}$, and integrate, $\int d\boldsymbol{r}\int d\boldsymbol{r}'\int d\tau$ for the left side:

$$-i\omega_n T\sum_{\boldsymbol{k}\boldsymbol{k}'\omega_n}\mathscr{G}_{\uparrow}(\boldsymbol{k},\boldsymbol{k}',\omega_n)e^{i[(\boldsymbol{k}-\boldsymbol{p}).\boldsymbol{r}+(\boldsymbol{k}'-\boldsymbol{p}').\boldsymbol{r}'-(\omega_n-\omega'_n)\tau]}\int d\boldsymbol{r}\int d\boldsymbol{r}'\int d\tau \tag{A.11}$$

and for the right side:

$$-\delta(\boldsymbol{r}-\boldsymbol{r}')e^{-i[\boldsymbol{p}.\boldsymbol{r}+\boldsymbol{p}'\boldsymbol{r}'+\omega'_n\tau]}\int d\boldsymbol{r}\int d\boldsymbol{r}'\int d\tau \tag{A.12}$$
$$-\xi_{\uparrow}T\sum_{\boldsymbol{k}\boldsymbol{k}'\omega_n}\mathscr{G}_{\uparrow}(\boldsymbol{k},\boldsymbol{k}',\omega_n)e^{i[(\boldsymbol{k}-\boldsymbol{p}).\boldsymbol{r}+(\boldsymbol{k}'-\boldsymbol{p}).\boldsymbol{r}'-(\omega_n-\omega'_n)\tau]}\int d\boldsymbol{r}\int d\boldsymbol{r}'\int d\tau$$
$$-\Delta_0 T\sum_{\boldsymbol{k}\boldsymbol{k}'\omega_n}\mathscr{F}^{+}_{\downarrow\uparrow}(\boldsymbol{k},\boldsymbol{k}',\omega_n)e^{i[(\boldsymbol{k}+\boldsymbol{q}-\boldsymbol{p}).\boldsymbol{r}+(\boldsymbol{k}'-\boldsymbol{p}')\boldsymbol{r}')-\omega_n\tau]}\int d\boldsymbol{r}\int d\boldsymbol{r}'\int d\tau.$$

Using the definition of the delta function $\int exp[i(m-m')b]dx=\delta_{m,m'}$ this reduces to:

$$-i\omega_n\mathscr{G}_{\uparrow}(\boldsymbol{k},\omega_n)=-\delta_{\boldsymbol{k}\boldsymbol{k}'}-\xi_{\uparrow}\mathscr{G}_{\uparrow}(\boldsymbol{k},\omega_n)-\Delta_0\mathscr{F}^{+}_{\downarrow\uparrow}(\boldsymbol{k}-\boldsymbol{q},\omega_n) \tag{A.13}$$

The same procedure is applied to the other GFs.

A.3 Rewritting the Gor'Kov GF

Expanding the denominator of the Gor'kov GF:

$$(i\omega_n - \xi(k+q)_\uparrow)(i\omega_n + \xi(\boldsymbol{k})_\downarrow) - \Delta_0^2 = -\omega_n^2 + i\omega_n\xi(k)_\downarrow - i\omega_n\xi(k+q)_\uparrow - \xi(k+q)_\uparrow\xi(k)_\downarrow - \Delta_0^2$$

Using the quasi-particle energies Eq(5.34):

$$\begin{aligned}(i\omega_n - \epsilon_\alpha)(i\omega_n + \epsilon_\beta) &= -\omega_n^2 + i\omega_n\epsilon_\beta - i\omega_n\epsilon_\alpha - \epsilon_\alpha\epsilon_\beta \\ &= -\omega_n^2 - i\omega_n[(\xi(k+q)_\uparrow - (\xi(k)_\downarrow)] - \epsilon_\alpha\epsilon_\beta\end{aligned} \tag{A.14}$$

$$\begin{aligned}\epsilon_\alpha\epsilon_\beta &= [\frac{1}{2}(\xi(k+q)_\uparrow - (\xi(k)_\downarrow) + \epsilon][-\frac{1}{2}(\xi(k+q)_\uparrow - \xi(k)_\downarrow) + \epsilon] \\ &= -\frac{1}{4}(\xi(k+q)_\uparrow - \xi(k)_\downarrow)^2 + \epsilon^2 \\ &= -\frac{1}{4}(\xi(k+q)_\uparrow - \xi(k)_\downarrow)^2 + \frac{1}{4}(\xi(k+q)_\uparrow + \xi(k)_\downarrow)^2 + \Delta^2 \\ &= \xi(k+q)_\uparrow\xi(k)_\downarrow + \Delta^2\end{aligned} \tag{A.15}$$

So that the denominator is:

$$(i\omega_n - \xi(k+q)_\uparrow)(i\omega_n + \xi(\boldsymbol{k})_\downarrow) - \Delta_0^2 = (i\omega_n - \epsilon_\alpha)(i\omega_n + \epsilon_\beta). \tag{A.16}$$

A.4 Finite Momentum Pairing Amplitude

We rewrite the pairing amplitude as follows:

$$\Delta(\boldsymbol{q}) = gT\sum_{k\omega_n}\frac{\Delta_0}{(i\omega_n - \epsilon_\alpha)(i\omega_n + \epsilon_\beta)} \tag{A.17}$$

Using our previous definitions Eqs(5.34) the fraction is split:

$$\frac{1}{(i\omega-\epsilon_\alpha)(i\omega+\epsilon_\beta)}=\frac{1}{2\epsilon}\Big(\frac{1}{(i\omega-\epsilon_\alpha)}-\frac{1}{(i\omega+\epsilon_\beta)}\Big) \tag{A.18}$$

Now examining the first fraction:

$$\sum_n \frac{1}{(i\omega_n-\epsilon_\alpha)}=\sum_n \frac{-\epsilon_\alpha}{\omega_n^2+\epsilon_\alpha^2} \tag{A.19}$$

The Matsubara frequencies are defined as $\omega_n = \pi T(2n+1)$, $n = 0 \pm 1 \pm 2 \pm 3...$ so $\sum_n \omega_n/(\omega_n^2+a)=0$. Using the identity Eq(5.25)

$$\sum_n \frac{1}{(i\omega_n-\epsilon_\alpha)}=\frac{-1}{2T}\sum_n \frac{\epsilon_\alpha}{2T}\frac{1}{[\pi(n+\frac{1}{2})]^2+(\frac{\epsilon_\alpha}{2T})^2}=\frac{-1}{2T}\tanh(\frac{\epsilon_\alpha}{2T}) \tag{A.20}$$

So the pairing amplitude is now:

$$\Delta(q)=\sum_k \frac{g\Delta_0}{4\epsilon}[\tanh(\frac{\epsilon_\alpha}{2T})+\tanh(\frac{\epsilon_\beta}{2T})]. \tag{A.21}$$

Bibliography

[1] M. R. Norman and C. Pepin. The electronic nature of high temperature cuprate superconductors. *Rep. Prog. Phys.*, 66:1547, 2003.

[2] A. Damascelli, Z. Hussin, and Z. X. Shen. Angle-resolved photoemission studies of the cuprate superconductors. *Rev. Mod. Phys.*, 75:473, 2003.

[3] N. W. Ashcroft and N. D. Mermin. *Solid State Physics.* Holt Saunnders, Philadelphia, 1976.

[4] S Blugel, G Gompper, E Koch, H Muller-Krumbhaar, R Spatscheck, and R Winkler. *Computational Condensed Matter Physics.* Forschungszntrum Julich GmbH, Julich, 2006.

[5] M. C. Gutzwiller. Effect of correlation on the ferromagnetism of transition metals. *Phys. Rev. Lett.*, 10(5):159, 1963.

[6] J Hubbard. Electron correlations in narrow energy bands. *Proc. Roy. Soc. A*, 276:238, 1963.

[7] J. Kanamori. Electron correlations and ferromagnetism of transition metals. *Prog. Theor. Phys.*, 30:275, 1963.

[8] N. F. Mott. *Metal-Insulator Transitions.* Taylor & Francis, London, 1990.

[9] J. Bardeen, L. N. Cooper, and J. R. Schrieffer. Theory of superconductivity. *Phys. Rev.*, 108(5):15, 1957.

[10] M. Cohen and P. W. Anderson. Comments on the maximum superconducting transition temperature. In D. H. Douglas, editor, *Superconductivity in d- and f-band Metals.* American Inst. of Physics, 1972.

[11] J. G. Bednorz and K. A. Müler. Possible high T_c superconductivity in the Ba-La-Cu-O system. *Z. Phys. B*, 64:189, 1986.

[12] P. Dai, B. C. Chakoumakos, G. F. Sun, K. W. Wong, Y. Xin, and D. F. Lu. Synthesis and neutron powder diffraction study of the superconductor HgBa2Ca2Cu3O_8 by Tl substitution. *Physica C*, 243:201, 1995.

[13] F.C. Zhang and T.M. Rice. Effective hamiltonian for the superconducting Cu oxides. *Phys. Rev. B*, 37:3759, 1988.

[14] E. Dagotto. Correlated electrons in high-temperature superconductors. *Rev. Mod. Phys.*, 66(3):763, 1994.

[15] A. S. Alexandrov. *Theory of Superconductivity From Weak to Strong Coupling.* IOP Publishing, Bristol, 2003.

[16] J. F. Annett, N. Goldenfeld, and A. J. Leggett. Experimental constraints on the pairing state of the cuprate superconductors: An emerging consensus. *J. Low Temp. Phys.*, 105:473, 1996.

[17] H. Ding, T. Tokoya, J. C. Campuzano, T. Takahashi, M. Randeria, M. R. Norman, T. Mochiku, K. Kandowaki, and J. Giapintzakis. Spectoscopic evidence for a pseudogap in the normal state of underdoped high-T_c superconductors. *Nature*, 382:51, 1996.

[18] G. M. Zhao. Experimental constraints on the physics of cuprates. *Phios. Mag. B*, 81:1335, 2001.

[19] P. W. Anderson. The resonating valence bond state in La_2CuO_4. *Sci.*, 235:1196, 1987.

[20] A. Paramekanti, M. Randeria, and N. Trivedi. High-T_c superconductors: A variational theory of the superconducting state. *Phys. Rev. B*, 70:21, 2004.

[21] K. Yamaji, T. Yanagisawa, T. Nakanishi, and S. Koike. Variational Monte Carlo study on the superconductivity in the two-dimensional Hubbard model. *Physica C*, 304:225, 1998.

[22] L. Spanu, M Lugas, F Becca, and S. Sorella. Magnetism and superconductivity in the t-t'-J model. *Phys. Rev. B*, 77:24510, 2008.

[23] T. A. Maier, M. Jarrell, T. C. Schulthess, P. R. C. Kent, and J. B. White. Systematic study of d-wave superconductivity in the 2d repulsive Hubbard model. *Phys. Rev. Lett.*, 95:237001, 2005.

[24] M. Imada and T. Aimi. Does simple 2d Hubbard model account for high T_c superconductivity in copper oxides? *J. Phys. Soc. Jpn.*, 76:113708, 2007.

[25] N. Furukawa and M. Imada. Two-dimensional Hubbard model - metal insulator transition studied by Monte Carlo calculation. *J. Phys. Soc. Jpn.*, 61:3331, 1992.

[26] M. Imada. Superconducting correlation of two-dimensional Hubbard model near half-filling. *J. Phys. Soc. Jpn.. Low Temp. Phys.*, 60:2740, 1991.

[27] S. Zhang, J. Carlson, and J. E. Gubernatis. Pairing correlations in the two-dimensional Hubbard model. *Phys. Rev. Lett.*, 78:4486, 1997.

[28] M. Guerrero, G. Ortiz, and J. E. Gubernatis. Correlated wave functions and the absence of long-range order in numerical studies of the Hubbard model. *Phys. Rev. B*, 59:1706, 1999.

[29] G. Zhao and D. E. Morris. Observation of a possible oxygen isotope effect on the effective mass of carriers in YBaCuO. *Phys. Rev. B*, 51:16487, 1995.

[30] G. M. Zhao, M. B. Hunt, H. Keller, and K. A. Müller. Evidence for polaronic supercarriers in the copper oxide superconductors LaSrCuO. *Nature*, 385:236, 1997.

[31] R. Khasanov, D.G. Eshchenko, H. Luetkens, E. Morenzoni, T. Prokscha, A. Suter, N. Garifianov, M. Mali, J. Roos, K. Conder, and H. Keller. Direct observation of the oxygen isotope effect on the in-plane magnetic field penetration depth in optimally doped YBaCuO. *Phys. Rev. B*, 92:57602, 2004.

[32] A. Lanzara, P. V. Bogdanov, X. J. Zhou, S. A. Kellar, D. L. Feng, E. D. Lu, T. Yoshida, H. Eisaki, A. Fujimori, K. Kishio, J. I. Shimoyama, T. Noda, S. Uchida, Z. Hussain, and Z. X. Shen. Evidence for ubiquitous strong electron–phonon coupling in high-temperature superconductor. *Nature*, 412:510, 2001.

[33] G. H. Gweon, T. Sasagawa, S. Y. Zhou, J. Graf, H. Takagi, D. H. Lee, and A. Lanzara. An unusual isotope effect in a high-transition-temperature superconductor. *Nature*, 430:187, 2004.

[34] X. J. Zhou, J. Shi, T. Yoshida, T. Cuk, W. L. Yang, V. Brouet, J. Nakamura, N. Mannella, S. Komiya, and Y. Ando *et al.* Multiple bosonic mode coupling in the electron self-energy of LaSrCuO. *Phys. Rev. Lett.*, 95:117001, 2005.

[35] W. Meevasana, N. J. C. Ingle, D.H. Lu, J.R. Shi, F. Baumberger, K. M. Shen, W. S. Lee, T. Cuk, H. Eisaki, and T. P. Devereaux *et al.* Doping dependence of the coupling of electrons to bosonic modes in the single-layer high-temperature $Bi_2Sr_2CuO_6$ superconductor. *Phys. Rev. Lett.*, 96:157003, 2006.

[36] D. Mihailovic, C.M. Foster, K. Voss, and A.J. Heeger. Application of the polaron-transport theory to $\sigma(\omega)$ in TlBaCaGdCuO, YBaCuO, and LaSrCuO. *Phys. Rev. B*, 42:7989, 1990.

[37] P. Calvani, M. Capizzi, S. Lupi, P. Maselli, A. Paolone, P. Roy, S.W. Cheong, W. Sadowski, and E. Walker. Polaron imprints in the infrared spectra of NdCuO. *Solid St. Commun.*, 91:113, 1994.

[38] R. Zamboni, G. Ruani, A. J. Pal, and C. Taliani. Evidence of strong electron-phonon coupling from infrared excited raman scattering in the YBaCuO superconducting system. *Solid St. Commun.*, 70:813, 1989.

[39] D. Reznik, L. Pintschovius, M. Ito, S. Iikubo, M. Sato, H. Goka, M. Fujita, K. Yamada, G. D. Gu, and J. M. Tranquada. Electron–phonon coupling reflecting dynamic charge inhomogeneity in copper oxide superconductors. *Nature*, 440:1170, 2006.

[40] A. S. Alexandrov and N. F. Mott. Lattice and spin bipolarons in metal oxides and doped fullerenes. *Journal of Superconductivity*, 7:599, 1994.

[41] S. Saxena. Superconductivity on the border of itinerant-electron ferromagnetism in UGe2. *Nature*, 406:587, 2000.

[42] C. Pfeiderer. Coexistence of superconductivity and ferromagnetism in the d-band metal $ZrZn_2$. *Nature*, 412:58, 2001.

[43] D. Aoki. Coexistence of superconductivity and ferromagnetism in URhGe. *Nature*, 413:613, 2001.

[44] J. Tallon. Coexisting ferromagnetism and superconductivity in hybrid rutheno-cuprate superconductors. *IEEE Trans. Appl. Supercond.*, 9:1696, 1999.

[45] P. Fulde and R.A. Ferrell. Superconductivity in a strong spin-exchange field. *Phys. Rev.*, 135:A550, 1964.

[46] A.I. Larkin and Y. N. Ovchinnikov. Inhomogeneous state of superconductors. *Sov. Phys. JETP*, 20:762, 1965.

[47] E. K. Gross. *Many-Particle Theory.* IOP Publishing, Bristol, 1991.

[48] R. Jastrow. Many-body problem with strong forces. *Phys. Rev.*, 98:1479, 1955.

[49] P. Fulde. *Electron Correlations in Molecules and Solids.* Springer, Berlin, 1995.

[50] N. N. Bogoljubov, V. V. Tolmachov, and D. V. irkov. A new method in the theory of superconductivity. *Fortschritte der Physik*, 6:605, 1958.

[51] H. Fröhlich. Electrons in lattice fields. *Phios. Mag. Supp.*, 3:325, 1954.

[52] G. D. Mahan. *Many-Particle Physics.* Plenum Press, New York, 1981.

[53] H. Fröhlich. Theory of the superconducting state: The ground state at the absolute zero of temperature. *Phys. Rev. Lett.*, 79:845, 1950.

[54] L. N. Cooper. Bound electron pairs in a degenerate fermi gas. *Phys. Rev.*, 104:1189, 1956.

[55] P. G. de Gennes. *Superconductivity of Metals and Aloys.* Addison-Wesley, New York, 1966.

[56] L. Pauling. Nature of the chemical bond. *Proc. N.A.S*, 39:551, 1953.

[57] P. W. Anderson. Resonating valence bond. *Mat. Res. Bull.*, 8:153, 1973.

[58] M. E. J. Newman and G. T. Barkema. *Monte Carlo Methods in Statistical Physics.* Oxford University Press, Oxford, 1999.

[59] J. R. Taylor. *Introduction to Error Analysis.* University Science Books, Mill Valley, 1982.

[60] N. Metropolis, A. W. Rosenbluth, M. N. Rosenbluth, and A. H. Teller. Equation of state calculation by fast computing machines. *J. Chem Phys.*, 21:1087, 1953.

[61] W. L. McMillan. Ground state of liquid He. *Phys. Rev.*, 138:A 442, 1965.

[62] A. I. M. Rae. *Quantum Mechanics.* IOP Publishing, Bristol, 2002.

[63] D. Ceperley, G. V. Chester, and M. H. Kalos. Monte Carlo simulation of a many-fermion system. *Phys. Rev. B*, 16(7):3081, 1977.

[64] S.Fahy, X. W. Wang, and S. G. Louie. Variational quantum Monte Carlo non-local psuedpotential approach to solids: Formlation and application to diamond, graphite and silicon. *Phys. Rev. B*, 42:3503, 1990.

[65] H. Anton and Chris Rorres. *Elementry Linear Algebra.* John Wiey & Sons, New York, 1994.

[66] H. Yokoyama and H. Shiba. Variational Monte-Carlo studies of Hubbard model. I. *J. Phys. Soc. Jpn.*, 56:1490, 1986.

[67] R. B. Jones and W. Yeung. Variational studies of the 2d Hubbard model: less than half filled. *J. Phys. Cond. Matt.*, 2:2975, 1989.

[68] H. Yokoyama and H. Shiba. Variational Monte-Carlo studies of Hubbard model. II. *J. Phys. Soc. Jpn.*, 55:3582, 1987.

[69] H. Yokoyama and H. Shiba. Variational Monte-Carlo studies of superconductivity in strongly correlated electron systems. *J. Phys. Soc. Jpn.*, 57:2482, 1988.

[70] Claudius Gros. Superconductivity in correlated wave funtions. *Phys. Rev. B*, 38:931, 1988.

[71] J. R. Schrieffer. *Theory of Superconductivity.* W. A. Benjamin, New York, 1964.

[72] E.H. Leib and F.Y. Wu. Absence of Mott transition in an exact solution of the short-range one-band model in one dimension. *Phys. Rev. Lett.*, 20:1445, 1968.

[73] M. Karbach and G. Müller. Introduction to the Bethe ansatz 1. *arXiv cond. mat.9809162*, 1998.

[74] J. Florencio and K. A. Chao. Antiferromagnetic ground state in the s-band Hubbard model. *Phys. Rev. Lett.*, 35:741, 1975.

[75] T. M. Hardy, J. P. Hague, J. H. Samson, and A. S. Alexandrov. Superconductivity in a Hubbard-Fröhlich model and in cuprates. *arXiv cond. mat.0806.2810*, 2008.

[76] Y. Kamihara, T. Watanabe, M. Hirano, and H. Hosono. Iron-based layered superconductor LaOFeAs with $T_c = 26K$. *J. Am. Chem. Soc.*, 130:3296, 2008.

[77] R. Heid, K.-P. Bohnen, R. Zeyher, and D. Manske. Momentum dependence of the electron-phonon coupling and self-energy effects in superconducting $YBa_2Cu_3O_7$ within the local density approximation. *Phys. Rev. Lett.*, 100:137001, 2008.

[78] P. W. Anderson, P. A. Lee, M. Randeria, T. M. Rice, N. Trivedi, and F. C. Zhang. The physics behind high-temperature superconducting cuprates: the 'plain vanilla' version of RVB. *J. Phys.: Condens. Matter*, 16:R755, 2004.

[79] H. Yokoyama, Y. Tanaka, M. Ogata, and H. Tsuchiura. Crossover of superconducting properties and kinetic-energy gain in two-dimensional Hubbard model. *J. Phys. Soc. Jpn.*, 73:1119, 2004.

[80] S. Sorella, G. B. Martins, F. Becca, C. Gazza, L. Capriotti, A. Parola, and E. Dagotto. Superconductivity in the two-dimensional t-J model. *Phys. Rev. Lett.*, 88:117002, 2002.

[81] T.A. Maier, M.S. Jarrell, and D.J. Scalapino. Understanding high-temperature superconductors with quantum cluster theories. *Physica C*, 460:13, 2007.

[82] J. F. Corney and P. D.Drummond. Gaussian phase-space representations for fermions. *Phys. Rev. B*, 73:125112, 2006.

[83] T.K. Lee, C.T. Shih, Y.C. Chen, and H.Q. Lin. Comment. *Phys. Rev. Lett.*, 89:279702, 2002.

[84] J. P. Hague. d-wave superconductivity from electron-phonon interactions. *Phys. Rev. B*, 73:060503(R), 2006.

[85] J. P. Hague, P. E. Kornilovitch, J. H. Samson, and A. S. Alexandrov. Superlight small bipolarons in the presence of a strong coulomb repulsion. *Phys. Rev. Lett.*, 98:037002, 2007.

[86] J. Bonča and S. A. Trugman. Bipolarons in the extended Holstein Hubbard model. *Phys. Rev. B*, 64:094507, 2001.

[87] A. S. Alexandrov. Bipolaron anisotropic flat bands, hall mobility edge, and metal-semiconductor duality of overdoped high-T_c oxides. *Phys. Rev. B*, 53:2863, 1996.

[88] J. P. Hague, P. E. Kornilovitch, J. H Samson, and A. S. Alexandrov. Superlight small bipolarons. *J. Phys. Cond. Matt.*, 19:255214, 2007.

[89] I. G. Lang and Yu. A. Firsov. Kinetic theory of semiconductors with low mobility. *Sov. Phys. JETP*, 16:1301, 1963.

[90] A. S. Alexandrov and P. E. Kornilovitch. Mobile small polaron. *Phys. Rev. Lett.*, 82:807, 1999.

[91] T. Bauer and C. Falter. The impact of dynamical screening on the phonon dynamics of lacuo. *arXiv cond. mat.0808.2765*, 2008.

[92] T. R. Sendyka, W. Dmowski, T. Egami, N. Seiji, H. Yamauchi, and S. Tanaka. Temperature dependance of the local structure of YBaCu0. *Phys. Rev. B*, 51:6747, 1995.

[93] A. S. Alexandrov. *Polarons in Advanced Materials*, volume 103 of *Springer Series in Material Sciences*. Springer, New York, 2007.

[94] A. S. Alexandrov and P. E. Kornilovitch. The Fröhlich-coulomb model of high-temperature superconductivity and charge segregation in the cuprates. *J. Phys.: Condens. Matter*, 14:5337, 2002.

[95] M. Krawiec, B.L. Györffy, and J.F. Annett. Andreev bound states in ferromagnet-superconductor nanostructures. *Physica C*, 387:7, 2003.

[96] M. Cuoco. Coexistance of ferromagnetism and singlet syuperconductivity via kinetic exchange. *Phys. Rev. Lett.*, 91:197003, 2003.

[97] M. Cuoco, P. Gentie, and C. Noce. General conditions for coexistance intinerant ferromagnetism and singet superconductvity. *J. Phys. Chem. Solids*, 67:157, 2006.

[98] R. D. Parks. *Seperconductivity.* Marcel Dekker, New York, 1969.

[99] T. Matsubara. A new approach to quantum-statistical mechanics. *Prog. Theor. Phys.*, 14:351, 1955.

[100] A. A. Abrikosov, L. P. Gorkov, and I. E. Dzyaloshinski. *Methods of Quantum Field Theory in Statistical Physics.* Prentice-Hall, New Jersey, 1963.